Optimal Decision Making under Uncertainty in Biomanufacturing

Optimal Decision Making under Uncertainty in Biomanufacturing

This thesis is part of the PhD thesis series of the Beta Research School for Operations Management and Logistics (onderzoeksschool-beta.nl) in which the following universities cooperate: Eindhoven University of Technology, Ghent University, Maastricht University, Tilburg University, University of Twente, VU Amsterdam, Wageningen University and Research, KU Leuven, Universiteit Hasselt.

A catalogue record is available from the Eindhoven University of Technology Library.

ISBN: 978-90-386-5456-0

Printed by Gildeprint

Cover picture: Barak, P, and EA Nater. 1997-201x. The Virtual Museum of Minerals and Molecules. online resource. http://virtual-museum.soils.wisc.edu.

Optimal Decision Making under Uncertainty in Biomanufacturing

PROEFSCHRIFT

ter verkrijging van de graad van doctor aan de
Technische Universiteit Eindhoven, op gezag van de
rector magnificus prof.dr.ir. F.P.T. Baaijens, voor een
commissie aangewezen door het College voor
Promoties, in het openbaar te verdedigen
op vrijdag 18 maart 2022 om 13:30 uur

door

Yeşim Koca

geboren te Osmangazi, Turkije

Dit proefschrift is goedgekeurd door de promotoren en de samenstelling van de promotiecommissie is als volgt:

voorzitter:	prof. dr. T. van Woensel
1^{e} promotor:	prof. dr. ir. I.J.B.F. Adan
co–promotor:	dr. T.G. Martagan
leden:	prof. dr. A. Krishnamurthy (Indian Institute of Management Bangalore)
	prof. dr. M. Grunow (Technical University of Munich)
	prof. dr. ir. J. van der Schaaf
adviseurs:	prof. dr. S. Bhulai (Vrije Universiteit Amsterdam)
	prof. dr. L.M. Maillart (University of Pittsburgh)

Het onderzoek of ontwerp dat in dit proefschrift wordt beschreven is uitgevoerd in overeenstemming met de TU/e Gedragscode Wetenschapsbeoefening.

Acknowledgments

When I moved to the Netherlands as a PhD student some four years ago, I expected that I would gain plenty of knowledge and experience. Yet, I could have never imagined this journey would help me grow this much, both in professional and personal aspects. I was surrounded by many people, contributing to my growth one way or another. I would like to thank each of them for their unique support throughout this journey.

First, I would like to express my sincere gratitude to my promoter, Ivo Adan. Thanks to your curiosity and enthusiasm for maths, I did not only strengthen the theoretical part of my research, but I also enjoyed doing it. I was amazed how you grasped the essence of my work during short meetings and pinpointed the holes by asking critical questions. I learnt so much from those meetings and your feedback over the last years. I appreciate your friendliness, support, and mentorship throughout my PhD.

Many thanks to my daily supervisor, Tugce Martagan for accepting me for this PhD position. You taught me the importance of visibility, presenting my work, and telling my story. I improved a lot in these aspects of research. Thank you for guiding me to be a better researcher.

I am grateful to Lisa Maillart for our collaboration, which resulted in Chapter 2

of this thesis. You were always motivating, and supportive. I enjoyed working with you, and learnt a lot from your feedback. Furthermore, I would like to thank Ananth Krishnamurthy, Martin Grunow, John van der Schaaf and Sandjai Bhulai for serving in my committee. Thank you for your time, suggestions, and comments that improved my thesis.

I was fortunate to have the great support of our industry partner, MSD Animal Health. I am grateful to Oscar Repping, Bram van Ravenstein and Marc Baaijens for their enthusiasm, hospitality, and their patience in introducing the biomanufacturing world to me. Thank you for all your input in my thesis.

I would like to thank all my previous colleagues from Hacettepe University, Department of Industrial Engineering. Thanks to the friendly and supportive environment you have provided, I really enjoyed the early stages of my career. This was a great motivation for me to start a PhD. Special thanks to Murat Caner Testik, Özlem Müge Aydın Testik, Banu Yüksel Özkaya, Volkan Sönmez and Hakan Birer. Thinking of my time with you brings a big smile on my face.

I am grateful to my colleagues from OPAC for their companionship. Mirjam, I really enjoyed sharing an office with you in the Paviljoen Building. I will miss our office chats, spotting campus wildlife from our window and practicing random Dutch words on our whiteboards. Thank you for your friendship beyond our office. İpek, thank you for being such a lovely and caring friend, and being there for me whenever I need. Özge, thank you for our long discussions about life and our spontaneous activities. I also would like to thank Sami, Volkan, Albina, Wendy, Simon, Claudia, Faranak, Natasja, Zümbül, Willem, Kay, Tarkan, Cansu, Sena, and everyone else. Due to Covid-19 lockdowns our daily interaction was interrupted. Still, I was lucky to get to know all of you over the coffee and lunch breaks, board game nights, conferences, road trips, skiing weeks, barbeques, and many other activities. Thank you for all those fun moments. Special thanks to Claudine and Jolanda for their amazing administrative support and friendliness.

Many thanks to my friends who helped me step away from my research and recharge. Thank you Caroline for our fun pole trainings full of laughter and sharing your positive energy with me. Thank you Gizem for our fun gaming days, and Betül for being there in every city I have lived in so far. My high school friends Merve and Pınar, and university friends, Emel, Ecem and Nurcihan, thanks a lot for proving that friendship resists distance and time. In addition, many thanks to the Jansen

family for their care and for making me feel at home.

Next, I would like to express my warm thanks to my amazing parents Gülsüm and Güner. Since my childhood you taught me the importance of logical thinking, working hard, having an open mind and being a fighter. These helped me so much in completing this thesis. Thank you for your patience, unconditional love, and continuous support.

Finally, my deepest gratitude goes to Sjors. We became a couple as two PhD students. This is why you understand me maybe better than anyone else. We created (sometimes nerd) inside jokes, laughed together and shared memories. You became one of my most enthusiastic supporters. I cannot imagine how my last couple of years would be without you. Thank you for believing in me and for your love.

February, 2022

Contents

1

Introduction

The biomanufacturing industry developed several revolutionary drugs (also known as biopharmaceuticals) to treat diseases and provide better health care services. More than 345 million patients worldwide survived from diabetes, cardiovascular diseases, cancer, and many others thanks to these biopharmaceuticals (The European Biopharmaceutical Enterprises, 2015). Due to the surge in the chronic diseases, inclination towards targeted therapy and growing elderly population, the demand for these drugs increases. The demand increase is so rapid that the market analyses anticipate 7.32% annual growth globally between the years 2021 and 2026 (Mordor Intelligence, 2020). The growing global demand is stretching production footprints, and markets are becoming increasingly sensitive to costs (McKinsey & Company, 2014). To keep pace, the competitive advantage is shifting from "science" to "operations" (McKinsey & Company, 2019); and practitioners look for novel methods to improve biomanufacturing efficiency.

Different than traditional pharmaceutical operations, producing medicines from chemicals and synthetic processes, biomanufacturing companies derive their products through biological processes using living cells (i.e., bacteria, viruses, mammalian cells). The resulting products are highly complex compared to traditional pharmaceuticals. For instance, a biopharmaceutical molecule can contain 25,000 atoms, while an aspirin contains only 21 atoms (McKinsey & Company, 2014). This complexity, and the use of living cells lead to many challenges including batch-

to-batch variability, uncertainties in yield and throughput, production planning difficulties, and high costs and lead times.

In this thesis we develop stochastic optimization models to address these challenges and improve biomanufacturing efficiency. We focus on a novel technique: *bleed–feed*, allowing biomanufacturers to skip intermediary setups. We investigate optimal bleed–feed decisions from different aspects and inform practitioners about its potential in improving biomanufacturing operations. Through industry collaboration with MSD Animal Health in Boxmeer, the Netherlands (MSD AH), we develop decision support tools, and elaborate on their real-world implementation.

The rest of this chapter is organized as follows. We first present an overview of the biomanufacturing operations, and explain the concept of bleed–feed (Section 1.1). Next, we introduce the challenges in decision making and provide our research questions (Section 1.2). Then, we explain the methodology used to answer the research questions and highlight our contributions (Section 1.3). Finally, we present the thesis outline (Section 1.4).

1.1. Biomanufacturing Operations and Bleed–feed

An overview of a biomanufacturing process flow is demonstrated in Figure 1.1. Biomanufacturing operations typically consist of two main steps: upstream processing (USP) and downstream processing (DSP). USP is the first production step where the living cells (i.e., viruses and bacteria) are grown. USP starts with preculture, where the seed (i.e., a small amount of inactive cells, such as 5mL) is fed with medium. In this step, the seed is activated and prepared for fermentation. In the fermentation process the cells are fed with medium to grow and produce the desired active ingredients. Along with cells, byproducts (also called as impurities or waste) also accumulate in the batch, as a result of cell metabolic activities. Thus, output of the fermentation is a batch mixture of active ingredients and byproducts. Downstream processing follows the fermentation process and focuses on purification of the fermentation output to meet regulatory requirements on quality, storage, and delivery. In this step impurities are separated from biomass to be stored safely until its shipment to the customer. Centrifugation, chromatography, and filtration are common downstream processing operations. Depending on the

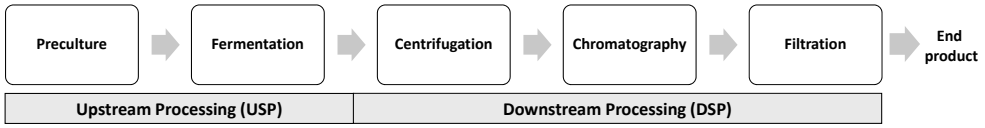

Figure 1.1: A general overview of biomanufacturing operations.

characteristics of the cell culture and regulations, different DSP operations can be applied in different orders.

The focus of this thesis is the upstream fermentation processes. Fermentation processes typically take place in bioreactors, which are stainless-steel vessels with a controlled environment to facilitate cell growth. Fermentation starts with a bioreactor setup, where the bioreactor is cleaned and sterilized and the seed culture (initial biomass) and medium are placed in the batch. The biomass consumes the medium and grows following certain growth phases as shown in Figure 1.2(a). Observe from Figure 1.2(a) that the fermentation starts with a small amount of initial biomass. The biomass grows exponentially over time in the exponential growth phase as it uses the medium. In the batch fermentation process medium is added only once, at the beginning of the fermentation process. Hence, nutrients deplete in the batch over time. Subsequently the cell growth slows down and the biomass enters the stationary phase, where the growth stops. Therefore, the batch is usually harvested in the stationary phase. When a batch is harvested, the bioreactor needs to be setup for a new fermentation process.

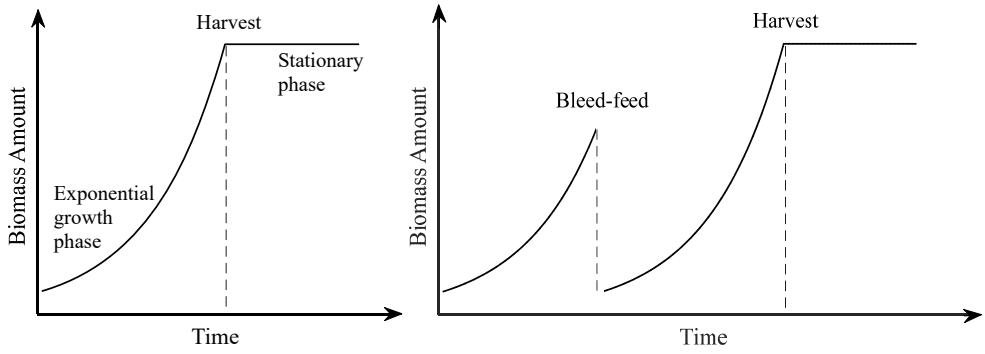

(a) Biomass growth without bleed–feed

(b) Biomass growth with bleed–feed

Figure 1.2: Biomass growth over time in current practice (a) and with bleed–feed (b).

The Bleed–feed Concept. The bioreactor setups are costly because they require highly specialized materials and labor. For instance, the consumables and reagents that are used in cleaning and sterilization of a bioreactor take around 16% of the total fermentation cost (Oyebolu et al., 2019; Mahal et al., 2021). This forces practitioners to find innovative ways to increase the biomass (and the associated rewards) obtained per setup as much as possible. In addition, setups are time consuming. Up to ten hours can be spent during a bioreactor setup (Sharma, 2019; Yang and Sha, 2019). This leads to lower throughput levels and fermentation profit per time unit. Therefore, there is a strong business case in the industry to reduce the number of setups.

Bleed–feed is a promising method to skip intermediary bioreactor setups. We illustrate the main idea behind bleed–feed in Figure 1.2(b). When bleed–feed is performed, some part of biomass accumulated in the bioreactor is extracted ("bleed") such that only a small amount of biomass remains inside the bioreactor. Then, fresh medium is added in the bioreactor ("feed"). The remaining biomass acts as a seed culture, and continues to grow in the exponential growth phase by using the new medium. In short, bleed–feed enables practitioners to skip a setup by prolonging the exponential growth phase.

The concept of "bleed" and "feed" exists in the fermentation systems for fed-batch, continuous batch and perfusion applications (Pollock et al., 2013; Muldowney, 2018; Walker, 2017; Kakes, 2018). Fed-batch systems continues to add fresh medium into the bioreactor during the fermentation. In continuous fermentation, next to continuous medium transfer into the batch, an equivalent amount of batch mixture is taken out of the bioreactor throughout the process. Perfusion is similar to continuous fermentation; the fundamental difference in a perfusion culture is that only the medium is extracted and the cells are kept in the system. Hence, bleed–feed is a new technique, as it is implemented in batch fermentation. It is performed almost instantaneously and can be perceived as starting a new batch *without* a new setup. Therefore, bleed–feed has unique trade-offs and challenges with high potential for improving biomanufacturing efficiency. Yet, its optimal implementation and potential impact has not been fully understood by the industry. We address these challenges and investigate the optimal bleed–feed decisions from various aspects to generate insights for biomanufacturers.

1.2. Challenges and Research Questions

In this section, we first elaborate on the challenges related to making bleed–feed decisions in different contexts and present the research questions. Then, we highlight common biomanufacturing challenges that are addressed in the last part of the thesis and focus on industry implementation of the proposed models.

High setup costs motivate biomanufacturers to produce as much yield as possible from a setup. We first assume the batch condition is regularly monitored and aim to maximize the yield obtained from a setup with bleed–feed. However, timing of bleed–feed is crucial for a successful implementation. Bleed–feed can only be implemented in the exponential growth phase. Otherwise, the cells do not grow in the next cultivation, and hence the batch needs to be harvested (meaning that bleed–feed failed). Determining the correct timing is not straightforward due to challenges derived by uncertain and complex nature of biomanufacturing. The duration of the exponential growth phase (i.e., time to enter the stationary phase) is stochastic. This is mainly because of the complex biological nature of living cells. This uncertainty introduces the trade-off on the bleed–feed time. If we implement the bleed–feed "too early" in order to avoid missing the exponential growth phase, we may not reach the highest yield from the batch. In contrast, if we are "too late" to bleed–feed in anticipation of obtaining higher biomass yield, then we lose the bleed–feed opportunity and we produce yield from only one cultivation.

Additionally, regulatory requirements permit only a limited number of bleed–feed implementation per bioreactor setup. These regulations are pre-specified by scientific evidence provided by biomanufacturers showing that batch safety and reliability are not at risk within these limits. Hence, these regulations are known to be overly strict in order to ensure safety for a wide range of settings. These rules affect the operational decisions, yet their impact is not fully understood in the industry. Biomanufacturers first need to understand the value of bleed–feed and the implications of adopting such policies in practice. Hence, we formulate the research questions as follows:

RQ 1. *What is an optimal condition-based bleed–feed policy that maximizes the total amount of biomass obtained from a bioreactor setup?*

RQ 2. *How are the potential benefits of bleed–feed affected by regulatory limitations?*

RQ 3. *What is the added value of implementing bleed–feed to current industry practice?*

Note that besides batch yield, processing time of the fermentation also increases with bleed–feed (because the bioreactor is occupied for a longer time period until the harvest). Therefore, understanding the implications of bleed–feed on throughput is important. In addition, time-based bleed–feed policies are also practically relevant, as they can easily be incorporated into production planning activities. For instance, biomanufacturing typically has a no-wait constraint, such that the batch needs to continue with subsequent operations immediately after it is harvested. In such settings time-based policies may be more attractive for practitioners.

Also, biomanufacturers can adjust the starting amount for the second cultivation (after bleed–feed) by controlling how much they extract from the first cultivation during bleed–feed. We observed from industry data that the start amount for the second cultivation affects the throughput. If the start amount is too little for the second cultivation, time to reach a certain biomass amount will be longer, and vice versa. Then, if we start the second cultivation with a high biomass amount, this implies we extract (obtain) less from the first cultivation during the bleed–feed (lowering the throughput). However, the exponential growth phase is likely to be shorter for the second cultivation (increasing the throughput). In contrast, if we start the second cultivation with a low biomass amount, this implies we extract (obtain) more from the first cultivation. Yet, the fermentation throughput may not increase, as the time needed to achieve a certain biomass level is longer for the second cultivation. Therefore, finding the balance between starting the second cultivation with "too much" or "too little" biomass can help making better bleed–feed decisions in optimizing the throughput. The trade-off between implementing the bleed–feed "too soon" versus "too late" (and the challenge in decision making) is still valid, as either case results in a suboptimal throughput due to suboptimal batch yield. These challenges lead to the following research questions:

RQ 4. *What is the optimal bleed–feed time for the first cultivation and the optimal starting biomass amount for the second cultivation in order to maximize the expected throughput?*

RQ 5. *What is the added benefit of jointly optimizing the bleed–feed time and the replenishment amount in practice?*

RQ 6. *How much improvement (in the expected throughput) can we achieve by*

implementing bleed–feed on current practice? Under which problem settings does bleed–feed offer a stronger business case for implementation, and under which setting adopting bleed–feed does not bring benefit?

Next to biomass growth, byproducts accumulate in fermentation as a result of metabolic activities of cells. These byproducts increase the toxicity in the culture environment, which might result in cell growth inhibition and reduction in batch quality. These byproducts are separated from the biomass (i.e., purified) in the DSP operations. The amount of byproducts affect the workload in the DSP. A batch with more byproducts might have to repeat certain steps in purification operations, thus incur higher costs. In this setting, if we bleed–feed too early, then we may not receive the highest yield and hence the revenue from the first cultivation. In addition, impurity level increases as a result of producing two cultivations, and purification cost increases. Contrarily, if we implement bleed–feed too late, the bleed–feed opportunity is lost and we harvest the batch with only one cultivation, leading to revenue corresponding to one cultivation alone. Yet, the impurity level and the purification cost will also be less in this case, as the impurity level corresponds to that from only one cultivation. Managing this trade-off and understanding how the cost parameters affect the bleed–feed decisions are important aspects for increasing the expected fermentation profit per time unit.

In addition, bleed–feed implementation requires operator interaction (i.e., initiating the medium transfer and extracting certain some part of the batch). However, in a biomanufacturing company working in shifts, no operators would be available during certain time periods. In this case, we must ensure that bleed–feed is implemented during a shift. Also, practitioners might tolerate some certain levels of bleed–feed failure risk. For instance, they might want to adjust the bleed–feed time in a risk-averse manner if they do not want to take the risk of missing the bleed–feed. Such restrictions limit the time that bleed–feed can be implemented, and the benefits obtained from it compared to flexible cases. Based on these challenges, we formulate the following research questions:

RQ 7. *What is the optimal bleed–feed time in order to maximize the fermentation profit per time unit, considering the impurity level in the batch?*

RQ 8. *How can we ensure that bleed–feed is implemented during a shift (i.e., when personnel is available), and that bleed–feed is implemented successfully with a certain*

probability level?

RQ 9. *How is the benefit obtained from bleed–feed affected by the constraints? What is the value of flexibility (i.e., having no restrictions on bleed–feed time) in bleed–feed decisions? Under which settings adopting bleed–feed does not bring benefit?*

In addition to aforementioned challenges related to bleed–feed decisions, we focus on other common challenges biomanufacturers face. We elaborate on the industry implementation of the proposed solutions. In particular, we address issues related to fermentation yield variability and production planning from our industry partner MSD AH, explained as follows:

Fermentation processes are highly unpredictable, and many factors affect the fermentation output. Even though the same fermentation process is conducted by using the identical settings (i.e., the cell type, physicochemical parameters, buffers, medium), one of the process lines produced significantly lower yield. Understanding the reason and improving the yield from a specific process line can be challenging, as life sciences literature does not necessarily capture the relationship between the specific fermentation yield of interest as a function of specific process parameters from different bioreactor technologies. Conducting laboratory scale experiments may not be possible due to capacity restrictions and scalability issues. Best configuration for fermentation parameters had to be determined under a limited number of industry scale runs.

In addition, production planning is challenging in biomanufacturing. The use of living cells causes variability in yield and processing times. Different products have different production requirements regarding equipment, necessary production steps and expertise of the operators. Equipment, such as bioreactors, can vary in size and technology, and processing times and end yield amount can be affected by equipment choices. There are interdependent production steps, with no-wait constraints (if products wait in between the production steps, contamination may occur, and quality may deteriorate so that the entire batch might be scrapped). Specialized equipment can be limited in number and shared between process lines. Operators are mostly scientists with different skill sets. Some operations can be carried out only by specific operators. Hence, production planning decisions are highly complicated. An automated and rigorous approach for production planning is crucial for companies.

1.3. Methodology and Contributions

In this section, we first elaborate on each chapter for the methodology used in order to answer the research questions, and the contributions. Then, we highlight the contributions of the thesis.

First, in Chapter 2 we develop a finite-horizon, discrete time Markov decision process (MDP) model to determine optimal condition-based bleed–feed policies to maximize expected total biomass obtained from a batch (RQ1). We analyze the structural properties of the optimal policies and show that the optimal bleed–feed policies have three-way control limit structure (on the cultivation age, cell growth rate, and the bleed–feed count) under mild conditions. We present a sufficient condition under which a risk-averse heuristic is optimal. We characterize the value function as a function of the regulatory requirements on bleed–feed number and show that the marginal benefit of an additional bleed–feed decreases and converges to a certain value (RQ2). In addition, we perform a case study from MSD AH to demonstrate the impact of bleed–feed implementation in practice (RQ3). We observe that bleed–feed brings benefits. In the base case, an increase of 137% is achieved in total biomass production from one setup with two bleed–feed implementations. Sensitivity analyses on system risks and the critical biomass level inform practitioners that low-risk batches and cultures with high critical biomass levels benefit more from bleed–feed implementation.

In Chapter 3, we develop a renewal model to find time-based bleed–feed policies for one bleed–feed. Our renewal model optimizes the bleed–feed time and the replenishment amount jointly to maximize fermentation throughput (RQ4). We explore the structural properties of the optimization problem to generate insights on optimal policies and assess the impact of batch risks on throughput. We present a sufficient condition under which the throughput function is convex for a specific period of bleed–feed time. Using this result, we explore the settings when implementing bleed–feed is not beneficial (RQ6). We enhance these results with a case study from MSD AH. We consider several relevant strategies to understand the potential benefits of optimizing the bleed–feed time and the replenishment amount jointly (RQ5). Further, we quantify the potential benefits of bleed–feed implementation in practice under different production settings (RQ6). Our numerical analysis shows that the expected throughput can be improved by 17%

with bleed–feed. We also observe that bleed–feed brings most benefit for fast-growing cells and that it is optimal not to adopt bleed–feed for slow-growing cell cultures.

Next, in Chapter 4 we extend our renewal model from Chapter 3 and find the bleed–feed time that optimizes the fermentation profit per time unit, considering practically relevant constraints (RQ7). In this chapter we take waste accumulation, its effects on the exponential growth phase, and the costs related to the purification of the batch (to remove waste) into account. We include constraints in our optimization model to capture relevant restrictions on the bleed–feed time related to operator availability to perform bleed–feed and the practitioner's risk-averse behavior (RQ8). We conduct a numerical analysis to generate managerial insights, and we relax some of the constraints to investigate the value of flexibility in bleed–feed decisions (RQ9). Further, we assess effects of restrictions on the bleed–feed time under different production configurations. Our results indicate that it is not necessarily better to implement bleed–feed at an earlier shift (to avoid missing the bleed–feed opportunity) if bleed–feed does not take place in a shift (when no operators are present). We also observe that implementing bleed–feed is not an attractive option if we have both the shift and the chance constraints.

In Chapter 5, we present a portfolio of operations research (OR) tools to improve biomanufacturing efficiency in collaboration with MSD AH. We demonstrate the use of OR methods in biomanufacturing. More specifically, the following tools are introduced: *(i) bleed–feed tool*, by using renewal reward theory to determine optimal bleed–feed time to optimize the fermentation throughput, *(ii) yield optimization tool*, by using Bayesian design of experiments to provide a methodological approach for determining the best fermentation configurations under limited number of experiments, and *(iii) rhythm wheel tool*, by using simulation-optimization to assess the feasibility of a weekly production schedule and create smart schedules to increase throughput and lower the lead times. We elaborate on the development of these tools and their implementation at MSD AH. Implementation of these tools at MSD AH had a significant impact with up to 50% increase in the batch yield, and an additional revenue of €50 million per year. The rhythm wheel tool allowed one extra batch production per week. Bleed–feed tool resulted in 85% increase in the batch yield per setup (using one bleed–feed).

Overall, this thesis demonstrates an example of how operations research can

complement biomanufacturing to improve operational decisions. We present problems and solution approaches that are relevant to both operations research and biomanufacturing communities. Biological dynamics and the operational trade-offs in biomanufacturing decision making are combined and lead to the formulation of optimization models. We work in collaboration with MSD AH, perform case studies with real world fermentation data and validate our models. The primary focus is on the bleed–feed problem, for which we develop novel analytical models to find optimal bleed–feed policies under different contexts. To the best of our knowledge, we are the first to address the bleed–feed problem and to present a successful industry scale implementation of bleed–feed. We develop generic models that can be extended to other companies, or industries with fermentation processes. The research outcomes have been internationally recognized in several platforms for its scalability and potential impact, including professional societies and the media (INFORMS, 2019; EURO, 2019; IFORS News, 2020; IMPACT, 2020; European Commission, 2020).

1.4. Outline

This thesis focuses on optimizing bleed–feed decisions from different aspects. First, Chapter 2 investigates condition-based bleed–feed policies to maximize the yield obtained from a setup, adapted from Koca et al. (2021b). Then, Chapter 3 generates time-based bleed–feed policies to maximize the expected throughput of a batch, based on Koca et al. (2021a). Next, Chapter 4 extends the renewal model from Chapter 3, and finds the optimal bleed–feed time considering practically relevant constraints. Chapter 5 presents a portfolio of decision support tools to improve biomanufacturing efficiency (Martagan et al., 2021). Finally, Chapter 6 presents the concluding remarks and future research directions.

We note that we rely on the same notation in the renewal models presented in Chapters 3, 4 and 5. However, Chapter 2 has a different theory, and its notation is independent from the other chapters. Chapters 2, 3 and 5 can be read individually. Chapter 4 is an extension of Chapter 3 and the literature review for Chapter 3 is valid also for Chapter 4. Thus, we do no present a separate literature review section in Chapter 4. Hence, we recommend reading Chapter 3 before starting with Chapter 4.

2

Increasing Biomanufacturing Yield with Bleed–Feed: Optimal Policies and Insights

2.1. Introduction

Upstream operations constitute the first step of biomanufacturing processes, and include activities related to fermentation (i.e., preparation of seed culture and media, bioreactor setup, fermentation process, and harvesting). Fermentation is generally conducted in a bioreactor, which is a stainless steel vessel equipped with several sensors. The fermentation process starts with a seed culture (i.e., living organisms such as bacteria or virus) and a special medium. We refer to the seed culture as *initial biomass*. The bioreactor provides a controlled environment in which the initial biomass grows and reproduces during fermentation. This growth pattern is shown in Figure 2.1(a). More specifically, in Figure 2.1(a), industry data is used to plot the biomass production (in grams) over time (hours) during a batch fermentation process. Figure 2.1(a) shows that the fermentation process starts with a small amount of initial biomass. Then, the biomass follows an exponential growth pattern, which is known as *exponential growth phase* of fermentation. In a batch fermentation process, a special medium is added only at the beginning of the process (before fermentation starts). This medium supports the exponential growth

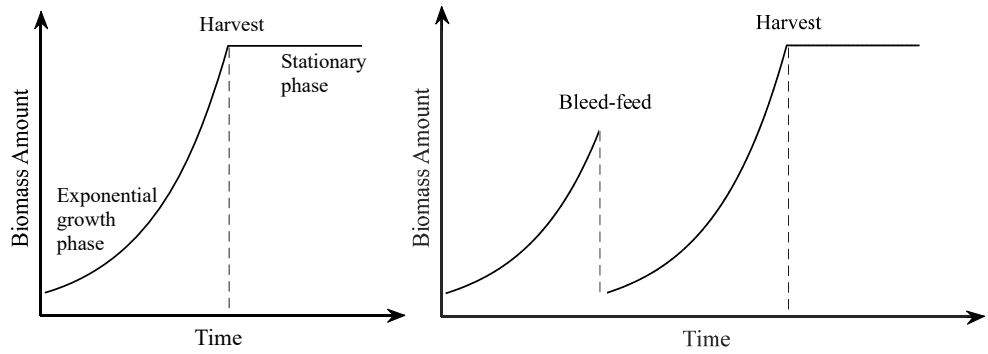

(a) Biomass growth without bleed–feed

(b) Biomass growth with bleed–feed

Figure 2.1: Biomass growth over time in current practice (a) and with bleed–feed (b).

of the biomass. However, the medium depletes as more biomass accumulates inside the batch, and the fermentation process enters the *stationary phase*. In this phase, the cells lose viability, and the bioreactor needs to be harvested. In our specific problem setting, the end-product obtained from fermentation is measured in terms of the total amount of biomass produced from the batch. This is because each of these biological cells (biomass) is essentially an active ingredient for a biopharmaceutical drug. Hence, the subsequent production steps process these active ingredients further into their final forms (e.g., vaccines, pills, etc.).

The bioreactor needs to be set up before a fermentation process is started. The setup activities include preparation of the seed culture and media; cleaning and sterilization of the bioreactor; and setup of other necessary equipment such as sensors. In practice, bioreactor setups require highly-specialized labor and materials, and are well-known to be costly. For example, the consumables and reagents alone (e.g., acid, caustic, water-for-injection, and steam used for cleaning and sterilization in each setup) constitute around 16% of the total fermentation costs (Oyebolu et al., 2019; Mahal et al., 2021). Such high setup costs motivate the industry to obtain as much biomass as possible from each bioreactor setup. The increasing adoption of single-use bioreactor technologies presents another motivation for maximizing the bioreactor yield in the industry (Low, 2020). The problem of increasing the total biomass production per setup (also known as *the problem of increasing upstream titer*) has been a popular research topic in the life sciences. As such, finding new ways of addressing this problem is recognized

as one of the critical requirements for succeeding in future markets (McKinsey & Company, 2014). To address this problem, we consider a novel technique for batch fermentation: "bleed–feed."

Bleed–Feed: Concept and Challenges

Figure 2.1(b) illustrates the basic dynamics of a bleed–feed operation using industry data. In simple terms, bleed–feed prolongs the exponential growth phase (Eppendorf, 2017; Muldowney, 2018; Kakes, 2018). To perform bleed–feed, the bioreactor operator first extracts the biomass that has accumulated inside the bioreactor ("bleed"). This is carried out such that only a small amount of biomass remains inside the bioreactor. Then, fresh medium is added to the bioreactor to help the remaining biomass grow and reproduce ("feed"). The bleed–feed operation is performed almost instantaneously and can be perceived as starting a new cultivation *without* a new setup. For example, Figure 2.1(b) shows that the remaining biomass functions as a seed culture after bleed–feed and continues to grow in the exponential growth phase. This is evidently a breakthrough technology with a high potential for improving biomanufacturing efficiency.

However, the specific timing of bleed–feed plays a critical role for success: bleed–feed needs to be performed during the exponential growth phase. When the cell culture enters the stationary phase, bleed–feed cannot be conducted, and the batch needs to be harvested.[1] The identification of the correct timing is not a trivial decision. The complex and uncertain nature of the biological systems introduce three critical challenges in decision-making:

(i) Uncertain duration of the exponential growth phase. The duration of the exponential growth phase (i.e., the time to enter the stationary phase) of most batch fermentation processes exhibits uncertainty. This is mainly owing to the complex biological nature of living cells. However, the process generally does not incur any risk of entering the stationary phase when the biomass amount is below a certain threshold value called "critical biomass." In addition, industry data shows that the cell growth is more likely to terminate as fermentation gets older.

(ii) Uncertain cell growth rate after bleed–feed. The response of living cells to bleed–feed

[1] We use the term "batch" to represent the production from when a bioreactor is set up until it is harvested, including multiple bleed–feeds.

is uncertain. Although it is established that they continue to grow in the exponential growth phase, their growth rate could be higher or lower compared to that of the original cell culture (the one used before the first bleed–feed).

(iii) Regulatory requirements on the number of bleed–feeds. According to regulatory requirements, only a limited number of bleed–feeds per bioreactor setup may be performed. These regulations are generally pre-specified, and biomanufacturers provide scientific evidence that substantiates the process' safety and reliability within these limits. However, these regulations are often known to be conservative to ensure safety in a wide range of settings. For example, in our specific case study, regulations permit only two bleed–feeds per setup.

From a practical perspective, challenge (i) described above creates a trade-off between performing the bleed–feed technique "too soon" and "too late." When performed too soon, we would not achieve the maximum biomass yield. When performed too late, we will miss the opportunity for performing bleed–feed. This motivates our first research question: *(1) what is an optimal bleed–feed policy that maximizes the total amount of biomass obtained from a bioreactor setup?*

As a consequence of the three challenges described above, there are conflicting opinions on the added value of bleed–feed to current practice, and biomanufacturers need a deeper understanding of their managerial choice before adopting such policies. In addition, the impact of regulations as described in (iii) is not fully understood in our context. Such exogenous policies affect operational decisions, yet their impact on the industry may in turn create the need for alternative regulatory policies. Moreover, challenges (i) and (ii) imply that bleed–feed may not improve the biomanufacturing efficiency if performed suboptimally. These observations motivate our second and third research questions: *(2) how are the potential benefits of bleed–feed affected by regulatory limitations; and (3) what is the added value of implementing bleed–feed to current industry practice?*

To address these research questions, we develop a Markov decision process (MDP) model, and analyze the structural characteristics of the value function and optimal bleed–feed policies. In addition, we present an industry case study to illustrate the use of the developed model and assess the potential room for improvement in practice. We develop answers to our aforementioned research questions, which yield the following insights for biomanufacturers:

1. Optimal bleed–feed policies have a control-limit structure. We show that optimal bleed–feed policies have a control-limit structure (i.e., a three-way control limit on the cultivation age, the cell growth rate, and the number of bleed–feeds performed) wherein it is optimal to perform bleed–feed above this control limit and not to do so below it. Such control-limits are useful to support industry implementation because these are simple to adopt in daily practice.

2. The marginal benefits of bleed–feed diminish as additional bleed–feeds are performed. Our analysis reveals that the marginal benefits of an additional bleed–feed are decreasing and converge to a certain value. More specifically, we show that the marginal benefits are only equal to the critical biomass if the regulators would permit more bleed–feeds.

3. Bleed–feed can provide significant benefits. We present an industry case study to quantify the potential impact of bleed–feed on practice. To generate broader insights, our numerical experiments assess the performance of two practically-relevant heuristics as a benchmark (i.e., a risk-averse heuristic, and the current practice with no bleed–feed). We observe an increase of 137% in batch yield per setup in the industry base case with two bleed–feeds.

In summary, our model formalizes our understanding of the challenges and trade-offs associated with bleed–feed. In addition, our results inform biomanufacturers and policy-makers on the potential impact of the bleed–feed technology on current practice.

The concept of "bleeding" and "feeding" has been used in continuous fermentation systems (Doran, 1995; Pollock et al., 2013; Muldowney, 2018). However, the use of bleed–feed in batch fermentation is novel and involves unique challenges, as described above.[2] To the best of our knowledge, we present the first successful industry-scale implementation in our context. We believe that our model can serve as a building block to support the industry's gradual transition from batch to (semi-)continuous processing in the near future.

This research has been conducted in close collaboration with MSD Animal

[2] In continuous systems, the cell culture is continuously fed and bled so that it maintains a steady-state condition. On the other hand, the problem of optimizing the bleed–feed time, the uncertainty in growth rate after bleed–feed, and the regulatory restrictions on the number of bleed–feeds are the distinguishing characteristics of batch processing applications.

Health, Boxmeer, the Netherlands.[3] MSD's facility in Boxmeer is a leading biomanufacturing hub of Europe. It specializes in both R&D and large-scale biomanufacturing to improve animal health. Hereafter, we use the term "MSD" to represent the Bacteriological Processing Department in Boxmeer. Although our work originates from MSD, this research addresses a common industry problem, and the resulting analytical models and insights can be generalized to other biomanufacturing companies. We also believe that our models can find future applications in other industries. In particular, certain applications in the food industry involve batch fermentation operations (e.g., yogurt, beer, and wine production) and may benefit from the use of the bleed–feed technology.

The remainder of this chapter is organized as follows. We review the relevant literature in Section 2.2. We present the optimization model in Section 2.3, and study the analytical results in Section 2.4. We present a model extension in Section 2.5 where failure risks depend on the bleed–feed count. We present an industry case study from MSD in Section 2.6, and the concluding remarks in Section 2.7.

2.2. Literature Review

Our work is closely related to two main streams of research: Section 2.2.1 elaborates on the relevant work in the life sciences, and Section 2.2.2 reviews relevant studies in Operations Management.

2.2.1 Relevant Literature in Life Sciences

Several studies in the life sciences address the problem of increasing upstream titer (i.e., total biomass obtained per setup). In particular, a large body of work focuses on the modeling and control of biological systems using mass-balance equations or kinetic models (Xing et al., 2010; Chang et al., 2011; Mutturi and Lidén, 2014; Villaverde et al., 2016). In addition, predictive models have been developed to estimate and control the biological dynamics of fermentation processes. These models generally focus on establishing a relationship between

[3]The company's official name is "Merck" in the United States and Canada, and "MSD" elsewhere.

the media composition, physicochemical parameters, and biomass production (Handlogten et al., 2018; Patel et al., 2016; Wang et al., 2019).

Although deterministic models are the most commonly used models in the life sciences, a few studies have also developed stochastic optimization models to increase fermentation titer. In particular, stochastic models are often used to control critical process parameters for supporting cell growth during fermentation. For example, an MDP model was built by Saucedo and Karim (1997) to determine an optimal feed rate that maximizes ethanol production in fed-batch fermentation. Subsequently, Peroni et al. (2005) used approximate dynamic programming to control feed rates and maximize the biomass formation in fed-batch fermentation. Similarly, Li et al. (2011) adopted a Q-learning approach to model fed-batch yeast fermentation and determined an optimal feed rate to increase biomass formation. Cheema et al. (2002) used the genetic algorithm to optimize operating conditions and improve gluconic acid production. Jabarivelisdeh and Waldherr (2018) also used the genetic algorithm and determined dynamic metabolic engineering strategies to maximize ethanol production in batch fermentation. We complement life science research with a rigorous theoretical analysis of optimal policies. While most studies in life science focus on controlling the dynamics of fermentation, we provide a theoretical analysis of optimal policies based on operational trade-offs and biological dynamics under uncertainty.

2.2.2 Relevant Literature in Operations Management

Although several industries have benefited from the use of Operations Management (OM) methodologies, OM applications in the context of biomanufacturing have not been widely studied. We refer to Kaminsky and Wang (2015) for a recent survey of analytical models for biopharmaceutical operations and supply chains.

Many of the existing OM studies focus on strategic or tactical decisions in biopharmaceutical supply chains, such as licensing contracts and R&D alliances (Crama et al., 2008; Xiao and Xu, 2012; Bhattacharya et al., 2015; Allain et al., 2016; Taneri and De Meyer, 2017), supply uncertainty and demand forecasting (Tomlin, 2009; Stonebraker and Keefer, 2009). A few OM studies considered the impact of regulations on licensing and innovation (Hermosilla, 2020; Moreira et al., 2020), and R&D investments (Arora et al., 2009; Rao, 2020) in the pharmaceutical

industry. A limited number of OM studies considered operational decisions in biomanufacturing. For example, Martagan et al. (2019) built an MDP framework to jointly optimize upstream batch sizing and downstream purification decisions. In a similar context, Xie et al. (2020) provided a Bayesian Network to capture the inter-dependence between process parameters and quality attributes. However, none of the aforementioned studies considered the problem of bleed–feed optimization.

Optimal stopping problems determine the optimal time to take an action to terminate a process. Several studies characterize structure of the optimal stopping policies, and develop algorithms to provide numerical solutions (Chow et al., 1964; Cox et al., 1979; Shiryaev, 2007; Dayanik et al., 2008; Oh and Özer, 2016). Applications of optimal stopping include option pricing, organ transplantation decisions and marketing (Ben-Ameur et al., 2002; Wu and Fu, 2003; Ciocan and Mišić, 2020; David and Yechiali, 1985; Terwiesch and Loch, 2004). Note that, the goal of bleed-feed action is not to terminate the process, but to prolong the fermentation by initiating new cultivations.

Machine maintenance is another stream of relevant OM research. This is because the transition of the batch to the stationary phase, and thus failing to implement bleed–feed can be considered as system failure, whereas bleed–feed operation resembles a maintenance activity. The field of machine maintenance has a rich history. Since the bleed–feed number that can be implemented on a batch is limited in our study, we focus on papers that are most directly relevant to our research, i.e., machine maintenance with a limited number of spare parts (replacements). For a comprehensive overview of the state-of-the-art, we refer to the review paper by De Jonge and Scarf (2019) and the book by Van Houtum and Kranenburg (2015). Earlier work on machine maintenance with a finite number of spare parts dates back to Derman et al. (1984). Therein, the authors assumed a continuous distribution for the lifetime of a machine, and determined age-dependent replacement policies. In a more recent study, Icten et al. (2013) extended this framework to build a discrete-time, condition-based MDP model. They optimized the lifetime of a system under a limited number of maintenance actions, and showed that optimal policies have a control-limit structure. However, our problem setting has several key differences. First, the replacement components are identical in Icten et al. (2013), whereas each bleed–feed results in a new value of cell growth rate in our setting. Second, although Icten et al. (2013) do allow for general transition probability matrices

rather than just advancing age by one or "failing," their transition probabilities are arbitrary and not calibrated for a specific application. Most importantly, Icten et al. (2013) assume that the rewards are *nonincreasing* in component condition, whereas ours are *nondecreasing* in cultivation age, which creates unique trade–offs. That is, more deteriorated components are more likely to fail and yield less reward in Icten et al. (2013), whereas in this chapter, the probability of entering the stationary phase increases in cultivation age while the biomass produced in a period increases.

In summary, our work has several contributions to both life sciences and OM. To the best of our knowledge, our work is the first attempt to optimize bleed–feed decisions under uncertainty. We characterize the structural properties of optimal bleed–feed policies; and analyze the behavior of the value function to understand the impact of regulatory restrictions. Our model has been validated with a real-world implementation at MSD and directly improved the business metrics.

2.3. Model Formulation

Our objective is to identify an optimal bleed–feed policy that maximizes the expected total biomass obtained per batch (subject to regulatory requirements). We formulate the bleed–feed problem as a discrete-time Markov decision process (MDP). All modeling assumptions presented in this section have been cross-validated with one year of implementation data. We present the details of the MDP model as follows.

Decision epochs: The fermentation process is monitored at discrete decision epochs $k = 0, 1, 2, \ldots$, corresponding to the time points $t = k\tau$. Here, τ represents a *period* (a constant time interval between two consecutive decision epochs). In practice, the length τ of a period can range from minutes to days depending on the cell characteristics (e.g., type of cells used, cell lifetime, cell growth rates, etc.) and process characteristics (e.g., type of bioreactor, etc.).

States: The state of the batch is denoted by (i, μ, n). The state $i \in \mathcal{I} = \{0, 1, \ldots, I\}$ is the *cultivation age*, and represents the time elapsed (in terms of decision epochs) from the start of the current cultivation. Each time a bleed–feed is performed, a special medium is added, and a new cultivation starts. Therefore, the cultivation age is $i = 0$ at the beginning of a fermentation process, and resets to $i = 0$ when

a bleed–feed is performed. We assume that the maximum achievable cultivation age is I considering the limitations in the cell viability during fermentation and the bioreactor capacity.

The state $\mu \in \mathcal{M} = [\mu_\ell, \mu_u]$ indicates the cell growth rate of a culture (i.e., the rate at which biomass accumulates during fermentation). In alignment with current practice, we assume that the cell growth rate μ is known at the beginning of the initial fermentation. In contrast, the cell growth rate after bleed–feed is uncertain and follows a general distribution $G(\mu)$ with finite support $[\mu_\ell, \mu_u]$. In practice, the bounds $\mu_u \geq \mu_\ell > 0$, as well as the distribution of the growth rate can be determined based on historical data and R&D studies. We let the random variable M denote the uncertain cell growth rate, and μ' its realization after bleed–feed. Post-implementation data indicates that the growth rate after bleed–feed does not depend on bleed–feed related parameters, such as cultivation age, growth rate before bleed–feed, number of bleed–feeds performed, etc. We can provide an intuitive explanation for this behavior from a biological perspective. When a bleed–feed is performed, a fresh medium is added and only a small amount of biomass remains inside the bioreactor as a seed culture. With the extraction of biomass and the addition of fresh medium, the fermentation process naturally "resets" itself without costly setups. Therefore, this uncertainty in growth rate is typically exogenous and mainly associated with the inherent uncertainty of biological dynamics.

The state $n \in \mathcal{N} = \{0, 1, \ldots, N\}$ represents the total number of bleed–feed operations performed since the setting up of the bioreactor (i.e., this state can be considered as a *bleed–feed count*). The term N denotes the regulatory limit with regard to the maximum number of bleed–feeds that can be performed on a batch. The regulatory limit N is generally pre-specified and known. Most often, N is limited to only one or two bleed–feeds per setup to ensure safety and quality. To be eligible for bleed–feed, biomanufacturers provide evidence to regulatory authorities on the process's safety and quality under N bleed–feeds (i.e., no safety and quality issues should arise because of mutation, impurities, contamination, etc.). Therefore, our state space does not include components related to batch safety or quality.

The state Δ denotes the stationary phase of fermentation, where the biomass growth stops and the batch is immediately harvested. The state Δ is an absorbing state with no rewards and represents the end of the decision-making process.

Actions: The action space includes two actions, $\{b, c\} \in \mathcal{A}$. Here, b denotes the bleed–feed, and c represents the continuation of fermentation until the next decision epoch. The only feasible action in states (i, μ, N) is c because no further bleed–feed is permitted.

State Transitions: As the fermentation evolves and the cultivation age i increases, additional biomass accumulates inside the bioreactor (see Figure 2.1). Therefore, we first provide relevant background on the underlying dynamics of fermentation. Let $m_{i\mu}$ denote the total amount of biomass produced by cultivation age $i \in \mathcal{I}$ when the cell growth rate is $\mu \in \mathcal{M}$. Biomass accumulates exponentially during the exponential growth phase. We use the well-known exponential cell growth function applied in chemical engineering to capture the amount of biomass accumulated $m_{i\mu}$ over the cultivation age i during the exponential growth phase (based on the cell growth rate μ):

$$m_{i\mu} = m_0(1 + \mu\tau)^i, \tag{2.1}$$

where m_0 denotes the initial amount of biomass (i.e., seed culture) (Monod, 1949; Doran, 1995). In common practice, the initial amount m_0 is pre-determined. The biomass amount is bounded due to the limitations in the fermentation dynamics and bioreactor capacity.

Let $1 - p_{i\mu}$ denote the probability of transitioning to the stationary phase Δ from state (i, μ, n). We observed from industry data that the transition probabilities $1 - p_{i\mu}$ are independent of the bleed–feed count n but dependent on the cultivation age i and cell growth rate μ. In particular, we observed that $1 - p_{i\mu} \leq 1 - p_{i+1\,\mu}$, i.e., the probability that the cell culture transitions to the stationary phase increases as the cultivation age i increases (under a specified growth rate μ). We can provide an intuitive explanation for these observations, i.e., the limited amount of medium depletes faster when the biomass amount m increases. As the medium inside the bioreactor is depleted, growth inhibition occurs and the cells lose viability. Subsequently, the cell culture becomes more likely to transition to the stationary phase. Moreover, it is intuitive that $1 - p_{i\mu}$ is independent of n, as the fermentation is "reset" at each bleed–feed with the addition of fresh medium and the extraction of biomass. To represent this behavior analytically, we let $\nu(m)$ denote the exponential rate at which the process transitions to the stationary phase when the biomass amount is m. Then, $1 - p_{i\mu} = \nu(m_{i\mu})\tau$. Appendix 2.C describes a procedure for estimating the rate function $\nu(m)$.

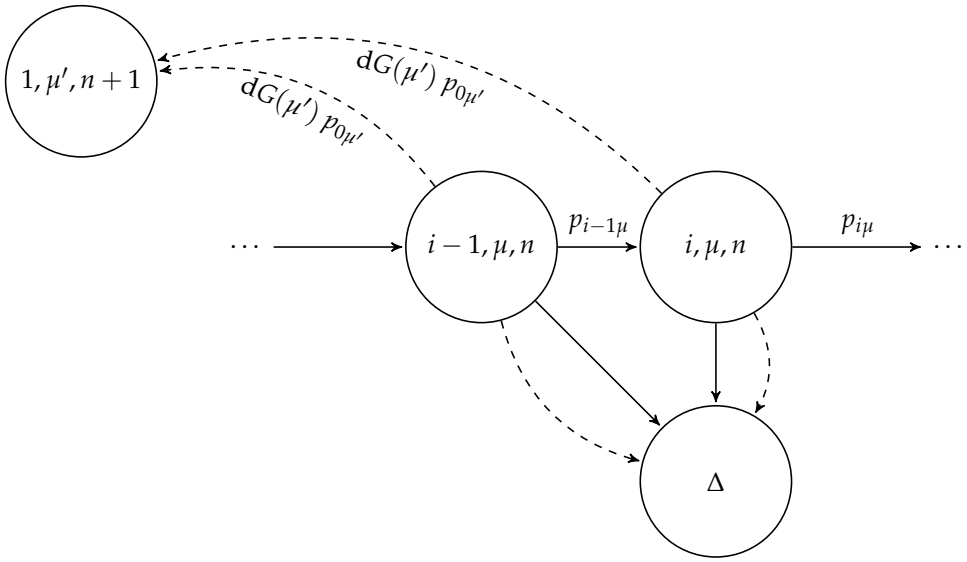

Figure 2.2: State transition diagram (solid arrows for the continue action, dashed arrows for the bleed–feed action).

Next, we elaborate on the state transitions associated with each action. The fermentation process starts in state $(i = 0, \mu, n = 0)$, where $\mu \in \mathcal{M}$ is known for the initial culture. The cell growth rate continues to be μ until a bleed–feed operation is performed. However, under the continue action c at state (i, μ, n), a critical risk for the decision-maker is the probability $1 - p_{i\mu}$ of transitioning to the stationary phase Δ. At the stationary phase Δ, the batch is harvested and the decision-making process terminates. This implies a lost opportunity for bleed–feed when $n < N$.

The solid arrows in Figure 2.2 show the state transitions under the continue action c. At a decision epoch, when we perform action c in state (i, μ, n), the biomass grows based on the dynamics shown in Equation (2.1) during that period. By the end of that period, *(i)* the culture continues to be in the exponential growth phase (with probability $p_{i\mu}$), which implies that the cultivation age increases from i to $i + 1$; or *(ii)* the culture transitions to the stationary phase Δ otherwise. The system immediately transitions to the stationary phase Δ at the maximum cultivation age I.

The dashed arrows in Figure 2.2 illustrate the state transitions under the bleed–feed action b. When we take action b in state (i, μ, n) at a decision epoch, the bleed–feed

operation is performed instantaneously (i.e., we keep the pre-specified amount m_0 inside the bioreactor as seed culture and add a special medium) and the cultivation age is reset to $i = 0$. Then, the cell culture adopts a new growth rate M. The realization of M is μ' with probability $\mathrm{d}G(\mu')$.[4] Hence, when we perform action b in state (i, μ, n) at a decision epoch, the system immediately transitions from state (i, μ, n) to $(0, \mu', n+1)$ with probability $\mathrm{d}G(\mu')$. Then, during period τ, the biomass grows with rate μ', and by the end of that period, *(i)* the culture stays in the exponential growth phase and the cultivation age increases from 0 to 1 (with probability $p_{0\mu'}$); or *(ii)* the culture transitions to the stationary phase Δ otherwise.

The cell culture does not transition to the stationary phase before a certain biomass amount is reached (see Figure 2.5 in Appendix 2.C for a real-world example). We call this biomass amount the *critical biomass*, $\tilde{m}$. Hence, the rate $\nu(m)$ is zero when the actual biomass amount is below this critical biomass $\tilde{m}$. However, $\nu(m)$ is increasing in m when the actual biomass amount exceeds the critical biomass $\tilde{m}$. This behavior implies that the likelihood of entering the stationary phase increases as more biomass accumulates. This trend is intuitive because the limited medium depletes and the cells lose viability faster at higher levels of biomass. In practice, the value of critical biomass $\tilde{m}$ depends on the cell culture and the application context (e.g., medium and bioreactor type). For example, we observed from industry data that the critical biomass could be as small as zero for several cell cultures while others were more robust (e.g., the cell culture considered in our case study has a critical biomass $\tilde{m} = 13$ grams). Lastly, we let $\tilde{\imath}_\mu$ be the cultivation age corresponding to the critical biomass level $\tilde{m}$. Hence, $p_{i\mu} = 1$ for $i < \tilde{\imath}_\mu$, and $p_{i-1\,\mu} > p_{i\mu}$ for $i \geq \tilde{\imath}_\mu$. Clearly, by (2.1), the critical age $\tilde{\imath}_\mu$ is nonincreasing in μ.

Rewards: The immediate reward is defined as $r_{i\mu} = m_{i+1\mu} - m_{i\mu}$ under the continue action c, and $r_{0\mu'} = m_{1\mu'} - m_0$ under the bleed–feed action b. This indicates that our reward function collects the incremental biomass amount produced during a period.[5] In our problem setting, the biomass amount $m_{i\mu}$ determines the rewards. Hence, we use Equation (2.1) to obtain the rewards associated with state (i, μ, n).

[4] When the cells continue growing after bleed–feed, the growth rate can be monitored. Hence, the cell growth rate after the bleed feed is uncertain before the bleed feed, but known after the bleed feed is implemented.

[5] We adopt this reward structure because our objective is to maximize the expected total biomass production. An alternative reward structure is also possible, where the cumulative biomass production is collected only by the end of the cultivation (i.e., rewards are collected either when the batch enters the stationary phase or when a bleed–feed is performed). We note that these two modeling approaches are essentially equivalent. We use the former for ease of exposition.

Next, we elaborate on the sequence of events associated with the reward collection process. Consider the case in which we perform the continue action c in state (i, μ, n). Here, we receive an immediate reward $r_{i\mu} = m_{i+1\mu} - m_{i\mu}$ (i.e., incremental biomass production during that period), and the system transitions either to state $(i+1, \mu, n)$ or the stationary phase Δ by the end of that period. Similarly, if we decide to perform a bleed–feed b in state (i, μ, n), the cultivation age is instantaneously reset to $i = 0$, we collect the reward $r_{0\mu'} = m_{1\mu'} - m_0$ based on the realized growth rate μ' during that period, and the system transitions either to state $(1, \mu', n+1)$ or Δ by the end of that period (see Figure 2.2 for an illustration on the system's dynamics).

Evidently, $p_{i\mu} > p_{i+1\,\mu}$, and $r_{i\mu} < r_{i+1\,\mu}$. That is, both risk of entering the stationary phase $1 - p_{i\mu}$ and immediate reward $r_{i\mu}$ increase in i for a given μ. This results in a challenging trade-off: as the cultivation age i increases, the biomass amount $m_{i\mu}$ also increases (from a practical perspective, this represents an opportunity for collecting higher rewards throughout the exponential cell growth phase). However, the risk of entering the stationary phase also increases as the cultivation age i increases (whereby, the chances of missing the bleed–feed opportunity increase). The decision-maker needs to balance this trade-off to maximize the expected total biomass yield.

Value function: We define $v(i, \mu, n)$ as the expected biomass production to go given that the current state is (i, μ, n). The objective is to identify optimal bleed–feed policies to maximize the value function $v(i, \mu, n)$. Let $C(i, \mu, n)$ and $B(n)$ be the expected biomass production under the actions continue c and bleed–feed b in state (i, μ, n), respectively. Then, the value function $v(i, \mu, n)$ satisfies the following optimality equations:

$$v(i,\mu,n) = \max \begin{cases} C(i,\mu,n) & \equiv r_{i\mu} + p_{i\mu} v(i+1,\mu,n), \\ B(n) & \equiv \mathbb{E}\big[C(0,M,n+1)\big] \end{cases} \tag{2.2}$$

valid for all $i < I$, $\mu \in \mathcal{M}$ and $n < N$, and

$$v(i,\mu,N) = C(i,\mu,N) \tag{2.3}$$

for all $i < I$ and $\mu \in \mathcal{M}$. Note that $v(I,\mu,n) = 0$ for all μ and n, and $v(\Delta) = 0$. For convenience, we set $B(N) = 0$, so (2.2) is also valid for $n = N$.

Observe from Equations (2.2) and (2.3) that our aim is to maximize the expected total biomass obtained from a batch, $v(0, \mu, 0)$, where μ is the cell growth rate at the beginning of fermentation. This objective function aligns with both existing studies in the life sciences and current industry practice that aim to obtain as much biomass as possible before harvest. This is because the activities associated with cleaning, sterilization and setup are cost-intensive (Mahal et al., 2021). In addition, discussions with MSD revealed that the costs associated with bleed–feed are rather small compared to the setup and harvest costs and therefore, negligible in practice. Nevertheless, in Appendix 2.B, we present an alternative model formulation with the objective of maximizing the total expected reward (profit) obtained from a batch, and extend our structural results. Our analysis in Appendix 2.B shows that the structural characteristics of optimal bleed–feed policies are robust to this alternative formulation.

2.4. Structural Analysis

In this section, we investigate the structural characteristics of the value function and optimal bleed–feed policies. These results provide a deeper understanding of the problem and insights on how optimal bleed–feed decisions should be made. In particular, we present sufficient conditions under which optimal bleed–feed policies have a control-limit structure in the cultivation age i (Section 2.4.1), cell growth rate μ (Section 2.4.2), and bleed–feed count n (Section 2.4.3). We also provide further insights on the value function (Section 2.4.4). All proofs are presented in Appendix 2.A.

2.4.1 Structural Analysis in the Cultivation Age

We first characterize the structural properties of the value function and optimal bleed–feed policies based on the cultivation age i. We start with Remark 2.1 and analyze the value function in Proposition 2.1.

Remark 2.1 The batch has no risk of entering the stationary phase before the critical age $\tilde{\imath}_\mu$. Hence, for $i < \tilde{\imath}_\mu$, it is optimal to continue fermentation and the value function is nonincreasing in i, i.e., $v(i+1, \mu, n) \leq v(i, \mu, n)$. However, for the value

function to be nonincreasing also for $i \geq \tilde{\imath}_\mu$, we need to impose a condition.

Proposition 2.1 *The value function $v(i, \mu, n)$ is nonincreasing in i for fixed $\mu \in \mathcal{M}, n \in \mathcal{N}$, provided the following condition holds:*

$$\frac{r_{i\mu} - r_{i-1\mu}}{r_{i\mu}} \leq p_{i-1\mu} - p_{i\mu}, \qquad \textit{for all } \tilde{\imath}_\mu \leq i < I, \mu \in \mathcal{M}. \tag{2.4}$$

Proposition 2.1 provides a sufficient condition for the value function $v(i, \mu, n)$ to be nonincreasing in i, i.e., the total biomass obtained from a batch does not increase as the cultivation age i increases. From a practical perspective, the left-hand side of (2.4) captures the (relative) increase in the immediate reward $r_{i\mu}$, and the right-hand side captures the decrease in the probability of successful batch growth $p_{i\mu}$, as the cultivation age transitions from $i-1$ to i. Thus, Condition (2.4) presents a constraint on how the immediate reward and the probability of biomass growth should change by a one-step increment in i, for $\tilde{\imath}_\mu \leq i < I$. The value function is nonincreasing in i if the increase in the reward is less than the decrease in the probability.

Based on our industry case study (Section 2.6), we conclude that Condition (2.4) is mild and realistic for most practical settings. In particular, we observe that the cell growth rates are generally small fractions (e.g., $\mu = 0.06$ in our case study), whereby the difference between the rewards obtained from two consecutive cultivation ages is relatively small compared to the increased risk of failure. Furthermore, we observe that the left-hand side of (2.4) is a constant rate and that the condition can be simplified further to $\frac{\mu\tau}{1+\mu\tau} \leq \min_i\{p_{i-1\mu} - p_{i\mu}\}$.

In Proposition 2.2, we analyze the difference $C(i, \mu, n) - B(n)$ in the value function under actions c and b. This establishes a preliminary result for analyzing the structural characteristics of optimal bleed–feed policies.

Proposition 2.2 *If Condition* (2.4) *holds, $C(i, \mu, n) - B(n) \leq C(i-1, \mu, n) - B(n)$ for all $\tilde{\imath}_\mu \leq i < I$, $\mu \in \mathcal{M}, n \in \mathcal{N}$.*

Proposition 2.2 states that $C(i, \mu, n) - B(n)$ is nonincreasing in i, i.e., the difference in the value function under actions c and b does not increase as the cultivation age i increases. This implies that when the difference drops below zero for a certain

cultivation age i and fixed μ and n, bleed–feed will be optimal for all cultivation ages greater or equal to i. This is summarized in Theorem 2.1.

Theorem 2.1 *If Condition* (2.4) *holds, for fixed $\mu \in \mathcal{M}$ and $n \in \mathcal{N}$, there exists a threshold $i^*(\mu, n)$, such that, for $i > i^*(\mu, n)$ it is optimal to bleed–feed in state (i, μ, n), and for $i \leq i^*(\mu, n)$ it is optimal to continue fermentation, where $i^*(\mu, n)$ is a cultivation-age-based control limit.*

Theorem 2.1 establishes the existence of an optimal control-limit policy in cultivation age i. That is, for a given cell growth rate μ and bleed–feed count n, it is optimal to bleed–feed if the cultivation age i exceeds a certain threshold value $i^*(\mu, n)$, and to continue otherwise. An intuitive explanation of this result is that the decision-maker becomes more willing to bleed–feed when the cultivation age i increases (i.e., as i increases, the risk of transitioning to the stationary phase increases and results in higher chances of missing the bleed–feed opportunity). From a practical perspective, Theorem 2.1 provides a simple and practical guideline to support bleed–feed decisions based on the cultivation age i. For example, at MSD, such cultivation-age-based optimal control-limits can be easily incorporated into production plans to support daily practice.

2.4.2 Structural Analysis in the Cell Growth Rate

Next, we analyze the structural characteristics of the value function in cell growth rate μ. We first present two monotonicty properties in Propositions 2.3 and 2.4, and establish our main result in Theorem 2.2. To establish these properties we impose the (mild) assumption that when the last cultivation age $I-1$ is reached, the optimal action is to bleed–feed. The assumption is valid throughout this section.

Assumption 2.1 *In all states $(I-1, \mu, n)$ with $\mu \in \mathcal{M}, n < N$, bleed–feed action b is optimal.*

Proposition 2.3 *For fixed $\mu \in \mathcal{M}$, $n < \mathcal{N}$, $v(i, \mu^+, n) \leq v(i, \mu, n)$ for all $i \geq \tilde{\imath}_{\mu^+}$ and $\mu^+ \geq \mu$, provided the following condition holds:*

$$\frac{r_{i-1\mu^+} - r_{i-1\mu}}{r_{i\mu^+}} \leq p_{i-1\mu} - p_{i-1\mu^+}, \qquad \text{for all } \tilde{\imath}_{\mu^+} \leq i < I, \mu \leq \mu^+ \in \mathcal{M}. \tag{2.5}$$

Proposition 2.3 provides a sufficient condition under which the value function $v(i, \mu, n)$ is nonincreasing in μ, i.e., the total biomass obtained from a batch does not increase as the cell growth rate μ increases. The left-hand side of (2.5) captures the (relative) increase in the immediate reward, and the right-hand side captures the decrease in the probability of successful growth when the cell growth rate increases from μ to μ^+. Hence, the condition ensures that the increase in immediate reward is lower than the decrease in the probability of successful growth when the growth rate increases. Condition (2.5) is mild and holds for the industry case study presented in Section 2.6.

In Proposition 2.4, we analyze the difference $C(i, \mu, n) - B(n)$. This is a preliminary result for analyzing the structure of optimal bleed–feed policies in μ.

Proposition 2.4 *If Condition* (2.5) *holds,* $C(i, \mu^+, n) - B(n) \leq C(i, \mu, n) - B(n)$ *for* $\tilde{\imath}_{\mu^+} \leq i < I - 1, \mu \leq \mu^+ \in \mathcal{M}, n < N$.

Proposition 2.4 shows that $C(i, \mu, n) - B(n)$ is nonincreasing in μ, i.e., the difference in the value function under actions c and b does not increase as the cell growth rate μ increases. This implies that if it is optimal to bleed–feed in state (i, μ, n), then it is also optimal to bleed–feed in state (i, μ^+, n) with $\mu^+ \geq \mu$.

Theorem 2.2 *If Condition* (2.5) *holds, for fixed* $i < I$ *and* $n \in \mathcal{N}$*, there exists a threshold* $\mu^*(i, n)$*, such that, for* $\mu > \mu^*(i, n)$ *it is optimal to bleed–feed, and for* $\mu \leq \mu^*(i, n)$ *it is optimal to continue fermentation, where* $\mu^*(i, n)$ *is a cell growth rate-based control limit.*

For a given cultivation age i and bleed–feed count n, Theorem 2.2 shows that it is optimal to bleed–feed if the cell growth rate μ exceeds a certain threshold value $\mu^*(i, n)$, and continue otherwise. This result also implies that the decision-maker becomes more willing to bleed–feed when the cell growth rate μ is higher (i.e., as μ increases, the risk of entering the stationary phase and hence the chances of missing the bleed–feed opportunity increase). From a practical perspective, Theorem 2.2 provides a simple guideline to support bleed–feed decisions based on the cell growth rate μ.

Remark 2.2 If the growth rate M is not random, but constant, $M = \mu$ say, then Assumption 2.1 immediately follows from Condition 2.4, since, by Proposition 2.2, we have $B(n) = C(0, \mu, n + 1) \geq C(I - 1, \mu, n + 1) = r_{I-1,\mu} = C(I - 1, \mu, n)$.

2.4.3 Structural Analysis in the Number of Bleed–feeds

In this section, we establish the structural characteristics in the number of bleed–feeds performed, n. Moreover, we analyze the behavior of the value function as a function of the regulatory limit N. We start our analysis with two monotonicity properties in Propositions 2.5 and 2.6.

Proposition 2.5 *The value function $v(i, \mu, n)$ is nonincreasing in n for fixed $i \in \mathcal{I}, \mu \in \mathcal{M}$.*

In Proposition 2.5, we show that the value function $v(i, \mu, n)$ is nonincreasing in n, i.e., the total biomass to be obtained from a batch does not increase as we perform more bleed–feeds (and approach the limit N). This result, together with Proposition 2.6, is used to establish the structural characteristics of optimal policies.

Proposition 2.6 *$C(i, \mu, n) - B(n) \leq C(i, \mu, n+1) - B(n+1)$ for all $i < I, \mu \in \mathcal{M}, n < N$.*

Proposition 2.6 states that $C(i, \mu, n) - B(n)$ is nondecreasing in n, i.e., the difference in the value function under actions c and b does not decrease as the number of bleed–feeds increases. This implies that for fixed i and μ, if it is optimal to continue at n, then it is also optimal to continue at $n+1$.

Theorem 2.3 *For fixed $i < I$ and $\mu \in \mathcal{M}$, there exists a threshold $n^*(i, \mu)$ such that for $n \leq n^*(i, \mu)$ it is optimal to bleed–feed, and for $n > n^*(i, n)$ it is optimal to continue fermentation, where $n^*(i, n)$ is the control limit in bleed–feed counter.*

Theorem 2.3 shows that optimal bleed–feed polices have a control-limit structure in the bleed–feed counter n. That is, for a given cultivation age i and cell growth rate μ, it is optimal to bleed–feed when the bleed–feed count is below a certain threshold value $n^*(i, \mu)$, and to continue otherwise. From a practical perspective, this result implies that the decision-maker is more willing to bleed–feed when only a few bleed–feeds have been performed. That is, one would take less risks of transitioning to the stationary phase at lower levels of n, because the opportunity for producing higher amounts of biomass through bleed–feed is lost when the process transitions to the stationary phase. On the other hand, Theorem 2.3 shows that, when the

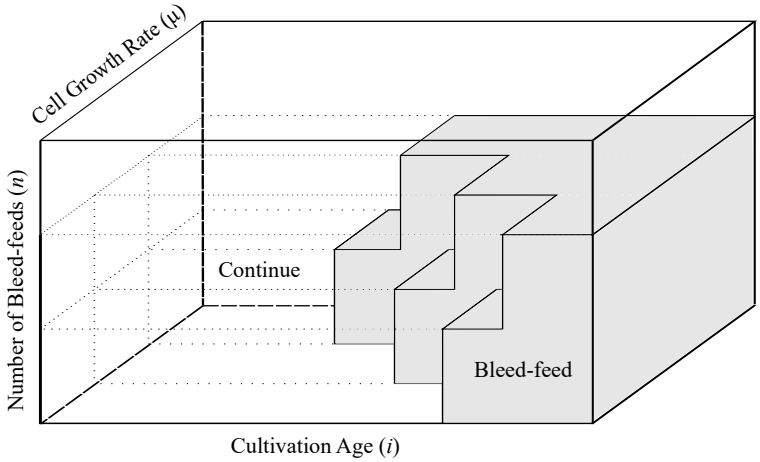

Figure 2.3: An illustration of the three-way control limit policy.

bleed–feed count approaches its maximum N, the decision-maker is willing to take higher risks of hitting the stationary phase and tends to continue the fermentation.

We can now conclude that the structure of the optimal policy is a three-way control limit. This is summarized in Corollary 2.1 and illustrated in Figure 2.3.

Corollary 2.1 *If Conditions* (2.4) *and* (2.5) *hold, there exists a three-way control limit policy, i.e.,*

- *for fixed $\mu \in \mathcal{M}, n \in \mathcal{N}$, there is a threshold $i^*(\mu, n)$ above which it optimal to bleed–feed,*
- *for fixed $i < I, n \in \mathcal{N}$, there is a threshold $\mu^*(i, n)$ above which it is optimal to bleed–feed,*
- *for fixed $i < I, \mu \in \mathcal{M}$, there is a threshold $n^*(i, \mu)$ above which it is optimal to continue.*

An immediate implication of the three-way control limit is that the thresholds are monotone in the parameters. This can be seen in Figure 2.3. Monotonicity of $i^*(\mu, n)$ is formalized in Corollary 2.2. The other two thresholds have similar properties.

Corollary 2.2 *If Conditions* (2.4) *and* (2.5) *hold, then:*

- *for fixed $\mu \in \mathcal{M}$, the threshold $i^*(\mu, n)$ is non-decreasing in n, i.e.,*

$$i^*(\mu, n+1) \geq i^*(\mu, n), \qquad n < N,$$

- *for fixed $n \in \mathcal{N}$, the threshold $i^*(\mu, n)$ is non-increasing in μ, i.e.,*

$$i^*(\mu^+, n) \leq i^*(\mu, n), \qquad \mu^+ \geq \mu \in \mathcal{M}.$$

Next, we focus on understanding the impact of regulations on bleed–feed operations. In industry, stringent regulations on the maximum bleed–feed count N can be perceived as a barrier towards bleed–feed implementation. Practitioners are concerned that regulatory requirements on bleed–feed count N may restrict the potential benefits of bleed–feed. To examine this issue, we analyze the behavior of the value function $\mathbb{E}[v(0, M, 0)]$ as a function of the maximum bleed–feed count N, where $\mathbb{E}[v(0, M, 0)]$ can be interpreted as the maximum expected total biomass produced by an arbitrary batch.

Theorem 2.4 *The expected total biomass $\mathbb{E}[v(0, M, 0)]$ obtained from an arbitrary batch increases in the maximum bleed–feed count N, where the marginal increments are decreasing and converge to the critical biomass $\tilde{m}$.*

Remark 2.3 More precisely, we prove that, if $\tilde{m} > 0$, then for sufficiently large N, the marginal increments are equal to

$$\mathbb{E}[\sum_{i<\bar{\imath}_M} \prod_{j=0}^{i-1} p_{jM} \cdot r_{iM}].$$

This quantity is close, but not identical to the critical biomass $\tilde{m}$, due to discretization of time. Further, if $\tilde{m} = 0$, then the marginal increments converge to 0 geometrically fast.

Theorem 2.4 shows that the expected total biomass obtained from an arbitrary batch exhibits diminishing returns in N, and converges to the critical biomass $\tilde{m}$ for sufficiently large N. This result provides a deeper understanding of the impact of regulations on bleed–feed operations. In practice, the relationship between biomanufacturers and regulators is bi-directional: regulatory constraints impact operational decisions in practice and industry implementation may also

shape regulatory policies. By characterizing the behavior of the value function as a function of the regulatory limit N, our analysis provides insights for both manufacturers and regulators.[6]

2.4.4 Further Insights

To generate further analytical insights, we analyze a risk-averse heuristic as a practically-relevant benchmark and provide a sensitivity analysis on risks $1 - p_{i\mu}$.

Risk-averse heuristic: a benchmark. As a practically-relevant benchmark, we consider a risk-averse heuristic and evaluate its performance. Recall that the bleed–feed opportunity is lost when fermentation enters the stationary phase. Because of the high risks involved in fermentation processes, practitioners may decide to adopt a risk-averse heuristic to implement bleed–feed with zero risk. Based on industry data, we know that the fermentation has no risk of entering the stationary phase before the critical age $\tilde{\imath}_\mu$. In addition, we know from Remark 2.1 that implementing bleed–feed before the critical age is suboptimal. Therefore, we consider a risk-averse heuristic which implements bleed–feed at the critical age $\tilde{\imath}_\mu$ with zero risk of failure. Theorem 2.5 presents a sufficient condition under which this risk-averse heuristic is optimal.

Theorem 2.5 *It is optimal to bleed–feed in state (i, μ, n) for $\tilde{\imath}_\mu \leq i \leq I-1, \mu \in \mathcal{M}, n < N$, if the following condition holds:*

$$\frac{r_{i\mu}}{r_{0\mu} + r_{1\mu} + ... + r_{\tilde{\imath}_\mu \mu} + \mathbb{E}[p_{\tilde{\imath}_M M} r_{I-1M}]} \leq 1 - p_{i\mu}, \qquad \text{for } \tilde{\imath}_\mu \leq i < I, \mu \in \mathcal{M}. \quad (2.6)$$

When Condition (2.6) holds, Theorem 2.5 indicates that the risk-averse heuristic is optimal. In other words, the critical age $\tilde{\imath}_\mu$ corresponds to the optimal cultivation-age-based control limit i^* presented in Theorem 2.1. To elaborate on the practical relevance of Theorem 2.5, we note that the term $r_{0\mu} + r_{1\mu} + ... + r_{\tilde{\imath}_\mu \mu}$ in Condition (2.6) is close to the critical biomass amount $\tilde{m}$. Hence, (2.6) indicates that if the reward at age $\tilde{\imath}_\mu$ divided by the critical biomass amount is less than the

[6] We note that Theorem 2.4 considers a hypothetical case in which the regulatory limit N is large. In practice, the regulations permit only a few (e.g., one or two) bleed–feeds. If the regulations would permit more bleed–feeds, we expect that the critical biomass $\tilde{m}$ would approach zero; and hence the marginal benefits would converge to zero in practice.

failure probability at age $\tilde{\imath}_\mu$, then it is optimal to bleed–feed at the critical age. On the other hand, we observe from (2.6) that if the critical biomass amount is small or the probability of batch failure at age $\tilde{\imath}_\mu$ is low, then Condition (2.6) may not hold and thus, implementing bleed–feed at the critical age may not be optimal. Hence, our analysis indicates that the risk-averse heuristic may not perform optimally for a wide range of practically-relevant scenarios. Yet, it can serve as a naïve heuristic for practitioners who aim to avoid failure risks. In Section 2.6, we provide a numerical analysis to assess the performance of this risk-averse heuristic compared to optimal policies.

Sensitivity analysis on risks. Recall that $1 - p_{i\mu}$ denotes the probability of entering the stationary phase at state (i, μ, n). Consider two batches with transition probabilities $p^1_{i\mu}$ and $p^2_{i\mu}$, respectively. We assume that these two batches are identical, except that the second batch has a higher risk of entering the stationary phase, i.e., $1 - p^1_{i\mu} \leq 1 - p^2_{i\mu}$ for all $i \in \mathcal{I}, \mu \in \mathcal{M}$. This means that the rate function of the second batch stochastically dominates the first one. Let $v^1(i, \mu, n)$ and $v^2(i, \mu, n)$ denote the value function of the first and second batch, respectively. We first present an upper bound on the value function in Lemma 2.1, and then compare these two batches in terms of their expected total biomass production in Proposition 2.7.

Lemma 2.1 *If Condition* (2.4) *holds, then*

$$\frac{r_{i\mu} + r_{i+1\mu} + ... + r_{\tilde{\imath}_\mu \mu}}{1 - p_{\tilde{\imath}_\mu \mu}} \geq v(i+1, \mu, n) \qquad \text{for } 0 \leq i < \tilde{\imath}_\mu, \mu \in \mathcal{M}, n \in \mathcal{N} \tag{2.7}$$

$$\frac{r_{i\mu}}{1 - p_{i\mu}} \geq v(i+1, \mu, n) \qquad \text{for } \tilde{\imath}_\mu \leq i \leq I-1, \mu \in \mathcal{M}, n \in \mathcal{N}. \tag{2.8}$$

Proposition 2.7 *Consider two identical batches, except that* $1 - p^1_{i\mu} \leq 1 - p^2_{i\mu}$ *for* $i \in \mathcal{I}, \mu \in \mathcal{M}$*, and assume Condition* (2.4) *holds, so the optimal policy for both batches has a control-limit in i. Then,*

(i) $v^1(i, \mu, n) \geq v^2(i, \mu, n)$ *for all* $i \in \mathcal{I}, \mu \in \mathcal{M}, n \in \mathcal{N}$*,*

(ii) if it is optimal to bleed–feed the first batch at state (i, μ, n)*, it is also optimal to bleed–feed the second batch at the same state, provided the following condition holds*

$$r_{I-1\mu}(p^1_{i\mu} - p^2_{i\mu}) \geq \mathbb{E}\big[p^1_{0M} \frac{r_{0M}}{1 - p^1_{0M}} - p^2_{0M} r_{I-1M}\big], \qquad \text{for } \tilde{\imath}_\mu \leq i < I. \tag{2.9}$$

Proposition 2.7 *(i)* shows that a batch with a lower risk produces higher total biomass, and *(ii)* presents a sufficient condition under which bleed–feed is implemented earlier to a batch with higher risk[7]. Condition (2.9) sets a lower bound on the difference between the successful growth probabilities, $p^1_{i\mu} - p^2_{i\mu}$. When this difference is sufficiently large, bleed–feed is performed earlier for the high-risk batch. For small values of $p^1_{0\mu}$ and $p^2_{0\mu}$, the right-hand side of (2.9) becomes negative, and the condition holds as the left-hand side is positive. However, Condition (2.9) becomes more restrictive for large values of $p^1_{0\mu}$. In such cases, the term $p^2_{0\mu} r_{I-1\mu}$ should be high or $r_{0\mu}$ should be small for the condition to hold. In our industry case study, we observed that $r_{0\mu}$ is relatively small, so that (2.9) holds for several practically-relevant scenarios.

2.5. Model Extension

The base model in Section 2.3 assumes that the probability of entering the stationary phase is independent of the bleed–feed count n.[8] However, this assumption might not necessarily hold for all fermentation processes (including cross-industry applications). To ensure generalizability and wider impact, we now relax this assumption and assume that the probability of entering the stationary phase $1 - p_{i\mu n}$ depends on the bleed–feed count n. In particular, we focus on the case when the fermentation encounters higher risks of entering the stationary phase as the bleed–feed count n increases, i.e., $1 - p_{i\mu n} \leq 1 - p_{i\mu n+1}$ for a given cultivation age i. In this extension, we shall assume that the cell growth behavior in Equation (2.1) and the reward structure are identical to the base model in Section 2.3. Hence, the value function $v(i, \mu, n)$ of the extended model satisfies the following optimality equations:

$$v(i,\mu,n) = \max \begin{cases} C(i,\mu,n) & \equiv r_{i\mu} + p_{i\mu n} v(i+1,\mu,n), \\ B(n) & \equiv \mathbb{E}\big[C(0,M,n+1)\big] \end{cases} \tag{2.10}$$

[7] When $p^1_{0\mu} = 1$, by using (2.7) of Lemma 2.1, we can replace the term $\mathbb{E}\big[p^1_{0M} \frac{r_{0M}}{1-p^1_{0M}}\big]$ in Condition (2.9) by $\mathbb{E}\big[p^1_{0M} \frac{r_{0M}+r_{1M}+\ldots+r_{i_M M}}{1-p^1_{i_M M}}\big]$.

[8] We validated this assumption with one-year of bleed–feed implementation data. However, our data involved only one bleed–feed per batch, $N = 1$.

valid for all $i < I$, $\mu \in \mathcal{M}$ and $n < N$, and

$$v(i, \mu, N) = C(i, \mu, N)$$

for all $i < I$ and $\mu \in \mathcal{M}$. Note that $v(I, \mu, n) = 0$ for all μ and n, and $v(\Delta) = 0$. Observe from (2.10) that the probabilities $p_{i\mu n}$ depend on the bleed–feed count n. We now revisit the structural results obtained from Section 2.4 to characterize the optimal bleed–feed policies for the extended model.

We first focus on the structural properties in the cultivation age i and the cell growth rate μ. In the extended model, structural properties described in Proposition 2.1, Proposition 2.2 and Theorem 2.1 continue to hold when the sufficient condition (2.4) is revised as $\frac{r_{i\mu} - r_{i-1\mu}}{r_{i\mu}} \leq p_{i-1\mu n} - p_{i\mu n}$. This implies that the extended model continues to have an optimal threshold-type policy in cultivation age i (for a given μ and n). Furthermore, Proposition 2.3, Proposition 2.4 and Theorem 2.2 also continue to hold for the extended model when the sufficient condition (2.5) is revised as $\frac{r_{i-1\mu^+} - r_{i-1\mu}}{r_{i\mu^+}} \leq p_{i-1\mu n} - p_{i-1\mu^+ n}$. Therefore, the extended model has an optimal threshold-type policy in μ (for a given i and n).

We now focus on the structural characteristics in the number of bleed–feeds n. It is easy to see that Proposition 2.5 and Theorem 2.4 continue to hold. However, Proposition 2.6 does not hold in the extended model. As a counterpart, Proposition 2.8 provides a sufficient condition under which $C(i, \mu, n) - B(n)$ is nonincreasing in n.

Proposition 2.8 *$C(i, \mu, n) - B(n) \geq C(i, \mu, n+1) - B(n+1)$ for all $i < I, \mu \in \mathcal{M}, n < N$ provided the following condition holds:*

$$r_{I-1\mu}(p_{i\mu n} - p_{i\mu n+1}) \geq \mathbb{E}\left[p_{0Mn+1} \frac{r_{0M}}{1 - p_{0Mn+1}} - p_{0Mn+2} r_{I-1M}\right] \quad \text{for } i < I, \mu \in \mathcal{M}, n < N. \tag{2.11}$$

Proposition 2.8 presents a sufficient condition under which the difference in value function under the actions continue c and bleed–feed b does not increase in the bleed–feed count n. This implies that the extended model continues to have an optimal threshold-type policy in n (for fixed i and μ), such that, it is optimal to continue below this threshold, and bleed–feed otherwise. Hence, the three-way control limit structure described in Corollary 2.1 continues to hold in the extended

model, except that it is now optimal to bleed–feed (instead of continue) above threshold n^*. This difference is attributed to the increasing failure risk under the extended model. Because the failure probabilities increase in the bleed–feed count n in the extended model, optimal policies tend to bleed–feed earlier than in the base model.

2.6. Numerical Analysis: An Industry Case Study

We present a numerical case study motivated by MSD Animal Health, Boxmeer, the Netherlands. We use the case study to demonstrate the potential impact of the bleed–feed optimization model in practice, and to provide a deeper understanding of the problem instances that have high potential for improvement. We first introduce the problem setting (Section 2.6.1), and present sensitivity analysis on the impact of the system's risk of transitioning to the stationary phase (Section 2.6.2), critical biomass level (Section 2.6.3), and the number of bleed–feeds permitted on a batch by the regulations (Section 2.6.4).

2.6.1 Problem Setting

This case study is generated based on three-years of fermentation data for a specific biopharmaceutical drug used in animal health (i.e., two years pre-implementation and one year post-implementation). The fermentation data obtained from MSD included an extensive set of measurements, including the initial biomass amounts, cell growth rates, time-to-enter the stationary phase, final biomass amounts, harvest times, and physico-chemical parameters. To protect confidentiality, we have disguised MSD's original data and used representative values in this case study.

We establish the main parameters used in the case study as follows. The fermentation starts with an initial biomass amount $m_0 = 1$ gram. The critical biomass amount is $\tilde{m} = 13$ grams, and the critical age is $\tilde{\imath} = 45$ hours. The maximum biomass amount that can be produced from a cell culture is 24 grams. In the first fermentation run (i.e., before the first bleed–feed), the cell growth rate is 0.06 cell divisions per hour. In the second fermentation (i.e., after the bleed–feed), our industry data shows that the cell growth rate follows a (discrete) uniform distribution in the interval $[0.045, 0.075]$ (see Figure 2.5(b) in Appendix 2.C). Hence,

the mean cell growth rate after a bleed–feed is $\mathbb{E}[M] = 0.06$ cell divisions per hour, and the coefficient of variation is $CV(M) = 0.14$. The maximum fermentation time is 72 hours because of the limitations in cell viability.

The rates of transitioning to the stationary phase $\nu(m)$ (for all possible values of biomass amount m) and the corresponding probabilities of successful batch growth $p_{i\mu}$ are estimated from industry data. Recall that transition rates $\nu(m)$ are calculated based on the biomass amount (as described in Section 2.3), and that the transition probabilities of the MDP model are determined from the transition rates by using the relationship $1 - p_{i\mu} = \nu(m_{i\mu})\tau$. We refer to Appendix 2.C for a detailed discussion on a procedure to estimate the transition rates. Appendix 2.C also presents the specific transition rates used in our case study.[9] In addition, we note that the industry data satisfied the monotonicity conditions described in Section 2.4.

In our case study, regulatory requirements limit the number of bleed–feeds to a maximum of two bleed–feeds per setup, i.e., $N = 2$. Note that $N = 2$ implies three cultivations per setup (i.e., no bleed–feed can be performed after the second one). The time between two decision epochs is set as $\tau = 1$ hour based on the feedback received from MSD. Nevertheless, we conducted a sensitivity analysis on smaller values of τ (i.e., $\tau \in \{0.25, 0.5\}$) and observed that the optimal policies and managerial insights were robust to finer levels of discretization. Hereafter, we refer to this setting as *base case.* We solved for the optimal policy using backward induction.

Analysis Overview. The main objective of this case study is to provide a deeper understanding of the potential impact of bleed–feed on current practice. For this purpose, we focus on (1) helping the biomanufacturing industry understand how implementing bleed–feed makes a difference on their operations and (2) quantifying the potential gains (in terms of the expected biomass production per setup) from the application of bleed–feed. We consider three practically-relevant strategies:

- Current practice (CP) harvests the batch as soon as it enters the stationary phase and does not use bleed–feed (this can also be interpreted as $N = 0$ for the model in Section 2.3). The strategy CP is our main benchmark because it

[9]Our numerical experiments used a step function which was empirically generated from industry data (see Figure 2.5(a) of Appendix 2.C). We note that it is possible to fit an exponential curve for the rate function, as shown in Figure 2.5. Additional numerical experiments confirm that our results are robust when this exponential function is used to approximate the empirical distribution.

represents the current practice.

- Risk-averse heuristic (RA) implements bleed–feed at the critical age $\tilde{\imath}$. This strategy represents a conservative approach that implements bleed–feed at no risk (see Section 2.4.4).
- Bleed–feed optimization (BO) maximizes the expected total biomass per setup and finds the optimal bleed–feed policies.

We identified a wide range of practically-relevant instances for our numerical analysis based on the input received from our industry partners. In particular, we understand that bio-processes can vary widely in terms of their their risk of entering the stationary phase and the critical biomass level. Therefore, we focus on sensitivity analysis on the risk of entering the stationary phase (Section 2.6.2), the critical biomass (Section 2.6.3) and the regulatory limit on the bleed–feed number allowed per batch (Section 2.6.4) to generate managerial insights for a wider audience (other companies or end-products in the industry). A key performance metric used in this section is the percentage improvement ($\%I_{RA}$ and $\%I_{BO}$) that could have been achieved by adopting risk-averse heuristic (RA) and bleed–feed optimization (BO) rather than current practice (CP).

2.6.2 Insights on the Risk of Entering the Stationary Phase

Although certain cell cultures are more reliable and stable (e.g., bacteria cells), others exhibit high risks of entering the stationary phase (e.g., viruses). To understand the impact of the transition probabilities on the room for improvement over CP, we performed sensitivity analysis on the rate of entering the stationary phase $\nu(m)$. Recall that Figure 2.5(a) in Appendix 2.C provides the rate function $\nu(m)$ of the base case. In this section, we multiply the base case's rate function $\nu(m)$ by a factor f to represent the following scenarios: *(i)* base case ($f = 1$), *(ii)* higher risk of transitioning to the stationary phase ($f = 1.1, 1.25, 1.5$), and *(iii)* lower risk of transitioning to the stationary phase ($f = \{0.9, 0.75, 0.5, 0.25, 0.1\}$). These scenarios are presented in Table 2.1.

Table 2.1 reports the value function $v(0, 0.06, 0)$ for each scenario under the strategies CP, RA and BO, and shows the corresponding percentage improvement $\%I$. In alignment with current regulations, the analysis is based on two bleed–feed

Table 2.1: Impact of transition risks on CP, RA and BO.

f	**CP**	**RA**	**BO**	$\%I_{RA}$	$\%I_{BO}$	i_0^*	i_1^*	ĩ
1.5	20.1	45.5	47.9	126%	139%	47	48	45
1.25	20.4	45.8	48.6	124%	138%	47	48	45
1.1	20.7	46.1	49.1	123%	137%	47	48	45
1	**20.8**	**46.2**	**49.5**	**122%**	**137%**	**48**	**49**	**45**
0.9	21.0	46.4	49.9	121%	138%	48	49	45
0.75	21.3	46.7	50.6	119%	138%	48	50	45
0.5	21.8	47.2	52.5	117%	141%	49	51	45
0.25	22.4	47.8	56.1	114%	151%	51	52	45
0.1	22.7	48.2	60.5	112%	166%	52	54	45

opportunities ($N = 2$). Columns i_0^* and i_1^* denote the optimal cultivation-aged-based threshold for the first and second bleed–feeds, respectively (i.e., at $n = 0$ and $n = 1$). For ease of exposition and brevity, Table 2.1 reports the optimal thresholds i_0^* and i_1^* at selected states (when $\mu' = 0.06$ and $n \in \{0, 1\}$).

First, we compare RA, BO and CP to quantify the potential room for improvement in each scenario. In Table 2.1, we observe that $\%I_{BO}$ ranges between 137% and 166%; and $\%I_{RA}$ ranges between 112% and 126%. In particular, Table 2.1 shows that in the base case setting of MSD, BO can help the company achieve an increase of 137% (and RA of 122%) in the total biomass production from one setup (with two bleed–feeds). Although two bleed–feeds may be perceived as two additional batches of biomass production, we observe that it does not triple the total biomass production (compared to CP) in any of the scenarios. This is mainly because we stop the cultivation earlier than CP when we bleed–feed (to avoid the risk of entering the stationary phase and losing the bleed–feed opportunity). This implies that BO compromises on the biomass production toward the end of the exponential growth phase to be able to perform bleed–feed. Hence, practitioners should understand that two additional cultivations with bleed–feed do not result in three full batches of biomass production in CP (without bleed–feed). Nevertheless, notable improvements (as reported in Table 2.1) can be achieved through BO by eliminating two intermediary setups.

For low-risk batches, Table 2.1 shows that improvement percentages are higher under BO, and lower under RA. The underlying intuition of this behavior can be explained as follows. Low-risk batches can accumulate more biomass at lower failure risks under each strategy. Hence, bleed–feed decisions can be postponed

without high risks of entering the stationary phase. Recall that RA implements bleed–feed at the critical biomass amount, whereas CP collects all the biomass until the stationary phase. This difference leads to lower improvements $\%I_{RA}$. On the other hand, BO collects higher amount of biomass with each bleed–feed, and hence $\%I_{BO}$ increases at lower risks. Hence, we observe that the business case for BO is stronger for the low-risk batches.

We now consider the optimal bleed–feed thresholds i_0^* and i_1^*. Table 2.1 shows that optimal policies tend to bleed–feed at higher cultivation ages i_0^* and i_1^*, as the risk of transitioning to the stationary phase decreases. This result is intuitive because the biomass is more likely to continue accumulating at lower risks. In addition, when we compare i_0^* and i_1^* of a given scenario, we observe that optimal bleed–feed thresholds increase in n. This indicates that the optimal bleed–feed policy becomes less conservative after the first bleed–feed and thus enables the growth of additional biomass for the second cultivation.

Table 2.1 shows that BO outperforms RA. Observe that the difference between the optimal bleed–feed thresholds i_0^* and i_1^* and the critical age $\tilde{\imath}$ increases when the batch exhibits lower risks of entering the stationary phase. This is because BO can wait longer to bleed–feed with lower risk of missing the bleed–feed opportunity. Subsequently, RA performs worse compared to BO for low-risk batches. This finding aligns with our structural insights (Section 2.4.4).

2.6.3 Insights on the Critical Biomass Level

In practice, cells might have different critical biomass levels depending on their biological characteristics (i.e., virus, bacteria or mammalian), the media (i.e., nutrients used in the media formulation) and the equipment used in the fermentation (i.e., bioreactor types and technologies). Therefore, we considered the following scenarios for the critical biomass: *(i)* base case, $\tilde{m} = 13$ grams, *(ii)* lower levels, $\tilde{m} = \{3, 5, 7, 9, 11\}$, and *(iii)* higher levels, $\tilde{m} = \{15, 17, 19\}$. In each scenario, we shifted our base rate function to the left (for lower $\tilde{m}$) or right (for higher $\tilde{m}$). Table 2.2 reports the value function $v(0, 0.06, 0)$ for each scenario under CP, RA and BO.

Observe from Table 2.2 that both $\%I_{RA}$ and $\%I_{BO}$ increase as the critical biomass $\tilde{m}$ increases. This trend is obtained because the process becomes more robust as the

Table 2.2: Impact of the critical biomass level in CP, RA and BO.

$\tilde{m}$	**CP**	**RA**	**BO**	$\%I_{RA}$	$\%I_{BO}$	i_0^*	i_1^*	$\tilde{\imath}$
19	22.9	59.9	64.6	161%	181%	54	54	51
17	22.7	55.8	59.8	146%	163%	52	53	49
15	22.1	51.2	54.7	131%	147%	50	51	47
13	**20.8**	**46.2**	**49.5**	**122%**	**137%**	**48**	**49**	**45**
11	18.6	39.7	43.2	113%	132%	46	47	42
9	16.2	32.6	36.4	101%	125%	43	45	38
7	13.8	26.3	29.5	90%	114%	40	42	34
5	11.2	19.6	22.8	74%	103%	36	38	28
3	8.5	12.7	15.8	49%	85%	31	34	19

critical biomass increases (i.e., no risk of entering the stationary phase before $\tilde{m}$). Subsequently, the expected total biomass production increases in $\tilde{m}$, and thus the potential benefits of bleed–feed also gets higher. This result implies that bleed–feed has a stronger business case when the critical biomass is high.

We now focus on the optimal bleed–feed thresholds i_0^* and i_1^*. Optimal bleed–feed times i_0^* and i_1^* decrease as the critical biomass $\tilde{m}$ decreases. This trend is intuitive because the risk of entering the stationary phase is higher at lower critical biomass levels. Yet, we observe from Table 2.2 that the difference between the optimal bleed–feed times i_0^* and i_1^* (used by BO) and the critical age $\tilde{\imath}$ (used by RA) increases as the critical biomass $\tilde{m}$ decreases. Recall that the process becomes more vulnerable (i.e., higher risks of entering stationary phase) at lower critical biomass levels $\tilde{m}$. Subsequently, RA underperforms compared to BO because it tends to bleed–feed sooner than optimal to avoid failure risks at low values of $\tilde{m}$. This risk-averse behavior leads to a larger difference between optimal policies (i_0^* and i_1^*) and the critical age $\tilde{\imath}$ when the critical biomass $\tilde{m}$ decreases. This finding aligns with the structural insights presented in Section 2.4.4.

2.6.4 Insights on Regulatory Requirements

We conduct numerical analysis on the maximum number of bleed–feeds permitted N. The regulatory bound N ensures that the batch is safe and reliable after bleed–feed (i.e., no safety or quality issues because of growth inhibitors and byproducts after bleed–feed; the cell growth behavior and the rate function is robust to the bleed–feed count). In this section, we relax this regulatory bound and analyze

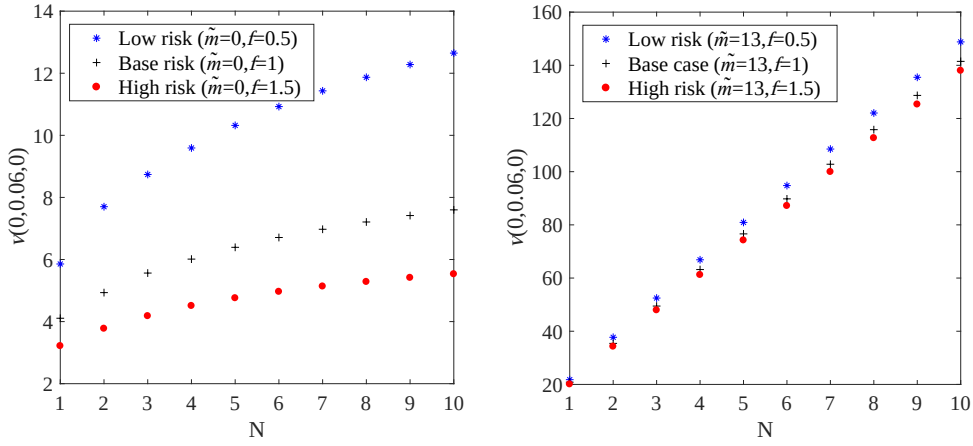

(a) $\tilde{m} = 0$ *(b)* $\tilde{m} = 13$

Figure 2.4: Analysis for the number of bleed–feeds permitted on a batch N for (a) $\tilde{m} = 0$ and (b) $\tilde{m} = 13$ grams.

the behavior of the value function in the bleed–feed count n. From a practical perspective, when the bleed–feed amount is large (by relaxing N), the cell culture is expected to become more vulnerable (i.e., the critical biomass would tend to zero and the batch would become more likely to enter the stationary phase). To capture this behavior in a realistic manner, our numerical analysis focuses on the case when the critical biomass amount is $\tilde{m} = 0$. We present the results also for $\tilde{m} = 13$ for the sake of completeness. In addition, we consider base risk ($f = 1$), high-risk ($f = 1.5$), and low-risk batches ($f = 0.5$) for both cases to provide a better understanding of the impact of risks and regulations. Figure 2.4(a) depicts the value function $v(0, 0.06, 0)$ under BO for $N = \{0, 1, \ldots, 10\}$, when $\tilde{m} = 0$, for a base risk ($\tilde{m} = 0$, $f = 1$), high-risk ($\tilde{m} = 0$, $f = 1.5$) and low-risk batch ($\tilde{m} = 0$, $f = 0.5$). Figure 2.4(b) presents the same for $\tilde{m} = 13$.

Recall Theorem 2.4 showing that the marginal increments of the expected total biomass are decreasing in n and converge to the critical biomass $\tilde{m}$. Figure 2.4(a) demonstrates this result for $\tilde{m} = 0$. Observe from Figure 2.4(a) that the increase in biomass production obtained by an additional bleed–feed decreases as more bleed–feeds are conducted on a batch. Moreover, if we increase N further, we observe that the total expected biomass converges to a bound in each case in Figure 2.4(a). This bound is lower for a high-risk batch, and higher for a low-risk batch. In addition,

we observe that the higher-risk batch converges to its bound at lower N values. Figure 2.4(b) depicts the result from Theorem 2.4 for $\tilde{m} = 13$. Observe that the value function increases in n when $\tilde{m} = 13$, as the increments in $v(0, 0.06, 0)$ in n converge to $\tilde{m}$. However, we note that Figure 2.4(b) can be misleading, as it does not capture the vulnerability of the cells as a result of increasing the number of bleed–feeds beyond the regulatory limit N. In practice, the relationship between manufacturers and regulators is bi-directional: exogenous constraints on the bleed–feed count N impact operational decisions in practice; and the industry implementation may also shape regulatory policies. Hence, our results provide a deeper understanding for practitioners by demonstrating the effects of an additional bleed–feed.

2.7. Conclusions

Bioreactor setups involve high cost of cleaning, sterilization, seed culture, labor, and materials (Oyebolu et al., 2019; Mahal et al., 2021). In addition, with increasing competition and growing market demand, maintaining a competitive advantage requires decision makers to balance short-term cost pressures against the long-term need to innovate (McKinsey & Company, 2019). In this context, the problem of increasing upstream titer has been gaining importance for improving biomanufacturing efficiency. To address this problem, we consider a new technology for batch fermentation: bleed–feed.

The bleed–feed technology allows biomanufacturers to "skip" a few of the bioreactor setups by extending the duration of the exponential growth phase in batch fermentation. Therefore, this technology presents an innovative approach for reducing costs and improving efficiency in batch-based biomanufacturing. However, the successful use of bleed–feed involves challenges and trade-offs that are unlike those in any other applications. For example, bleed–feed can be performed only in the exponential growth phase. As the duration of the exponential growth phase is random, there is a critical trade-off between performing bleed–feed too soon or too late. In addition, regulatory requirements restrict the number of bleed–feeds (per setup) to a pre-specified limit, which are generally known to be conservative to ensure safety and reliability. All these factors obstruct the potential benefits of bleed–feed technology.

To address these challenges, we built an analytical framework to optimize bleed–feed decisions. In particular, we developed an MDP model and analyzed the structural properties of optimal bleed–feed policies. Moreover, we characterized the behavior of the value function as a function of the regulatory limit N. Counter-intuitive to the generally-held opinion in industry, we showed that the marginal benefits of an additional bleed–feed are decreasing and converge to the critical biomass, as the regulatory limit N increases. We observe that bleed–feed brings benefits. Our case study shows that batch yield per setup can increase by 137% in the base case (with two bleed–feeds).

2.A. Proofs

Proof of Proposition 2.1. Fix $\mu \in \mathcal{M}$ and $n \in \mathcal{N}$. By induction in i we show

$$v(i,\mu,n) \leq v(i-1,\mu,n), \qquad i > 0. \tag{2.12}$$

For $i = I$, we have $v(I,\mu,n) = 0 \leq v(I-1,\mu,n)$. Hence, (2.12) is valid for $i = I$. Now we assume that (2.12) is valid for i where $i > \tilde{\imath}_\mu$. Then we show that (2.12) also holds for $i-1$. From (2.4) we have (note that $p_{i-2\mu} - p_{i-1\mu} > 0$)

$$\begin{aligned}\frac{r_{i-1\mu} - r_{i-2\mu}}{p_{i-2\mu} - p_{i-1\mu}} &\leq r_{i-1\mu} \\ &\leq r_{i-1\mu} + p_{i-1\mu} v(i,\mu,n) \\ &= C(i-1,\mu,n) \\ &\leq v(i-1,\mu,n). \end{aligned} \tag{2.13}$$

Rearranging (2.13), we obtain

$$\begin{aligned} r_{i-1\mu} - r_{i-2\mu} &\leq (p_{i-2\mu} - p_{i-1\mu}) v(i-1,\mu,n) \\ &= p_{i-2\mu} v(i-1,\mu,n) - p_{i-1\mu} v(i-1,\mu,n) \\ &\leq p_{i-2\mu} v(i-1,\mu,n) - p_{i-1\mu} v(i,\mu,n), \end{aligned} \tag{2.14}$$

where (2.14) follows from the induction hypothesis. Rearranging terms yields

$$C(i-1,\mu,n) = r_{i-1\mu} + p_{i-1\mu} v(i,\mu,n) \leq r_{i-2\mu} + p_{i-2\mu} v(i-1,\mu,n) = C(i-2,\mu,n). \tag{2.15}$$

Hence,

$$v(i-1,\mu,n) = \max\{C(i-1,\mu,n), B(n)\} \leq \max\{C(i-2,\mu,n), B(n)\} = v(i-2,\mu,n).$$

Finally, for $0 < i < \tilde{\imath}_\mu$ we have $p_{i-1\mu} = 1$, so $v(i-1,\mu,n) = \max\{r_{i-1\mu} + v(i,\mu,n), B(n)\} \geq v(i,\mu,n)$. □

Proof of Proposition 2.2. The inequality $C(i,\mu,n) - B(n) \leq C(i-1,\mu,n) - B(n)$ reduces to $C(i,\mu,n) \leq C(i-1,\mu,n)$. The latter inequality follows from the proof of Proposition 2.1. □

Proof of Theorem 2.1. The proof is an immediate consequence of Proposition 2.2. □

Proof of Proposition 2.3. Fix $\mu < \mu^+ \in \mathcal{M}$ and $n < \mathcal{N}$. By induction in i we show

$$v(i,\mu^+,n) \leq v(i,\mu,n), \quad i \geq \tilde{\imath}_{\mu^+}. \tag{2.16}$$

Assumption 2.1 is required for the first induction step: For $i = I-1$ we have $v(I-1,\mu^+,n) = v(I-1,\mu,n) = B(n)$. Hence, (2.16) is valid for $i = I-1$. Now we assume that (2.16) is valid for i where $i > \tilde{\imath}_{\mu^+}$. We show that (2.16) also holds for $i-1$. From (2.5) we have (note that $p_{i-1\mu} - p_{i-1\mu^+} > 0$):

$$\begin{aligned}
\frac{r_{i-1\mu^+} - r_{i-1\mu}}{p_{i-1\mu} - p_{i-1\mu^+}} &\leq r_{i\mu^+} \\
&\leq r_{i\mu^+} + p_{i\mu^+} v(i+1,\mu^+,n) \\
&= C(i,\mu^+,n) \\
&\leq v(i,\mu^+,n).
\end{aligned} \tag{2.17}$$

Rearranging (2.17), we obtain:

$$\begin{aligned} r_{i-1\mu^+} - r_{i-1\mu} &\leq (p_{i-1\mu} - p_{i-1\mu^+})v(i,\mu^+,n) \\ &= p_{i-1\mu}v(i,\mu^+,n) - p_{i-1\mu^+}v(i,\mu^+,n) \\ &\leq p_{i-1\mu}v(i,\mu,n) - p_{i-1\mu^+}v(i,\mu^+,n), \end{aligned} \tag{2.18}$$

where (2.18) follows from the induction hypothesis. Rearranging terms we get:

$$C(i-1,\mu^+,n) = r_{i-1\mu^+} + p_{i-1\mu^+}v(i,\mu^+,n) \leq r_{i-1\mu} + p_{i-1\mu}v(i,\mu,n) = C(i-1,\mu,n). \tag{2.19}$$

Hence,

$$v(i-1,\mu^+,n) = \max\{C(i-1,\mu^+,n), B(n)\} \leq \max\{C(i-1,\mu,n), B(n)\} = v(i-1,\mu,n),$$

which completes the proof. □

Proof of Proposition 2.4. The inequality $C(i,\mu^+,n) - B(n) \leq C(i,\mu,n) - B(n)$ reduces to $C(i,\mu^+,n) \leq C(i,\mu,n)$. The latter inequality follows from the proof of Proposition 2.3. □

Proof of Theorem 2.2. The proof is an immediate consequence of Proposition 2.4. □

Proof of Proposition 2.5. Suppose that in each state (i,μ,n) with $n < N$, we apply the optimal action for state $(i,\mu,n+1)$ (note that the only feasible action in states (i,μ,N) is c). Let $v'(i,\mu,n)$ denote the expected biomass production under this policy. Then,

$$v(i,\mu,n) \geq v'(i,\mu,n) = v(i,\mu,n+1).$$

□

Proof of Proposition 2.6. Proposition 2.5 implies that $B(n) \geq B(n+1)$. By

induction in i, we show

$$C(i,\mu,n) - B(n) \leq C(i,\mu,n+1) - B(n+1). \tag{2.20}$$

For $i = I-1$ we have $C(i,\mu,n) = C(i,\mu,n+1) = r_{I-1\mu}$. Therefore,

$$C(i,\mu,n) - B(n) = C(i,\mu,n+1) - B(n) \leq C(i,\mu,n+1) - B(n+1).$$

Hence, (2.20) is valid for $i = I-1$. Now assume that (2.20) is valid for i. Then, we show that it also holds for $i-1$. By (2.20), we have $C(i,\mu,n) \leq C(i,\mu,n+1) + B(n) - B(n+1)$. Therefore,

$$\begin{aligned} v(i,\mu,n) - v(i,\mu,n+1) &= \max\{C(i,\mu,n), B(n)\} - \max\{C(i,\mu,n+1), B(n+1)\} \\ &\leq \max\{C(i,\mu,n+1) + B(n) - B(n+1), B(n)\} \\ &\quad - \max\{C(i,\mu,n+1), B(n+1)\} \\ &= B(n) - B(n+1) \end{aligned}$$

and thus

$$\begin{aligned} C(i-1,\mu,n) - C(i-1,\mu,n+1) &= p_{i-1\mu}(v(i,\mu,n) - v(i,\mu,n+1)) \\ &\leq p_{i-1\mu}(B(n) - B(n+1)) \;\leq\; B(n) - B(n+1). \end{aligned}$$

□

Proof of Theorem 2.3. The proof is an immediate consequence of Proposition 2.6. □

Proof of Lemma 2.1. If Condition (2.4) holds, then the value function is nonincreasing in i:

$$v(i,\mu,n) = \max\{C(i,\mu,n), B(n)\} \geq v(i+1,\mu,n). \tag{2.21}$$

If $v(i,\mu,n) = B(n)$, then $v(i+1,\mu,n) = B(n)$ from Theorem 2.1, and (2.21) holds. If

$v(i,\mu,n) = C(i,\mu,n)$ for $0 \leq i < \tilde{\imath}_\mu$ we have:

$$\begin{aligned} v(i,\mu,n) = C(i,\mu,n) &= r_{i\mu} + v(i+1,\mu,n) \\ &= r_{i\mu} + r_{i+1\mu} + ... + r_{\tilde{\imath}_\mu\mu} + p_{\tilde{\imath}_\mu\mu} v(\tilde{\imath}_\mu + 1,\mu,n) \geq v(i+1,\mu,n). \end{aligned}$$

Then, from Proposition 2.1,

$$r_{i\mu} + r_{i+1\mu} + ... + r_{\tilde{\imath}_\mu\mu} + p_{\tilde{\imath}_\mu\mu} v(i+1,\mu,n) \geq v(i+1,\mu,n),$$

so

$$\frac{r_{i\mu} + r_{i+1\mu} + ... + r_{\tilde{\imath}_\mu\mu}}{1 - p_{\tilde{\imath}_\mu\mu}} \geq v(i+1,\mu,n).$$

If $v(i,\mu,n) = C(i,\mu,n)$ for $\tilde{\imath}_\mu \leq i \leq I-1$ we have:

$$v(i,\mu,n) = C(i,\mu,n) = r_{i\mu} + p_{i\mu} v(i+1,\mu,n) \geq v(i+1,\mu,n),$$

thus

$$\frac{r_{i\mu}}{1 - p_{i\mu}} \geq v(i+1,\mu,n).$$

□

Proof of Theorem 2.4. From Equation (2.2) we have for $n = 0,\ldots,N$:

$$\begin{aligned} v(0,\mu,n) &= \max\{B(n), r_{0\mu} + p_{0\mu} v(1,\mu,n)\} \\ &= \max\{B(n), r_{0\mu} + p_{0\mu} B(n), r_{0\mu} + p_{0\mu} r_{1\mu} + p_{0\mu} p_{1\mu} v(2,\mu,n)\} \\ &= \cdots \\ &= \max\{B(n), r_{0\mu} + p_{0\mu} B(n), r_{0\mu} + p_{0\mu} r_{1\mu} + p_{0\mu} p_{1\mu} B(n), \cdots, \\ &\quad r_{0\mu} + p_{0\mu} r_{1\mu} + \cdots + p_{0\mu} \cdots p_{I-3\mu} r_{I-2\mu} + p_{0\mu} \cdots p_{I-2\mu} B(n), \\ &\quad r_{0\mu} + p_{0\mu} r_{1\mu} + \cdots + p_{0\mu} \cdots p_{I-3\mu} r_{I-2\mu} + p_{0\mu} \cdots p_{I-2\mu} r_{I-1\mu}\}. \end{aligned}$$

This can be written as

$$v(0,\mu,n) = \max_{0 \leq i \leq I} \{a_{i\mu} + b_{i\mu} B(n)\},$$

where

$$b_{i\mu} = \prod_{j=0}^{i-1} p_{j\mu}, \quad 0 \le i < I, \quad b_I = 0,$$

and

$$a_{i\mu} = \sum_{j=0}^{i-1} b_{j\mu} r_{j\mu}, \quad 0 \le i \le I.$$

Note that $b_{i+1\mu} = b_{i\mu} p_{i\mu} \le b_{i\mu}$ and $a_{i+1\mu} = a_{i\mu} + b_{i\mu} r_{i\mu} \ge a_i$. We first consider the special case that the growth rate M is not random, but constant, $M = \mu$ say. Then $B(n) = v(0, \mu, n+1)$, so the above equation can be written as

$$v(0, \mu, n) = \max_{0 \le i \le I} \{a_{i\mu} + b_{i\mu} v(0, \mu, n+1)\}, \qquad n = 0, 1, \ldots N,$$

where $v(0, \mu, N+1) = 0$. Since we want to investigate the behavior of $v(0, \mu, 0)$ as N tends to infinity, it is convenient to write $w(\mu, n) = v(0, \mu, N-n)$, where n denotes the remaining number of bleed–feeds. For $w(\mu, n)$ we get the recursion

$$w(\mu, n) = f_\mu(w(\mu, n-1)), \quad n = 0, 1, \ldots, N,$$

starting with $w(\mu, -1) = v(0, \mu, N+1) = 0$, where

$$f_\mu(x) = \max_{0 \le i \le I} \{a_{i\mu} + b_{i\mu} x\}.$$

Then the maximum total expected biomass from a batch is $v(0, \mu, 0) = w(\mu, N)$.

Since $a_{0\mu} = 0$ and $b_{0\mu} = 1$ we immediately have

$$w(\mu, n) \ge a_{0\mu} + b_{0\mu} w(\mu, n-1) = w(\mu, n-1), \quad n \ge 0. \tag{2.22}$$

So the benefit of bleed–feed increases. The function $f_\mu(x)$ is the maximum of convex, non-decreasing linear functions, and hence, $f_\mu(x)$ is convex, non-decreasing and piece-wise linear. Then we have

$$\begin{aligned} w(\mu, n+1) - w(\mu, n) &= f_\mu(w(\mu, n)) - f_\mu(w(\mu, n-1)) \\ &\le f'_\mu(w(\mu, n))(w(\mu, n) - w(\mu, n-1)) \\ &\le w(\mu, n) - w(\mu, n-1), \end{aligned} \tag{2.23}$$

where f'_μ is the (left) derivative. Hence, the marginal benefit is decreasing.

For $i > \tilde{\imath}_\mu$, let $w^*_{i\mu}$ be the intersection point of $a_{i\mu} + b_{i\mu}x$ and $a_{\tilde{\imath}_\mu\mu} + b_{\tilde{\imath}_\mu\mu}x$, so (note that $b_{\tilde{\imath}_\mu\mu} = 1 > b_{i\mu}$)

$$w^*_{i\mu} = \frac{a_{i\mu} - a_{i_\mu\mu}}{1 - b_{i\mu}}, \quad i > \tilde{\imath}_\mu,$$

and let $w^*_\mu = \max_{i>i_\mu} w^*_{i\mu}$. Then, clearly,

$$f_\mu(x) = a_{i_\mu\mu} + x, \qquad x \geq w^*_\mu. \tag{2.24}$$

If the critical biomass $\tilde{m} > 0$, i.e., $\tilde{\imath}_\mu > 0$, we have

$$w(\mu, n) \geq a_{\tilde{\imath}_\mu\mu} + b_{\tilde{\imath}_\mu\mu} w(\mu, n-1) = a_{\tilde{\imath}_\mu\mu} + w(\mu, n-1),$$

so the benefit $w(\mu, n)$ grows to infinity as n tends to infinity. By (2.24), we have, for sufficiently large n,

$$w(\mu, n) = a_{\tilde{\imath}_\mu\mu} + w(\mu, n-1).$$

Hence, the marginal benefit decreases to and, at some point, coincides with $a_{\tilde{\imath}_\mu\mu}$. Now we consider the case $\tilde{m} = 0$, or in other words, $\tilde{\imath}_\mu = 0$. Then $a_{\tilde{\imath}_\mu\mu} = a_{0\mu} = 0$, so we have, by (2.24),

$$f_\mu(x) = x, \quad x \geq w^*_\mu. \tag{2.25}$$

Since $w(\mu, -1) = 0 \leq w^*_\mu$ and $f_\mu(x)$ is non-decreasing, $w(\mu, n) \leq w^*_\mu$ implies that $w(\mu, n+1) = f_\mu(w(\mu, n)) \leq f_\mu(w^*_\mu) = w^*_\mu$. Hence, by induction, $w(\mu, n) \leq w^*_\mu$ for all n. So $w(\mu, n)$ is an increasing, bounded sequence. Therefore, its limit exists and it is equal to w^*_μ, since for all $n \geq 0$,

$$\begin{aligned} w^*_\mu - w(\mu, n) = f_\mu(w^*_\mu) - f_\mu(w(\mu, n-1)) &\leq b_{1\mu}(w^*_\mu - w(\mu, n-1)) \\ &\leq \cdots \\ &\leq b^{n+1}_{1\mu}(w^*_\mu - w(\mu, -1)) = b^{n+1}_{1\mu} w^*_\mu. \end{aligned}$$

Hence, if the critical biomass $\tilde{m} = 0$, the benefit converges geometrically fast to w^*_μ.

The above holds when the growth rate is not random. For random growth rate M we have the recursion

$$w(n) = \mathbb{E}[f_M(w(n-1))], \quad n = 0, 1, \ldots, N,$$

starting with $w(-1) = 0$. Then the maximum expected total biomass from an arbitrary batch is $\mathbb{E}[v(0, M, 0)] = w(N)$. Similar to (2.22) and (2.23) we have

$$w(n) = \mathbb{E}[f_M(w(n-1))] \geq \mathbb{E}[w(n-1)] = w(n-1)$$

and

$$w(n+1) - w(n) = \mathbb{E}[f_M(w(n)) - f_M(w(n-1))] \leq \mathbb{E}[w(n) - w(n-1)] = w(n) - w(n-1).$$

Hence, $w(n)$ is increasing, and the marginal benefits decrease.

Since $p_{i\mu}$ and $r_{i\mu}$ are continuous in μ, we have that $a_{i\mu}$, $b_{i\mu}$ and w^*_μ are also continuous in μ. So $w^* = \max_\mu w^*_\mu$ exists. If the critical biomass $\tilde{m} > 0$, i.e., $\tilde{\imath}_\mu > 0$ for $\mu \in \mathcal{M}$, we have

$$w(n) = \mathbb{E}[f_M(w(n-1)] \geq \mathbb{E}[a_{\tilde{\imath}_M M} + w(M, n-1)] = \mathbb{E}[a_{\tilde{\imath}_M M}] + w(n-1),$$

so the benefit $w(n)$ grows to infinity as n tends to infinity. Since (2.24) is valid for $x \geq w^*$ and $\mu \in \mathcal{M}$, we have, for sufficiently large n,

$$w(n) = \mathbb{E}[f_M(w(n-1)] = \mathbb{E}[a_{\tilde{\imath}_M M}] + w(n-1)$$

Hence, the marginal benefit decreases to and, at some point, coincides with $\mathbb{E}[a_{\tilde{\imath}_M M}]$. This quantity is close to the critical biomass $\tilde{m}$, but not exactly equal to $\tilde{m}$, due to discretization of time.

In case the critical biomass $\tilde{m} = 0$, i.e., $\tilde{\imath}_\mu = 0$ for $\mu \in \mathcal{M}$, we have that (2.25) is valid for $x > w^*$ and $\mu \in \mathcal{M}$. Since $w(-1) = 0 \leq w^*$ and $f_\mu(x)$ is non-decreasing for $\mu \in \mathcal{M}$, $w(n) \leq w^*$ implies that $w(n+1) = \mathbb{E}[f_M(w(n))] \leq \mathbb{E}[f_M(w^*)] = w^*_\mu$. Hence, by induction, $w(n) \leq w^*$ for all n. So $w(n)$ is an increasing, bounded sequence and thus, its limit exists. This limit is equal to w^*, since for all $n \geq 0$,

$$\begin{aligned} w^* - w(n) = \mathbb{E}[f_M(w^*) - f_M(w(n-1))] &\leq \mathbb{E}[b_{1M}(w^* - w(n-1))] \\ &= \mathbb{E}[b_{1M}](w^* - w(n-1)) \\ &\leq b^*_1(w^* - w(n-1)), \end{aligned}$$

where $b^*_1 = \max_\mu b_{1\mu} < 1$ Hence, if $\tilde{m} = 0$, the benefit converges geometrically fast to w^*. □

Proof of Proposition 2.7. By induction in i and n we show *(i)*:

$$v^1(i,\mu,n) \geq v^2(i,\mu,n). \tag{2.26}$$

For states (I,μ,n) and $(i,\mu,N+1)$ we have $v^1(I,\mu,n) = v^2(I,\mu,n) = v^1(i,\mu,N+1) = v^2(i,\mu,N+1) = 0$, hence (2.26) holds. Assume (2.26) holds for (i,μ,n) and $(1,\mu,n+1)$. We now show (2.26) also holds for $(i-1,\mu,n)$. Then, from the induction assumption and $p^1_{i\mu} \geq p^2_{i\mu}$ we have:

$$C^1(i-1,\mu,n) = r_{i-1\mu} + p^1_{i-1\mu} v^1(i,\mu,n) \geq r_{i-1\mu} + p^2_{i-1\mu} v^2(i,\mu,n) = C^2(i-1,\mu,n),$$

and

$$r_{0\mu} + p^1_{0\mu} v^1(1,\mu,n+1) \geq r_{0\mu} + p^2_{0\mu} v^2(1,\mu,n+1),$$

Thus,

$$B^1(n) = \mathbb{E}\big[C^1(0,M,n+1)\big] \geq \mathbb{E}\big[C^2(0,M,n+1)\big] = B^2(n),$$

Hence,

$$v^1(i-1,\mu,n) = \max\{C^1(i-1,\mu,n), B^1(n)\} \geq \max\{C^2(i-1,\mu,n), B^2(n)\} = v^2(i-1,\mu,n).$$

This completes the proof of *(i)*. We prove *(ii)* by showing that $C^1(i,\mu,n) - B^1(n) \geq C^2(i,\mu,n) - B^2(n)$. From Condition (2.9):

$$\begin{aligned}
r_{I-1\mu}(p^1_{i\mu} - p^2_{i\mu}) &\geq \mathbb{E}\big[p^1_{0M} \frac{r_{0M}}{1-p^1_{0M}} - p^2_{0M} r_{I-1M}\big] \\
&\geq \mathbb{E}\big[p^1_{0M} v^1(1,M,n+1)\big] - \mathbb{E}\big[p^2_{0M} C^2(I-1,M,n+1)\big] && (2.27)\\
&\geq \mathbb{E}\big[p^1_{0M} v^1(1,M,n+1)\big] - \mathbb{E}\big[p^2_{0M} v^2(I-1,M,n+1)\big] && (2.28)\\
&\geq \mathbb{E}\big[p^1_{0M} v^1(1,M,n+1)\big] - \mathbb{E}\big[p^2_{0M} v^2(1,M,n+1)\big] && (2.29)\\
&= B^1(n) - B^2(n), && (2.30)
\end{aligned}$$

where (2.27) follows from (2.8) of Lemma 2.1 and the fact that $C(I-1,\mu,n+1) = r_{I-1\mu}$, (2.28) follows from the fact that $v^2(I-1,\mu,n) \geq C^2(I-1,\mu,n)$ and (2.29)

from Proposition 2.1. Rearranging (2.30):

$$\begin{aligned}
B^2(n) - B^1(n) &\geq -r_{I-1\mu}(p^1_{i\mu} - p^2_{i\mu}) \\
&= -C^1(I-1,\mu,n)(p^1_{i\mu} - p^2_{i\mu}) \\
&\geq -v^1(I-1,\mu,n)(p^1_{i\mu} - p^2_{i\mu}) && (2.31)\\
&\geq -p^1_{i\mu}v^1(i+1,\mu,n) + p^2_{i\mu}v^1(i+1,\mu,n) && (2.32)\\
&\geq -p^1_{i\mu}v^1(i+1,\mu,n) + p^2_{i\mu}v^2(i+1,\mu,n) = -C^1(i,\mu,n) + C^2(i,\mu,n), && (2.33)
\end{aligned}$$

where (2.31) follows from the fact that $C^1(I-1,\mu,n) \leq v^1(I-1,\mu,n)$, (2.32) follows from Proposition 2.1, and (2.33) from Proposition 2.7 *(i)*. Rearranging (2.33) we obtain $C^1(i,\mu,n) - B^1(n) \geq C^2(i,\mu,n) - B^2(n)$.

For $i < \tilde{\imath}_\mu$, the difference $C^1(i,\mu,n) - C^2(i,\mu,n)$ remains constant (since $r_{i\mu}$ is the same for the two batches, and $p^1_{i\mu} = p^2_{i\mu} = 1$). Thus, $C^1(i,\mu,n) - B^1(n) \geq C^2(i,\mu,n) - B^2(n)$. □

Proof of Theorem 2.5. By induction in i, we show that the following holds for $\tilde{\imath}_\mu \leq i \leq I-1, \mu \in \mathcal{M}$ and $n < N$:

$$C(i,\mu,n) \leq B(n). \tag{2.34}$$

For $i = I-1$, from Condition (2.6) we have:

$$\begin{aligned}
C(I-1,\mu,n) = r_{I-1\mu} &\leq (1-p_{I-1\mu})(r_{0\mu} + r_{1\mu} + ... + r_{\tilde{\imath}_\mu\mu} + \mathbb{E}[p_{\tilde{\imath}_M M} r_{I-1M}]) \\
&\leq r_{0\mu} + r_{1\mu} + ... + r_{\tilde{\imath}_\mu\mu} + \mathbb{E}[p_{\tilde{\imath}_M M} r_{I-1M}] \\
&= r_{0\mu} + r_{1\mu} + ... + r_{\tilde{\imath}_\mu\mu} + \mathbb{E}[p_{\tilde{\imath}_M M} C(I-1,M,n+1)] \\
&\leq r_{0\mu} + r_{1\mu} + ... + r_{\tilde{\imath}_\mu\mu} + \mathbb{E}[p_{\tilde{\imath}_M M} v(I-1,M,n+1)] && (2.35)\\
&\leq r_{0\mu} + r_{1\mu} + ... + r_{\tilde{\imath}_\mu\mu} + \mathbb{E}[p_{\tilde{\imath}_M M} v(\tilde{\imath}_M+1,M,n+1)] && (2.36)\\
&= \mathbb{E}[r_{0\mu} + v(1,M,n+1)] = \mathbb{E}[C(0,M,n+1] = B(n),
\end{aligned}$$

where (2.35) follows from the fact that $C(I-1,\mu,n) \leq v(I-1,\mu,n)$ and (2.36) from Proposition 2.1. Hence, (2.34) is true for $i = I-1$. Now, assume (2.34) holds for $\tilde{\imath}_\mu + 1$. We show that it also holds for $\tilde{\imath}_\mu$. Rearranging Condition (2.6) for $i = \tilde{\imath}_\mu$ we

have:

$$\begin{aligned}
\frac{r_{\tilde{\imath}_\mu \mu}}{1-p_{\tilde{\imath}_\mu \mu}} &\leq r_{0\mu} + r_{1\mu} + ... + r_{\tilde{\imath}_\mu \mu} + \mathbb{E}[p_{\tilde{\imath}_M M} r_{I-1M}] \\
&= r_{0\mu} + r_{1\mu} + ... + r_{\tilde{\imath}_\mu \mu} + \mathbb{E}[p_{\tilde{\imath}_M M} C(I-1, M, n+1)] \\
&\leq r_{0\mu} + r_{1\mu} + ... + r_{\tilde{\imath}_\mu \mu} + \mathbb{E}[p_{\tilde{\imath}_M M} v(I-1, M, n+1)] \qquad (2.37) \\
&\leq r_{0\mu} + r_{1\mu} + ... + r_{\tilde{\imath}_\mu \mu} + \mathbb{E}[p_{\tilde{\imath}_M M} v(\tilde{\imath}_M + 1, M, n+1)] \qquad (2.38) \\
&= \mathbb{E}[r_{0\mu} + v(1, M, n+1)] = \mathbb{E}[C(0, M, n+1] = B(n),
\end{aligned}$$

where (2.37) follows from the fact that $C(I-1, \mu, n) \leq v(I-1, \mu, n)$ and (2.38) from Proposition 2.1. Rearranging:

$$C(\tilde{\imath}_\mu, \mu, n) = r_{\tilde{\imath}_\mu \mu} + p_{\tilde{\imath}_\mu \mu} v(\tilde{\imath}_\mu + 1, \mu, n) = r_{\tilde{\imath}_\mu \mu} + p_{\tilde{\imath}_\mu \mu} B(n) \leq B(n) \qquad (2.39)$$

where (2.39) follows from the induction assumption. □

Proof of Proposition 2.8. The proof is similar to that of Proposition 2.7*(ii)*, hence it is omitted. □

2.B. Maximizing the Expected Reward per Batch

We present an alternative model formulation with the objective of maximizing the reward (profit) obtained from a single batch. Immediate rewards are now defined as $r_{i\mu} = g(m_{i+1\mu} - m_{i\mu})$, where g denotes the revenue obtained per unit biomass produced in the bioreactor. Let the direct costs for harvesting and for bleed–feed be constants, represented as c_h and c_b, respectively. The costs are ordered such that $c_b < c_h$. We note that the cell growth behavior (as represented in Equation (2.1)) and the transition probabilities remain identical.

Since every batch is eventually harvested, we can omit the harvest cost. We define $v(i, \mu, n)$ as the maximum expected reward given the current state is (i, μ, n). Then,

the value function $v(i,\mu,n)$ satisfies:

$$v(i,\mu,n) = \max \begin{cases} C(i,\mu,n) & \equiv r_{i\mu} + p_{i\mu} v(i+1,\mu,n), \\ B(n) & \equiv \mathbb{E}\big[C(0,M,n+1)\big] - c_b \end{cases}$$

valid for all $i < I$, $\mu \in \mathcal{M}$ and $n < N$, and $v(i,\mu,N) = C(i,\mu,N)$ for all $i < I$ and $\mu \in \mathcal{M}$. Note that $v(I,\mu,n) = 0$ for all μ and n, and $v(\Delta) = 0$. We now show that structural results presented in Section 2.4 are robust to the alternative model formulation.

First, we focus on the structure in fermentation age i. Since $B(n)$ is constant in i in the alternative model (as in the main model), showing the result for $C(i,\mu,n)$ is sufficient. Note that $C(i,\mu,n)$ is identical in both models, except in the alternative model the immediate rewards $r_{i\mu}$ are multiplied by constant revenue per unit biomass amount g. Recall Condition (2.4): $\frac{r_{i\mu}-r_{i-1\mu}}{r_{i\mu}} \leq p_{i-1\mu} - p_{i\mu}$. In the alternative model, the left hand side of the condition can be written as:

$$\begin{aligned} &\frac{g(m_{i+1\mu} - m_{i\mu}) - g(m_{i\mu} - m_{i-1\mu})}{g(m_{i+1\mu} - m_{i\mu})} \\ &= \frac{g(m_0(1+\mu\tau)^{i+1}) - g(m_0(1+\mu\tau)^{i}) - g(m_0(1+\mu\tau)^{i}) + g(m_0(1+\mu\tau)^{i-1})}{g(m_0(1+\mu\tau)^{i+1}) - g(m_0(1+\mu\tau)^{i})} \\ &= \frac{\mu\tau}{1+\mu\tau}. \end{aligned}$$

Observe that g cancels out in the condition, implying that the structure of the value function in i does not depend on revenue obtained per unit biomass amount g in the alternative model. Hence, Proposition 2.1 is valid. Using similar arguments, it is easy to show that Propositions 2.2, 2.3, 2.4 and 2.5, and Theorems 2.1, 2.2, and 2.3 continue to hold. We omit the details for brevity.

2.C. Estimation of the Transition Rate Function

We only sketch the approach adopted to estimate the rate function (and omit the details) because of confidentiality concerns. Let $F_\mu(m)$ denote the (long-run) fraction of batches that transition to the stationary phase at a biomass amount of at most m, and $f_\mu(m)$ be the corresponding density, i.e., $f_\mu(m) = F'_\mu(m)$, for

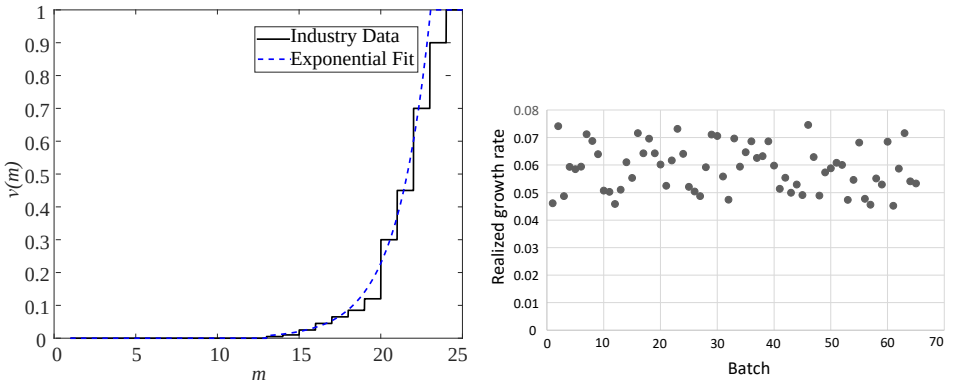

(a) The rate function $\nu(m)$. *(b)* Growth rate of batches.

Figure 2.5: Base case parameters used in the case study.

batches that grow at the rate $M = \mu$. Let Δ be a small time interval. Then, given that the biomass is m at time t, the probability that a batch will transition to the stationary phase at a biomass amount between m and $m(1+\mu\Delta)$ (recall that the growth is exponential) satisfies $f_\mu(m)\mu m\Delta = \nu(m)\Delta(1-F_\mu(m))$. Hence, $\frac{f_\mu(m)}{1-F_\mu(m)} = \frac{\nu(m)}{\mu m}$. Note that the rate of transitioning $\nu(m)$ depends only on the biomass m, and not on the growth rate μ. Solving the above differential equations yields $1-F_\mu(m) = e^{-\int_{m_0}^{m}\frac{\nu(x)}{\mu x}dx}$, $m \geq m_0$, where m_0 is the initial biomass. The function $F_\mu(m)$ can be estimated directly from data, and discretized at points $m = 1,2,\ldots$. If we then approximate $f_\mu(m) \approx F_\mu(m+1) - F_\mu(m)$, we obtain an estimate for the transition rate function $\frac{F_\mu(m+1)-F_\mu(m)}{1-F_\mu(m)} = \frac{\nu(m)}{\mu m}$, which can be rewritten as $\nu(m) = \mu m\frac{F_\mu(m+1)-F_\mu(m)}{1-F_\mu(m)}$ for $m = 1,2,\ldots$. The growth rate M is random. Therefore, by taking the expectation, we obtain the (more robust) estimate $\nu(m) = \int_{\mu_l}^{\mu_u}\mu m\frac{F_\mu(m+1)-F_\mu(m)}{1-F_\mu(m)}dP(M=\mu)$. By discretizing M with the possible values $\mu_1,\mu_2,\ldots$, this equation reduces to $\nu(m) = \sum_{\mu_i}\mu_i m\frac{F_{\mu_i}(m+1)-F_{\mu_i}(m)}{1-F_{\mu_i}(m)}P(M=\mu_i)$ for $m = 1,2,\ldots$.

Figure 2.5 illustrates the rate function used in our numerical experiments. We used representative values considering confidentiality.

3

Optimizing the Fermentation Throughput in Biomanufacturing with Bleed–Feed

3.1. Introduction

Biomanufacturing operations start with upstream processing, where living cells, such as viruses and bacteria, are grown in a controlled environment to produce the desired active ingredients. Upstream processing includes operations such as preparation of seed culture, preparation of medium, fermentation and harvest. The output obtained from fermentation varies across different drugs but it often represents biomass, protein or antibody. In the remainder of this chapter, we use the term "biomass" to represent the output of fermentation.

Fermentation processes typically take place in a bioreactor which is a stainless steel vessel, providing a controlled environment to facilitate cell growth. The bioreactor needs to be set up before a fermentation process starts. During these setup activities, the bioreactor is first cleaned and sterilized, and then a seed culture (initial biomass) and medium are placed inside the bioreactor. The biomass growth follows a specific pattern during fermentation, as shown in Figure 3.1(a). We observe from

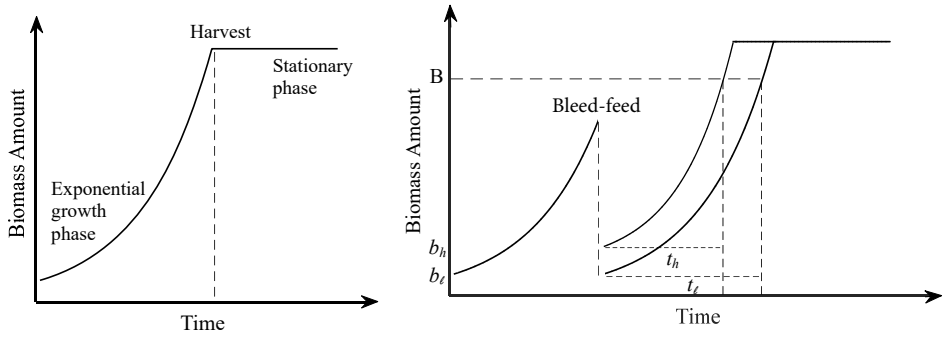

(a) Biomass growth without bleed-feed. *(b)* Biomass growth with bleed-feed.

Figure 3.1: Biomass growth over time in current practice (a) and with bleed–feed (b).

Figure 3.1(a) that the fermentation starts with a small amount of initial biomass. This biomass consumes the medium and grows exponentially over time. This specific phase of fermentation is known as the *exponential growth phase*. In batch fermentation, medium is added only once, at the beginning of the fermentation process. Thus, the limited amount of medium depletes over time and the biomass growth stops. This specific phase of fermentation is called the *stationary phase*. A common practice is to harvest the batch in the stationary phase. After the harvest, the bioreactor is set up for a new fermentation process.

Bioreactor setups can be labor intensive and time consuming (Yang and Sha, 2019). For example, up to ten hours can be spent during a bioreactor setup (Sharma, 2019). This results in long bioreactor occupation times and low throughput levels. Therefore, there is a strong business case in the industry to reduce bioreactor setups and thereby improve throughput. For this purpose, *bleed–feed* is perceived as a promising technique to skip intermediary bioreactor setups. The main dynamics of bleed–feed are demonstrated in Figure 3.1(b). When the bleed–feed technique is performed, we extract ("bleed") some of the biomass that accumulated inside the bioreactor and add ("feed") fresh media for the remaining biomass. The biomass in the remaining culture acts as a seed for the next cultivation, and uses the fresh medium to continue growing. Thus, bleed–feed technique enables practitioners to skip one setup by prolonging the exponential growth phase. In other words, the bleed–feed technology enables us to produce two cultivations from one setup. The batch is harvested when the second cultivation reaches its predetermined harvest time.

Although bleed–feed presents an opportunity to increase throughput, its implementation can be challenging in practice. In particular, we can bleed–feed only in the exponential growth phase for a successful implementation. Otherwise, the technique does not work as the biomass growth stops before the second cultivation. However, the duration of the exponential growth phase is stochastic due to inherent randomness of biological systems. Subsequently, this uncertainty introduces a critical trade-off on the timing of bleed–feed. On the one hand, if we are "too late" to bleed–feed in anticipation of obtaining a higher biomass yield, the bleed–feed opportunity is lost and we harvest the batch with only one cultivation. On the other hand, if we are "too early" to bleed–feed, we may not receive the highest yield from the first cultivation and thus obtain a sub-optimal throughput. Managing this trade-off is crucial for a successful implementation to increase throughput.

The starting biomass amount for the first cultivation (before bleed–feed) is predetermined by manufacturing protocols. However, the biomanufacturer is allowed to control the starting biomass amount of the second cultivation to achieve the highest benefit from bleed–feed.[1] For brevity, we call the problem of optimizing the starting biomass amount as the *replenishment problem*. Industry data shows that the replenishment problem itself involves a critical trade-off: when the starting biomass amount is "too little" for the second cultivation, the time needed to achieve a certain biomass amount is likely to be longer. For example, Figure 3.1(b) illustrates two scenarios with low (b_ℓ) and high (b_h) starting biomass amounts in the second cultivation (assuming the same cell growth rate for both cases). Consider a certain biomass amount to be produced in the second cultivation B. Then, we observe from Figure 3.1(b) that the time needed to produce B units of biomass is longer (i.e., $t_\ell > t_h$) when the starting biomass amount is lower (i.e., $b_\ell < b_h$). This behavior is mainly caused by the exponential growth pattern of biomass, and has complex implications on the expected throughput. When we start the second cultivation with a high biomass, this implies that we obtain (extract) only a little biomass from the first cultivation during bleed–feed (thus lowering the throughput). However, the exponential growth phase is likely to be shorter for the second cultivation (thus increasing the throughput). In contrast, when we start the second cultivation with a low biomass, this implies that we obtain (extract) a high biomass yield from the first cultivation. However, the expected throughput of the system may not necessarily

[1]The starting biomass amount of the second cultivation is controlled by adjusting the amount of biomass extracted from the first cultivation during bleed–feed.

be higher, as the time needed to achieve a certain biomass level is longer in the second cultivation. Therefore, starting the second cultivation with "too much" or "too little" biomass would lead to a sub-optimal throughput for the system. By modeling this complex relationship between the initial biomass and the exponential growth duration, we can make better bleed–feed decisions to maximize the expected throughput.

Based on the aforementioned challenges and trade-offs of biomanufacturers, we formulate our research questions as follows:

- What is the optimal bleed–feed time for the first cultivation and the optimal replenishment amount (i.e., starting biomass amount) for the second cultivation in order to maximize the expected throughput?
- What is the added benefit of jointly optimizing the bleed–feed time and the replenishment amount in practice?
- How much improvement (in the expected throughput) can we achieve by implementing bleed–feed on current practice? Under which problem settings (e.g., risk of entering the stationary phase, setup duration, etc.) does bleed–feed offer a stronger business case for implementation?

To answer these research questions, we developed a stochastic optimization model using renewal reward theory, and analyzed the structural properties of the model. We summarize our contributions as follows. Bleed–feed is a novel technique with a high potential for improving biomanufacturing efficiency. However, its optimal implementation and potential impact is not fully understood. We develop a novel analytical model that combines the biological dynamics with operational trade-offs of bleed–feed. To the best of our knowledge, our study is the first to build an analytical model to jointly optimize the bleed-feed time and the replenishment amount to maximize biomanufacturing throughput. We explore the structural properties of the optimization problem to generate insights on optimal policies and assess the impact of risks. In addition, we present an industry case study from MSD Animal Health (Boxmeer, the Netherlands) to quantify the potential impact of bleed–feed implementation on practice. To generate broader insights, our numerical experiments assess the performance of three practically-relevant strategies as a benchmark: *(i)* "current practice" which does not implement bleed–feed; *(ii)*

"naive bleed–feed policy" which implements bleed–feed in a risk-averse manner without optimization; and *(iii)* "bleed–feed optimization" which assumes a fixed start amount for the second cultivation and optimizes the bleed–feed time alone (inspired from Koca et al. (2021b)). Comparing the performance of these benchmark strategies help us understand the potential benefits of jointly optimizing the bleed–feed time and the replenishment amount on practice. Numerical experiments indicate that our optimization framework can improve the expected throughput by 17% compared to current practice.

Our model is generic to address a wide range of applications including biopharmaceutical research and development, and large-scale biomanufacturing. Although our research has been primarily inspired by the biomanufacturing industry, applications of bleed–feed technology is relevant to several other industries that use fermentation (e.g., food processing industry for wine or yogurt making, biofuel production with ethanol fermentation, etc.).

The remainder of the chapter is organized as follows. We discuss the relevant literature in Section 3.2. We formulate the renewal model in Section 3.3 and explore properties of the optimization problem in Section 3.4. We present a case study in Section 3.5 and concluding remarks in Section 3.6.

3.2. Literature Review

This study is closely related to the following areas: (i) modeling and optimization of fermentation processes in life sciences, and (ii) applications of Operations Research methodologies in biomanufacturing.

In life sciences, many studies work on improving the fermentation titer (i.e. total biomass obtained from a batch) and productivity (i.e. titer produced in the batch per unit time). Commonly, mass balance equations and kinetic models are built to control fermentation systems (Chang et al., 2011; Villaverde et al., 2016; Nakanishi et al., 2017; D'anjou and Daugulis, 2001). Some studies develop predictive models to estimate the relationship between process parameters and fermentation yield. By controlling these parameters, the fermentation titer and productivity are increased (Cunha et al., 2002; Colletti et al., 2011; Handlogten et al., 2018). Additionally, stochastic models are developed to improve fermentation titer and productivity.

These studies often focus on controlling process parameters to support cell growth (Kapadi and Gudi, 2004; Kachrimanidou et al., 2020; Li et al., 2011; Peroni et al., 2005; Wang et al., 2019). However, the life sciences literature mostly focuses on the chemical and biological dynamics of fermentation. To complement the life sciences research, our study combines the biological dynamics of fermentation with operational trade-offs and business implications of bleed–feed, and our insights can be extended to other industries.

The concept of "bleed" (extracting material from the batch) and "feed" (adding fresh medium to the culture) exists in fermentation literature for continuous batch, fed-batch and perfusion fermentation applications (Doran, 1995; Walker, 2017; Muldowney, 2018). However, the implementation of bleed–feed in batch fermentation mode is a new technique, and has unique trade-offs and challenges as described in Section 3.1. Hence, a rigorous analytical modeling of bleed-feed decisions is essential before its implementation, as practitioners need a better understanding on the potential benefits of this new technology.

Applications of Operations Research (OR) methodologies in the biomanufacturing industry is relatively understudied. We refer to Kaminsky and Wang (2015) for a survey of analytical models in biomanufacturing. Limon and Krishnamurthy (2020) analyzed a queuing system using matrix-geometric methods to address resource allocation decisions in downstream purification processes. Zeng et al. (2018) proposed a constrained Gaussian process method to predict scaffold biodegradation. Sahling and Hahn (2019) adopted a heuristic approach to address dynamic lot sizing problem in biomanufacturing. In the OR literature, renewal models are mainly studied in the context of maintenance (Sabri-Laghaie and Noorossana, 2016; Bei et al., 2019; Cherkaoui et al., 2018; Wang, 2000; Rebaiaia et al., 2017) and inventory management (Çetinkaya and Lee, 2000; Karamatsoukis and Kyriakidis, 2009; Chang and Ho, 2010; Boone et al., 2000; Maddah and Jaber, 2008). To the best of our knowledge, our study is the first attempt to develop a stochastic optimization model of bleed–feed decisions using the renewal reward theory to optimize biomanufacturing throughput. To date, only a limited number of studies adopted OR methodologies to optimize fermentation processes in biomanufacturing. For example, Xie et al. (2020) adopted Bayesian network approach to model the dependencies between process parameters and quality to improve the performance of fermentation processes. Martagan et al. (2016) built

a Markov Decision Process (MDP) model to determine condition-based harvesting policies to increase fermentation efficiency. However, none of the aforementioned papers addressed the bleed–feed problem.

Koca et al. (2021b) presented a first attempt in modeling the bleed–feed problem in biomanufacturing (Chapter 2). They built an MDP model to generate condition-based policies that maximize the fermentation yield. Our study is different from Koca et al. (2021b) in several fundamental aspects: we optimize both the bleed–feed time and the replenishment amount (i.e., the biomass amount kept inside the batch after bleed-feed) simultaneously. In contrast, Koca et al. (2021b) only focus on optimizing the bleed-feed time alone and assume a fixed replenishment amount. Our numerical experiments show that joint optimization of bleed–feed time and replenishment amount can lead to a significant improvement in fermentation throughput. In addition, the replenishment problem itself involves unique trade-offs as explained in Section 3.1. Besides, we develop an analytical model to maximize throughput; whereas Koca et al. (2021b) analyze condition-based policies to maximize yield. This implies that our bleed-feed policy is a time-based policy that takes into account the long setup times in biomanufacturing. Such time-based policies are also practically-relevant as they can be easily incorporated into production planning activities.

In summary, this chapter contributes to both life sciences and operations research. The bleed–feed problem is new and practically-relevant with a high potential to improve biomanufacturing throughput. We address the problem of jointly optimizing the bleed-feed time and the replenishment amount by combining the underlying biological dynamics of fermentation with operational trade-offs of bleed–feed. We present an industry case study and provide insights about the potential benefits of bleed–feed.

3.3. Model Formulation

We formulate a renewal model to optimize the bleed–feed time t_b for the first cultivation and starting biomass amount b_2 for the second cultivation, with the objective of maximizing the expected throughput $R(t_b, b_2)$ (i.e., expected yield per time unit). A fermentation (renewal) cycle starts with a bioreactor setup and

continues until a harvest operation. Recall that bleed–feed is performed only in the exponential growth phase but the duration of the exponential growth phase is stochastic (ex-ante). Hence, if the culture is in the exponential growth phase at a certain bleed–feed time t_b (ex-post), then bleed–feed is successful and we obtain two cultivations from one setup. In this case, the second cultivation (after bleed–feed) continues for a fixed processing time t_h, which is specified by manufacturing protocols. If the batch is not in the exponential growth phase at time t_b (ex-post), then bleed–feed fails and the batch is harvested with only one cultivation. A new cycle begins each time the batch is harvested.

We build an optimization model that captures the trade-offs in bleed–feed decisions. On the one hand, the biomanufacturer faces with a trade-off on bleed–feed time t_b ("too soon" versus "too late") which affects the chances of successful bleed–feed. On the other hand, there is a trade-off on starting amount b_2 ("too much" versus "too little") which affects the performance of second cultivation. Both trade-offs have a direct impact on the expected throughput of the system. To establish our objective function and build our optimization model, we first elaborate on the expected length of a fermentation cycle (Section 3.3.1) and expected yield obtained in a fermentation cycle (Section 3.3.2). Table 3.1 summarizes the notation.

3.3.1 Length of a Fermentation Cycle

Each fermentation cycle starts with a bioreactor setup. Setup activities (i.e., cleaning, sterilization, medium and seed culture transfer) are standardized, and their duration is known in advance. We let s denote the fixed duration of a bioreactor setup.

Our model focuses on a *time-based* bleed–feed policy, i.e., we define a fixed bleed–feed time t_b ex-ante and do not change our decision during fermentation. In practice, biomanufacturers often prefer to adopt time-based policies, because of production planning restrictions. For example, there is a no-wait constraint such that the batch needs to immediately continue with subsequent purification operations after harvest. In such settings, time-based policies are easier to implement in practice. We note that the bleed–feed time is negligible, as it takes relatively short time (i.e., only 1-2 minutes) with respect to the overall fermentation time (i.e., several days or weeks until the first bleed–feed). Hence, it is practically-

Table 3.1: Notation used in the renewal model.

b_i	Initial biomass amount for the ith cultivation.
$\mathbb{E}[Y(t_b, b_2)]$	Expected yield obtained in a fermentation cycle when bleed–feed is performed at time t_b and the second cultivation starts with b_2 units biomass.
$f(m)$	Density of batches that enter the stationary phase at a biomass m.
$F(m)$	Long-run fraction of batches that enter the stationary phase at a biomass of at most m.
$g(t\|b)$	Probability density function (pdf) of time to enter the stationary phase given starting amount of b units biomass.
$G(t\|b)$	Cumulative distribution function (cdf) of time to enter the stationary phase given starting amount of b units biomass.
m'	The critical biomass amount.
$m(t, b)$	Biomass accumulation during the exponential growth phase by time t, when the fermentation starts with b units biomass.
μ	Biomass growth rate.
$\nu(m)$	Rate of entering stationary phase under m units of biomass.
$R(t_b, b_2)$	Expected throughput when bleed–feed is performed at time t_b and the second cultivation starts with b_2 units biomass.
s	Bioreactor setup duration.
t_b	Time to bleed–feed.
T_i	Random time to enter the stationary phase at the ith cultivation.
t_i	Realization of the exponential growth phase's duration for the ith cultivation.
t_h	Time to harvest a cultivation.
$Z(t, b)$	Random yield obtained from a cultivation by time t when the starting biomass amount is b.

relevant to assume that the bleed–feed implementation is instantaneous.

Consistent with current good manufacturing practices (CGMPs), the second cultivation (after bleed–feed) needs to be harvested at a fixed harvest time t_h. For example, if we decide to implement bleed–feed at time t_b, this implies that the bioreactor will be occupied during $t_b + t_h$ time units (t_b for the first, and t_h for the second cultivation). Therefore, the fermentation cycle length when we bleed–feed at time t_b is deterministic, and given as $s + t_b + t_h$.

3.3.2 Expected Yield Obtained in a Fermentation Cycle

Let $\mathbb{E}[Y(t_b, b_2)]$ denote the expected biomass yield obtained from a fermentation cycle, when we perform bleed–feed at time t_b and start the second cultivation with b_2 units biomass. In a fermentation process, the expected biomass yield depends on a complex relationship between the starting biomass amount, random time to enter the stationary phase, and biomass growth rate during the exponential growth phase. Therefore, we establish an analytical model to capture the impact of these critical parameters on the expected yield.

The term b_i denotes the biomass amount at the beginning of cultivation $i \in \{1, 2\}$, where $i = 1$ represents the first cultivation (before bleed–feed) and $i = 2$ the second one (after bleed–feed). We note that the first cultivation always starts with a certain biomass amount b_1, which is prespecified by manufacturing protocols. However, as part of bleed–feed decisions, the biomanufacturer can control and optimize the starting biomass amount b_2 for the second cultivation. The decision b_2 affects the risk (probability) of entering the stationary phase.

Let the random variable T_i (with realization t_i) denote the time to enter the stationary phase in cultivation i. The random variable T_i has probability density function $g(t_i|b_i)$, and distribution function $G(t_i|b_i) = P(T_i \leq t_i|b_i)$ for cultivation i. We note that the density function $g(t_i|b_i)$ depends on the starting biomass amount b_i. We made this modeling assumption based on the analysis of three-years of industry data. In particular, we observed that the time needed to achieve a certain biomass level is longer when the starting biomass amount is lower (see Figure 3.1(b) for an illustration based on real-world data). The underlying intuition of this behavior can be explained as follows: when we have more biomass, the limited amount of medium depletes faster. As a result, growth inhibition occurs and the fermentation enters the stationary phase earlier. This implies that a high amount of initial biomass b_2 does not necessarily lead to high yield, because the process is more likely to enter the stationary phase earlier.

We let the function $m(t, b)$ represent the biomass accumulation by time t (as long as the batch is in the exponential growth phase) when the fermentation starts at time $t = 0$ with b units of biomass. Based on well-known fermentation models in

chemical engineering, the biomass accumulation by time $t \geq 0$ is modelled as:

$$m(t, b) = be^{\mu t}, \tag{3.1}$$

where μ denotes the growth rate, and b the initial biomass Doran (1995). The exponential growth continues for the cultivation i until the cultivation enters the stationary phase at the realized time t_i.

In this setting, the yield obtained from cultivation i is random, because the duration of the exponential phase is random with realization t_i. Therefore, we use Equation (3.1) to formulate the random yield obtained from cultivation i when we start with b_i units biomass and stop at time t:

$$Z(t, b_i) = \begin{cases} b_i e^{\mu T_i} & \text{if } T_i \leq t, \\ b_i e^{\mu t} & \text{if } T_i > t. \end{cases} \tag{3.2}$$

Observe from Equation (3.2) that the random yield obtained from cultivation i by time t depends on the realization of T_i. When the exponential growth T_i stops before time t, i.e., $t_i < t$, the biomass yield obtained from cultivation i by time t is $b_i e^{\mu t_i}$ (i.e., recall that biomass accumulates only until the realized time t_i). Otherwise, the biomass yield is $b_i e^{\mu t}$, as the process is still in the exponential growth phase by time t.

We let $\mathbb{E}[Y(t_b, b_2)]$ denote the total expected yield obtained from both the first and the second cultivation under bleed–feed time t_b (for the first cultivation) and starting biomass amount b_2 (for the second cultivation). We formulate $\mathbb{E}[Y(t_b, b_2)]$ as:

$$\mathbb{E}[Y(t_b, b_2)] = \mathbb{E}[Z(t_b, b_1)] + (1 - G(t_b|b_1)) \left[\mathbb{E}[Z(t_h, b_2)] - b_2\right]. \tag{3.3}$$

In Equation (3.3), $\mathbb{E}[Z(t_b, b_1)]$ represents the expected yield of the first cultivation. Using Equation (3.2), $\mathbb{E}[Z(t_b, b_1)]$ can be written as $\mathbb{E}[Z(t_b, b_1)] = \int_0^{t_b} b_1 e^{\mu t_1} g(t_1|b_1) dt_1 + \int_{t_b}^{\infty} b_1 e^{\mu t_b} g(t_1|b_1) dt_1$. The first summand represents the biomass produced from the first cultivation when bleed–feed fails ($t_1 \leq t_b$). The second summand is the biomass production in the first cultivation when bleed–feed is successful ($t_1 > t_b$). In this case, the bleed–feed time limits the cell growth, and yield becomes $b_1 e^{\mu t_b}$. Thus, we can also rewrite the second summand as $\int_{t_b}^{\infty} b_1 e^{\mu t_b} g(t_1|b_1) dt_1 = (1 - G(t_b|b_1)) b_1 e^{\mu t_b}$. The term $1 - G(t_b|b_1)$ in (3.3)

represents the probability of a successful bleed–feed. If bleed–feed is successful, then we produce the second cultivation with the expected yield $\mathbb{E}[Z(t_h, b_2)] - b_2 = \int_0^{t_h} b_2 e^{\mu t_2}\, g(t_2|b_2) dt_2 + \int_{t_h}^{\infty} b_2 e^{\mu t_h}\, g(t_2|b_2) dt_2 - b_2$. The first summand represents the yield obtained from the second cultivation when the exponential growth ends before the harvest time, $t_2 \leq t_h$. The second summand captures the case when the exponential growth does not end before the prespecified harvest time, $t_2 > t_h$. When $t_2 > t_h$, the harvest time t_h limits the biomass growth, and hence the cultivation yield becomes $b_2 e^{\mu t_h}$. Therefore, we have $\int_{t_h}^{\infty} b_2 e^{\mu t_h}\, g(t_2|b_2) dt_2 = (1 - G(t_h|b_2))\, b_2 e^{\mu t_h}$. If bleed–feed is successful, we subtract b_2 from the second cultivation yield since b_2 was produced in the first cultivation and was already in the batch during the second. The randomness in the yield is captured by probability distribution of the exponential growth phase's duration (i.e., $g(t_i|b_i)$ for $i = \{1, 2\}$).

Recall that the replenishment problem involves a critical relationship between the starting amount b_2 and the duration of the exponential growth phase. Because of the exponential growth pattern described in Equation (3.1), it takes longer to achieve a certain biomass amount when b_2 is too small (see Figure 3.1(b) for an illustration). To capture this relationship analytically, we define a rate function: let $\nu(m)$ denote the rate of entering the stationary phase when there are m units biomass inside the bioreactor. The rate function $\nu(m)$ can be obtained from industry data (see Appendix 3.B for details). In our analytical model, we use the rate function $\nu(m(t, b_i))$ to estimate the probability density function $g(t_i|b_i)$, as explained in Section 3.3.2.1.

3.3.2.1 Establishing the Probability Distribution to Stationary Phase from the Rate Function

We now establish the probability density function $g(t|b)$ from the rate function $\nu(m)$. Consider a random time to enter stationary phase T, with distribution function

$$G(t|b) = P(T \leq t|b), \quad t \geq 0,$$

where b represents the initial biomass. The function $\nu(m)$ is the transition rate to the stationary phase when the biomass amount is m. Then, we have

$$g(t|b)dt \quad = \quad P(T > t|b) \cdot P(T < t + dt|T > t, b)$$

$$= \quad (1 - G(t|b))\, \nu(m(t,b))dt.$$

Hence,

$$\frac{g(t|b)}{1 - G(t|b)} = \nu(m(t,b))$$

and integrating this equation yields (by using that $G(0,b) = 0$)

$$\log(1 - G(t|b)) = -\int_0^t \nu(m(s,b))ds,$$

thus,

$$1 - G(t|b) = e^{-\int_0^t \nu(m(s,b))ds}, \quad t \geq 0.$$

The probability density function is $g(t|b) = G'(t|b)$. For the expectation, we get

$$\mathbb{E}[T|b] = \int_0^\infty (1 - G(t|b))dt = \int_0^\infty e^{-\int_0^t \nu(m(s,b))ds}dt.$$

Thus, once we obtain the rate function $\nu(m)$ from the industry data (as explained in Appendix 3.B) we can establish the probability density function of entering the stationary phase $g(t|b)$.

3.3.3 The Objective Function and the Optimization Model

We formulate our optimization model to determine a bleed–feed policy $\pi(t_b, b_2)$ that maximizes the expected throughput $R(t_b, b_2)$. By using the fermentation cycle length presented in Section 3.3.1, and the expected yield of a fermentation cycle in Section 3.3.2, we formulate our objective function as follows:

$$R(t_b, b_2) = \frac{\mathbb{E}[Z(t_b, b_1)] + (1 - G(t_b|b_1))\,[\mathbb{E}[Z(t_h, b_2)] - b_2]}{s + t_b + t_h}. \tag{3.4}$$

Equation (3.4) denotes the expected throughput (i.e., expected yield produced per unit time) as a function of the bleed–feed time t_b (for the first cultivation) and starting amount b_2 (for the second cultivation). Using Equation (3.4), we solve the following two-dimensional optimization problem to maximize the expected throughput:

$$\max \quad R(t_b, b_2) \tag{3.5}$$

$$\begin{aligned} \text{s.t.} \quad & 0 < b_2 \leq b_1, \\ & 0 \leq t_b \leq t_h. \end{aligned}$$

In problem (3.5), the first constraint ensures that the starting biomass b_2 of the second cultivation is lower than b_1. The amount b_1 represents the maximum possible amount to start a cultivation, as defined by current manufacturing protocols. Nevertheless, the protocols provide an opportunity to control the biomass amount b_2 on the range $(0, b_1]$, as part of bleed–feed decisions. In common practice, the harvest time t_h represents a prespecified bound on the cultivation processing time. Hence, the second constraint ensures that the bleed–feed time t_b does not exceed the predefined fermentation time t_h. Our model takes these practical boundaries into account to find an optimal $\pi(t_b, b_2)$ to maximize throughput $R(t_b, b_2)$.

For computational efficiency, we can reduce the problem (3.5) into two sequential, one-dimensional optimization problems as follows. Consider our objective function:

$$\max_{t_b, b_2} R(t_b, b_2) = \max_{t_b} \frac{1}{s + t_b + t_h} \left[\mathbb{E}[Z(t_b, b_1) + (1 - G(t_b|b_1)) \max_{b_2} (\mathbb{E}[Z(t_h, b_2)] - b_2) \right].$$

Note that the expected yield obtained from the second cultivation $\mathbb{E}[Z(t_h, b_2)]$ depends only on the starting amount of the second cultivation b_2 and not on the bleed–feed time t_b. Hence, we can first solve the inner optimization problem (the first one-dimensional problem) to find b_2^* maximizing $\mathbb{E}[Z(t_h, b_2)] - b_2$. Then, we can substitute b_2^* in the original optimization problem to have the second one-dimensional problem as:

$$= \max_{t_b} \frac{1}{s + t_b + t_h} \left[\mathbb{E}[Z(t_b, b_1) + (1 - G(t_b|b_1)) (\mathbb{E}[Z(t_h, b_2^*)] - b_2^*) \right].$$

3.4. Properties of the Optimization Problem

In this section, we consider the optimization problem (3.5) and explore the properties of the expected throughput function $R(t_b, b_2)$. We generate insights on optimal policies (Section 3.4.1) and analyze the impact of system's risks (Section 3.4.2). All proofs are presented in Appendix 3.A.

3.4.1 Insights on Optimal Policies

Insights on the optimal bleed–feed time t_b^*. The cell culture does not transition to the stationary phase before a certain biomass amount is reached. We refer to this biomass amount as the "critical biomass level," m'. Hence, the probability of entering to the stationary phase is typically zero when the actual biomass amount is below this critical biomass m'. In practice, the value of critical biomass m' is known and depends on the cell culture and equipment used in fermentation. Subsequently, the "critical biomass time" t' denotes the time when m' is reached. Then, we have $m' = b_i e^{\mu t'}$, and hence $t' = \frac{1}{\mu} \log \frac{m'}{b_i}$. Therefore, $\nu(m) = 0$ for $m \leq m'$, and $g(t|b_i) = 0$ for $t \leq t'$.

We now explore the impact of parameters m' and t' on optimal bleed–feed policies. For this purpose, we let $\pi(t_b, b_2)$ represent a bleed–feed policy which performs the bleed-feed at time t_b and starts the second cultivation with b_2 units of biomass. We formalize our insights in Lemma 3.1 and Proposition 3.1.

Lemma 3.1 *For a fixed biomass amount b_2, the expected biomass yield $\mathbb{E}[Y(t_b, b_2)]$ under the bleed–feed policy $\pi(t_b, b_2)$ increases in the bleed-feed time t_b for $0 \leq t_b \leq t'$, where t' is the critical biomass time.*

Lemma 3.1 indicates that the expected yield $\mathbb{E}[Y(t_b, b_2)]$ obtained from the bleed–feed policy $\pi(t_b, b_2)$ is increasing in bleed–feed time t_b when $0 \leq t_b \leq t'$. However, this insight is not necessarily valid for the expected throughput. This is because the fermentation cycle time also increases when the expected yield obtained from the batch increases in t_b (where $0 \leq t_b \leq t'$). When the additional yield does not outweigh the extended fermentation time, the expected throughput may decrease in t_b (when $0 \leq t_b \leq t'$). From a practical perspective, Lemma 3.1 implies that it is optimal not to perform bleed–feed before the critical biomass time t'. We further explore this insight in Proposition 3.1.

Proposition 3.1 *$R(t_b, b_2)$ is convex in t_b for $0 \leq t_b \leq t'$ and fixed b_2, if the following condition holds:*

$$\frac{\mu}{2} > \frac{1}{s + t_h}. \tag{3.6}$$

Proposition 3.1 presents a sufficient condition under which the expected throughput

function $R(t_b, b_2)$ is convex in t_b when $0 \leq t_b \leq t'$ for a given b_2. Condition (3.6) sets a lower bound on the growth rate μ in terms of fermentation processing rate (i.e., setup time s and harvest time t_h). This condition may not hold when the biomass growth rate μ is too small or when the fermentation setup and cultivation harvest time is too short. Nevertheless, we validated with industry data that Condition (3.6) is mild and holds for a wide range of practically-relevant settings (i.e., Condition (3.6) holds for the base case and all other scenarios considered in case study in Section 3.5).

Convexity of the expected throughput $R(t_b, b_2)$ in $0 \leq t_b \leq t'$ implies that we need to analyze the boundary conditions (i.e., when $t_b = 0$ and $t_b = t'$) to maximize throughput. Therefore, we compare the two extreme scenarios, namely the bleed–feed policies $\pi(t', b_2)$ (when we bleed–feed at time t') and $\pi(0, b_2)$ (when we bleed–feed at time 0) for a fixed b_2. Note that bleed–feeding at $t_b = 0$ represents the case when bleed–feed is not implemented. Next, we observe that bleed-feeding at time t' is better than bleed–feeding at time 0, if:

$$R(t', b_2) = \frac{\mathbb{E}[Z(t', b_1)] + \mathbb{E}[Z(t_h, b_2)] - b_2}{s + t' + t_h} \geq \frac{\mathbb{E}[Z(0, b_1)] + \mathbb{E}[Z(t_h, b_2)] - b_2}{s + t_h} = R(0, b_2). \quad (3.7)$$

In (3.7), $\mathbb{E}[Z(t', b_1)] = b_1 e^{\mu t'} = m'$ and $\mathbb{E}[Z(0, b_1)] = b_1$. Rearranging the terms, we obtain:

$$\frac{m'}{s + t' + t_h} - \frac{b_1}{s + t_h} \geq \frac{\mathbb{E}[Z(t_h, b_2)] - b_2}{s + t_h} - \frac{\mathbb{E}[Z(t_h, b_2)] - b_2}{s + t' + t_h}. \quad (3.8)$$

When we bleed–feed earlier than t', the bleed–feed is successful because there is no risk of entering the stationary phase when $t_b \leq t'$. Therefore, the expected yield produced from the second cultivation $\mathbb{E}[Z(t_h, b_2)]$ is constant for all $t_b \leq t'$ for a fixed b_2. On one hand, if we bleed–feed at t' instead of at time 0, the fermentation cycle increases, and hence the throughput from the second cultivation decreases. On the other hand, bleed–feeding at time t' leads to increased yield form the first cultivation compared to the case when we bleed–feed at time 0. Thus, (3.8) implies that, if the decrease in throughput in the second cultivation is smaller than the increase in the throughput from the first cultivation, than bleed–feeding at time t' is better than bleed–feeding at time 0, and vice versa. In addition, we validated that (3.8) holds for the industry case study presented in Section 3.5.

Our analysis presents a sufficient condition under which the optimal bleed–feed

time is at t' or later, where $t' = \frac{1}{\mu} \log \frac{m'}{b_1}$ and m' is fixed. Hence, when the initial biomass level b_1 or growth rate μ is small, the time to reach the critical biomass amount t' is high. In such cases, the left hand side of (3.8) decreases, while the right hand side increases. As a result, bleed–feeding at time 0 might be better than bleed–feeding at time t'. We further investigate the optimal bleed–feed time through a comprehensive numerical analysis in Section 3.5.

Insights on the optimal starting biomass amount for the second cultivation b_2^*. Recall that the yield $\mathbb{E}[Z(t_h, b_2)] - b_2$ obtained from the second cultivation (when the bleed–feed is successful) depends only on b_2. Hence, the amount b_2 for which $\mathbb{E}[Z(t_h, b_2)] - b_2$ is maximized would be the optimal start amount for the second cultivation. Proposition 3.2 shows that $\mathbb{E}[Z(t_h, b_2)] - b_2$ is concave in b_2 for a special case, where the rate function $\nu(m)$ is linearly increasing in the biomass m.

Proposition 3.2 *$\mathbb{E}[Z(t_h, b_2)] - b_2$ is concave in b_2 when the rate function $\nu(m)$ is linearly increasing in the biomass amount m.*

Proposition 3.2 focuses on a special case of the problem to study the concavity of $\mathbb{E}[Z(t_h, b_2)] - b_2$ in b_2. We note that the complex nature of the rate function $\nu(m)$ challenges the proof of Proposition 3.2 for more generic cases.

We now present a boundary for the optimal start amount b_2^* by using the relations obtained from industry data: $\nu(m) = 0$ for $m \leq m'$, and $\nu(m) = 1$ for $m > H$, where H denotes the maximum possible biomass obtained from a cultivation due to limitations in cell viability and growth. When $\nu(m) = 0$, the first derivative of $\mathbb{E}[Z(t_h, b_2)] - b_2$ is equal to $e^{\mu t_h} - 1$, which is positive. This means that the expected yield obtained from the second cultivation is increasing in b_2. Thus, we reach the critical biomass amount until the second cultivation ends, i.e., $b_2 e^{\mu t_h} = m'$, resulting in at least $b_2 = \frac{m'}{e^{\mu t_h}}$. Similarly, when $\nu(m) = 1$, the first derivative of $\mathbb{E}[Z(t_h, b_2)] - b_2$ is equal to -1, meaning that the expected yield obtained from the second cultivation is decreasing in b_2. Then, we do not to exceed the maximum biomass amount that can be produced until the second cultivation ends, i.e., $b_2 e^{\mu t_h} = H$, resulting in at most $b_2 = \frac{H}{e^{\mu t_h}}$. Since we have a constraint on b_2 as $b_2 \leq b_1$ in problem (3.5), the upper bound would be $\min(b_1, \frac{H}{e^{\mu t_h}})$. As a result b_2^* would be in the interval $[\frac{m'}{e^{\mu t_h}}, \min(b_1, \frac{H}{e^{\mu t_h}})]$.

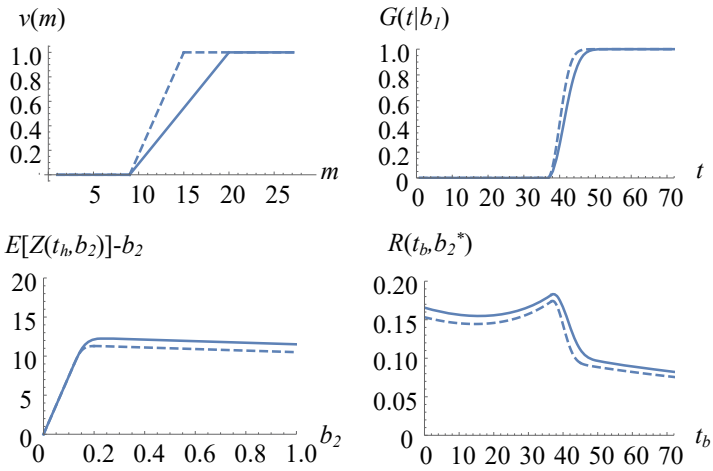

Figure 3.2: Plots of $v(m), G(t|b_1)$, $\mathbb{E}[Z(t_h, b_2)] - b_2$ and $R(t_b, b_2^*)$, for the industry base case (solid line), and a scenario with a higher risk of entering the stationary phase (dashed line).

3.4.2 Insights on the Risk of Entering the Stationary Phase

We evaluate the impact of risk of entering the stationary phase on the expected throughput. For this purpose, we consider two batches with identical initial biomass amount b_1 and growth rate μ, on which we implement the same bleed–feed policy $\pi(t_b, b_2)$. We shall assume that these two batches are identical except for their risk of entering the stationary phase. To assess their difference in risk, we adopt the concept of stochastic ordering Ross (1996).

Proposition 3.3 *If the time to enter the stationary phase for batch A is stochastically larger than the time to enter the stationary phase for batch B, the throughput of batch A under a bleed–feed policy $\pi(t_b, b_2)$ is higher than the throughput of batch B under the same bleed–feed policy.*

If the rate function to enter stationary phase for one batch stochastically dominates the other one (when everything else is identical), then the latter batch has stochastically larger time to enter stationary phase than the former. This means that, when a batch has higher rate to enter stationary phase, it is more likely for this batch to stop growing at early biomass levels. Hence, the expected yield and the expected throughput for this batch will be lower.

To visualize Proposition 3.3, Figure 3.2 presents two scenarios obtained from our case study. The solid line represents the base case obtained from industry data, and the dashed line represents a scenario where the batch has a stochastically lower time to enter the stationary phase. For these two batches, Figure 3.2 plots (i) the rate function of entering the stationary phase $\nu(m)$ over m; (ii) the cumulative distribution function $G(t|b_1)$ over t; (iii) the yield obtained from the second cultivation $\mathbb{E}[Z(t_h, b_2)] - b_2$ over b_2; and (iv) the expected throughput $R(t_b, b_2^*)$ over t_b. Observe from Figure 3.2 that the resulting expected yield from the second cultivation $\mathbb{E}[Z(t_h, b_2)] - b_2$ and the expected throughput $R(t_b, b_2^*)$ are lower for the high-risk batch.

3.5. Case Study

We present a case study from MSD in Boxmeer, the Netherlands. We use the case study to *(i)* demonstrate the room for improvement by the bleed–feed implementation, and *(ii)* investigate the additional benefit of jointly optimizing the bleed–feed time and the starting biomass amount for the second cultivation. For our numerical analysis, we identified a wide range of practically-relevant configurations with our industry partners. We understand that the performance of fermentation processes varies for different cell cultures (i.e., viruses or bacteria), medium (i.e., different types and formulations), and equipment (i.e., bioreactor mechanism and size). Therefore, we present a comprehensive sensitivity analysis to generate managerial insights for the industry. First, we explain the data collection and present the base case (Section 3.5.1). Then, we conduct numerical experiments on critical process parameters, such as, biomass growth rate (Section 3.5.2), failure risks (Section 3.5.3), and setup duration (Section 3.5.4).

3.5.1 Data Collection and the Base Case

In the case study, we use three-years of fermentation data for a specific active ingredient of an animal drug. This data was obtained from various measurements performed by MSD. More specifically, the data consisted of two main data sets including: *(i)* fermentation information (e.g, initial biomass amount, end biomass amount, growth rate, etc.) and *(ii)* physicochemical parameters monitored through

the fermentation (e.g., pH, temperature, oxygen levels, etc.) for each batch. The latter were in terms of plots, showing the process parameter versus time. Specific pattern changes in these plots were used to detect different growth phases during the fermentation. These plots were available in paper format and needed to be transformed into digital form manually. Then, the two data sets were combined into one master data file for determining the case study parameters.

We establish the case study parameters as follows: The fermentation starts with $b_1 = 1$ gram biomass. The biomass growth rate is $\mu = 0.06$ cell divisions per hour. The rate function is obtained from the data as explained in Appendix 3.B. Figure 3.3 depicts the rate function used in the base case and the corresponding probability density function for the time to enter stationary phase (given that $b_1 = 1$ gram). Observe from Figure 3.3(a) that the critical biomass level is $m' = 9$ grams. Due to the growth limiting factors (e.g., cell characteristics and media formulation) the biomass can reach at most $H = 20$ grams. Finally, time to harvest a cultivation is $t_h = 72$ hours, and setup duration is $s = 8$ hours. We refer this setting as the *base case* in our numerical analysis. We note that all parameters presented in this section are representative values to protect confidentiality.

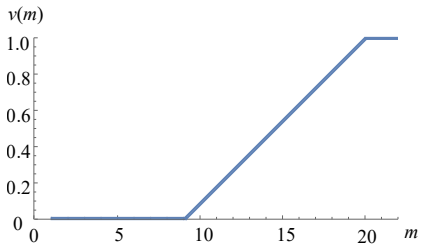

(a) The rate function $v(m)$.

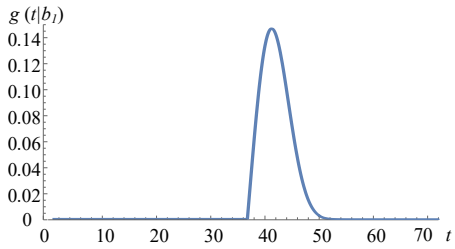

(b) The corresponding probability density function $g(t|b_1)$.

Figure 3.3: The rate function used in the base case (a) and the corresponding probability density function (b).

To establish a benchmark and assess the potential benefits of our model, we consider the following strategies in our case study [2]:

(i) Current practice (CP) harvests the batch at the harvest time t_h without implement-

[2]Note that it is also possible to define another strategy where the starting amount is optimized alone by assuming a predefined bleed–feed time. For ease of exposition, we did not include this strategy in our numerical experiment (i.e., its performance was sensitive to the assumption on bleed–feed time and the results were not practically-relevant).

ing bleed–feed. The harvest time t_h is exogenously prespecified by manufacturing protocols. This strategy represents the current industry practice, as bleed–feed is a novel technique and has not been implemented yet.

(ii) Naive Bleed–feed Policy (NBP) implements bleed–feed at critical biomass time t'. Under this strategy, we assume that b_2 is fixed at $b_2 = b_1$. We consider NBP because it is a simple and practically-relevant heuristic, as Section 3.4 indicates that optimal bleed–feed time can be only at t' or later.

(iii) Bleed–feed optimization (BO) maximizes the expected throughput by finding the optimal bleed–feed time alone. Under this strategy, we assume that b_2 is fixed at $b_2 = b_1$. This strategy aligns with the work of Koca et al. (2021b).

(iv) Joint bleed–feed optimization (JBO) corresponds to our renewal model (described in Section 3.3) and optimizes both the bleed–feed time t_b and the starting biomass amount for the second culture b_2 to maximize the expected throughput.

To assess the room for improvement with bleed–feed implementation, we compute the percentage improvement ($\%I$) in the expected throughput that could have been achieved by NBP, BO and JBO instead of CP. We used Mathematica software to solve the numerical experiments.[3]

We present the results for the base case in Table 3.2. We observe that the expected throughput in CP is $R = 0.156$. It is optimal to bleed–feed at time $t_b^* = 37.3$ for BO and $t_b^* = 37.2$ for JBO. By optimizing the bleed–feed time alone with BO, we can already achieve 13% improvement on the expected throughput. By jointly optimizing the bleed–feed time and the replenishment amount with JBO, the percentage improvement increases to 17%. We obtain that the optimal initial biomass amount for the second cultivation is $b_2^* = 0.2$ grams in JBO. Note that this b_2^* value is less than $b_2 = b_1 = 1$ gram used in BO. This is because JBO considers the relationship between the starting biomass b_2 and the duration of the exponential growth phase, whereas BO omits this trade-off. We observe that the performance ($\%I$) of NBP and BO are similar, yet NBP performs bleed–feed slightly earlier than BO.

Figure 3.4 plots the expected throughput $R(t_b)$ as a function of the bleed–feed

[3]To evaluate JBO, we optimized the bleed–feed time t_b and the replenishment amount b_2 simultaneously. Note that the reduced problem (i.e., solving two sequential, one-dimensional optimization problems) would produce the same results, as described in Section 3.3.3.

Table 3.2: Base case results and the room for improvement on current practice.

CP	NBP			BO			JBO			
R	t'	$R(t')$	$\%I$	t_b^*	$R(t_b^*)$	$\%I$	t_b^*	b_2^*	$R(t_b^*, b_2^*)$	$\%I$
0.156	36.6	0.176	12%	37.3	0.177	13%	37.2	0.2	0.183	17%

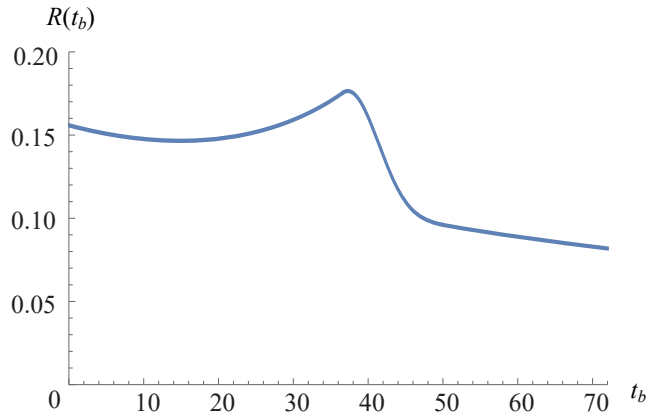

Figure 3.4: Base case throughput $R(t_b)$ versus t_b in BO strategy.

time t_b under the BO strategy (i.e., for $b_2 = b_1 = 1$ gram). First, we observe from Figure 3.4 that the expected throughput $R(t_b)$ is not necessarily concave in t_b. However, we see that the throughput reaches its maximum at $t_b^* = 37.3$, with one peak point. This behavior illustrates the trade-off between the bleed–feed time and biomass yield. Bleed–feeding too early (before $t_b^* = 37.3$) results in lower yield and throughput. Bleed–feeding too late (after $t_b^* = 37.3$) causes a steep decrease in throughput as bleed–feed is more likely to fail.

Figure 3.5 presents a surface plot showing the expected throughput $R(t_b, b_2)$ for JBO strategy as a function of bleed–feed time t_b and the biomass amount b_2. We obtained Figure 3.5 by optimizing t_b and b_2 simultaneously (by solving the two-dimensional optimization problem in Equation (3.5)). Note that reducing this joint optimization problem into two sequential, one-dimensional optimization problems would lead to the same results (as explained in Section 3.3.3). For illustration, Figure 3.6 shows $\mathbb{E}[Z(t_h, b_2)] - b_2$ in b_2 (Figure 3.6(a)), and $R(t_b, b_2^*)$ in t_b (Figure 3.6(b)), which are obtained by solving the reduced optimization problems. We observe from Figure 3.5 and 3.6 that the expected throughput reaches its maximum at $b_2^* = 0.2$ and $t_b^* = 37.2$.

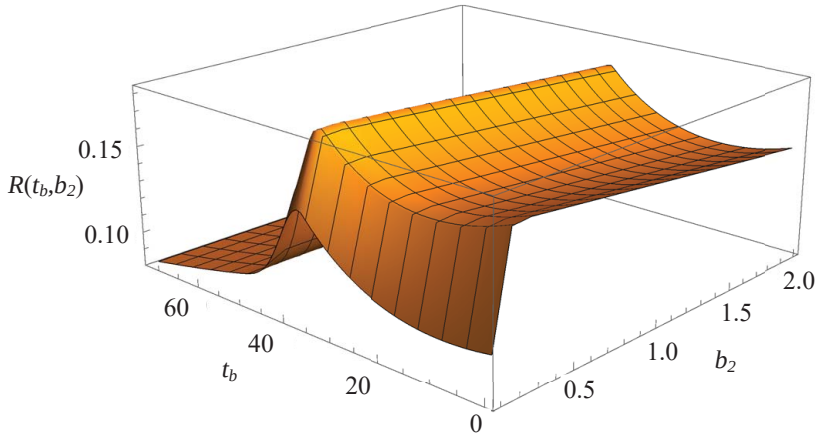

Figure 3.5: Surface plot depicting base case throughput $R(t_b, b_2)$ versus t_b and b_2 in JBO strategy, when t_b and b_2 are optimized simultaneously.

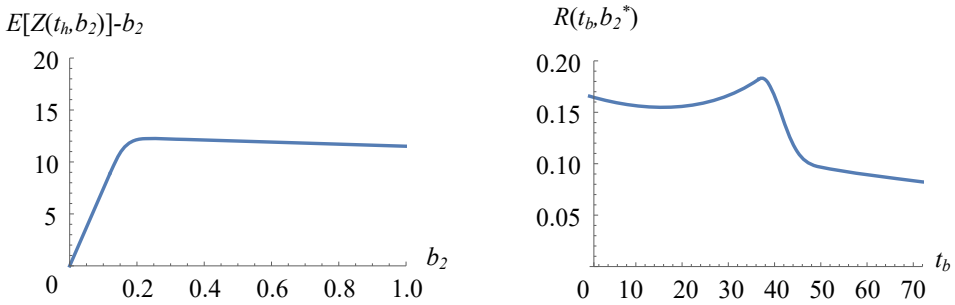

(a) $\mathbb{E}[Z(t_h, b_2)] - b_2$ versus b_2.

(b) $R(t_b, b_2^*)$ versus t_b for b_2^*.

Figure 3.6: Reducing two-dimensional JBO into two sequential one-dimensional optimization problems.

We now investigate the behavior of the objective function under b_2 and t_b. In Figure 3.6(a), the expected yield first increases in b_2 steeply, and then decreases slowly. The underlying reason can be explained as follows: the optimal amount b_2^* in JBO ensures that we can obtain the highest yield possible from the second cultivation by capturing the complex dynamics of cell growth (given biomass growth rate μ, the probability to enter stationary phase and the harvest time t_h). If we start with a lower biomass then b_2^*, the cell growth might not end before the prespecified harvest time t_h in the second cultivation and we harvest with

little yield. Hence, the expected yield increases sharply in b_2 until we reach b_2^* in Figure 3.6(a). In contrast, when we start the second cultivation with more biomass then b_2^*, this does not necessarily imply that we produce high yield in the second cultivation as the growth is limited (due to the trade-off between starting biomass and duration of the exponential growth). When we start with higher biomass than b_2^* in the second cultivation, this means that we extract less biomass from the first cultivation while the yield from second cultivation remains almost constant. Hence, the overall expected yield decreases so as the throughput. Consistent with our result from Section 3.4.1, Figure 3.6(a) shows that $\mathbb{E}[Z(t_h, b_2)] - b_2$ is concave in b_2. In Figure 3.6(b), we observe a similar pattern for $R(t_b, b_2^*)$ in t_b (as in Figure 3.4) and hence omit the discussion. From practical point of view, these observations imply bleed–feeding too late and/or starting the second cultivation with too little biomass is worse off (in terms of expected throughput) than bleed–feeding too early and/or starting with too much biomass.

3.5.2 Sensitivity on Biomass Growth Rate

Biomass growth rate μ can be different across cell cultures based on the biological characteristics (virus or bacteria), medium and equipment used. Hence, we considered the following scenarios for the biomass growth rate: *(i) base case*, $\mu = 0.06$, *(ii) slow growth*, $\mu = \{0.04, 0.045, 0.05, 0.055\}$, and *(iii) fast growth*, $\mu = \{0.065, 0.07, 0.075, 0.08\}$. Table 3.3 presents these scenarios in the first column, and reports the optimal expected throughput R, optimal bleed–feed times t_b^* and the optimal amount b_2^* to start the second cultivation under relevant strategies. Columns $\%I$ show the percentage improvements in the expected throughput under the strategies NBP, BO and JBO compared to CP. Bold entries represent the base case.

We observe from Table 3.3 that as the growth rate μ increases, the throughput R increases in all strategies (since the expected yield increases for a fast-growing batch). With bleed–feed (in BO and JBO strategies), we see that the faster the biomass grows, the earlier the optimal bleed–feed time becomes. The reason is that a fast-growing batch consumes the medium faster and enters the stationary phase earlier. The system tends to bleed–feed earlier to avoid entering the stationary phase and losing the bleed–feed opportunity. Additionally, as growth rate μ increases, the optimal starting amount b_2^* decreases. This is because of the relationship between

Table 3.3: Sensitivity on the biomass growth rate μ.

	CP	**NBP**			**BO**			**JBO**			
μ	R	t'	$R(t')$	$\%I$	t_b^*	$R(t_b^*)$	$\%I$	t_b^*	b_2^*	$R(t_b^*, b_2^*)$	$\%I$
0.04	0.147	54.9	0.147	0%	0	0.147	0%	0	—	0.147	0%
0.045	0.150	48.8	0.155	4%	49.5	0.156	4%	49.4	0.6	0.158	6%
0.05	0.152	43.9	0.163	7%	44.6	0.163	7%	44.6	0.4	0.168	10%
0.055	0.154	39.9	0.170	10%	40.6	0.170	11%	40.6	0.3	0.176	14%
0.06	**0.156**	**36.6**	**0.176**	**12%**	**37.3**	**0.177**	**13%**	**37.2**	**0.2**	**0.183**	**17%**
0.065	0.158	33.8	0.182	15%	34.5	0.183	15%	34.4	0.2	0.190	20%
0.07	0.160	31.4	0.187	17%	32.1	0.188	17%	32.0	0.1	0.196	22%
0.075	0.162	29.3	0.192	18%	30.0	0.194	19%	29.9	0.1	0.202	24%
0.08	0.164	27.5	0.197	20%	28.1	0.198	21%	28.1	0.1	0.207	26%

the staring amount and the duration of the exponential growth phase, as explained in Section 3.1. Consistent with analytical results, NBP performs the bleed–feed slightly earlier than BO. However, we observe that the performance ($\%I$) of NBP and BO are similar in all scenarios considered in Table 3.3.

As biomass grows faster, the biomass yield increases and the fermentation cycle time of the first cultivation decreases (because the optimal policy tends to bleed–feed earlier). Subsequently, throughput R and the improvement percentage $\%I$ increase for both BO and JBO at higher growth rates μ. However, the increase in $\%I$ decreases in μ. This behavior is associated with the exponential growth behavior of the biomass: for fast-growing cells, the exponential growth phase ends earlier and hence the optimal bleed-feed times (and fermentation cycle times) become closer between the scenarios. We also observe from Table 3.3 that the additional benefit obtained by joint optimization JBO increases as the batch grows faster. The underlying intuition of this behavior can be explained as follows. Recall that BO uses a heuristic that starts the second cultivation with the same amount as the first one, i.e., $b_2 = b_1$. However, we observe from Table 3.3 that the optimal amount b_2^* (suggested by JBO) is lower than b_1 (suggested by BO) and decreases in μ. Hence, the difference between b_2^* and b_1 increases when the growth rate μ gets higher. For practitioners, these observations indicate bleed–feed (both BO and JBO strategies) have stronger business case for fast-growing batches, and the additional benefits provided by JBO become more pronounced as the growth rate μ increases.

Table 3.3 indicates that $t_b^* = 0$ when $\mu = 0.04$. This implies that it is optimal not to

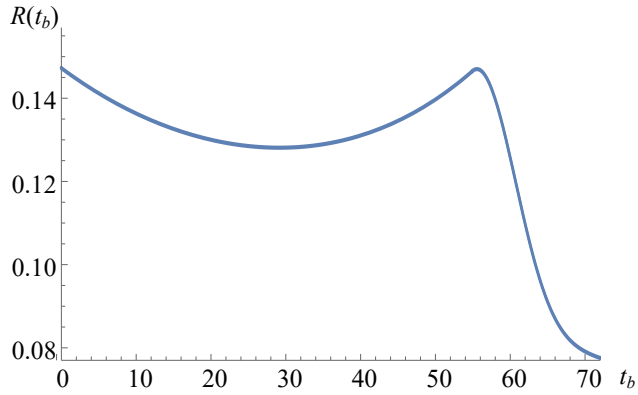

Figure 3.7: Throughput $R(t_b)$ versus bleed–feed time t_b in BO strategy for slow growth ($\mu = 0.04$).

bleed–feed when the biomass growth rate is too small. To visualize this behavior, Figure 3.7 plots the expected throughput $R(t_b)$ as a function of bleed–feed time t_b under BO strategy when $\mu = 0.04$. We observe from Figure 3.7 that the biomass grows so slowly that the system needs too much time until any significant biomass is obtained in the first cultivation. Thus, it becomes optimal to produce only one batch without bleed–feed. We note that this result is consistent with our analysis in Section 3.4.1. For practitioners, these observations imply that bleed–feed is not an attractive option for slow growing cell cultures.

3.5.3 Sensitivity on the Risk of Entering the Stationary Phase

We now investigate the impact of the risk of entering the stationary phase on optimal throughput and bleed–feed policies.

3.5.3.1 Sensitivity on Critical Biomass Level

Recall that the rate of transitioning to the stationary phase starts to be greater than zero when the biomass amount reaches the critical level m'. In our sensitivity analysis, we considered the following scenarios for the critical biomass level: *(i) base case*, $m' = 9$ grams, *(ii) lower critical biomass level*, $m' = \{1, 3, 5, 7\}$ grams, and *(iii) higher critical biomass level*, $m' = \{11, 13, 15\}$ grams. Table 3.4 presents

Table 3.4: Sensitivity on the critical biomass level m'.

	CP	**NBP**			**BO**			**JBO**			
m'	R	t'	$R(t')$	$\%I$	t_b^*	$R(t_b^*)$	$\%I$	t_b^*	b_2^*	$R(t_b^*, b_2^*)$	$\%I$
1	0.040	0	0.040	0%	4.7	0.041	2%	1.4	0.1	0.051	28%
3	0.074	18.3	0.081	9%	20.5	0.082	10%	20.0	0.2	0.090	21%
5	0.104	26.8	0.115	11%	28.2	0.116	12%	28.0	0.2	0.124	19%
7	0.131	32.4	0.147	12%	33.4	0.148	13%	33.3	0.2	0.154	18%
9	**0.156**	**36.6**	**0.176**	**12%**	**37.3**	**0.177**	**13%**	**37.2**	**0.2**	**0.183**	**17%**
11	0.180	40.0	0.204	13%	40.4	0.205	13%	40.4	0.3	0.210	17%
13	0.203	42.7	0.230	13%	43.1	0.231	14%	43.1	0.3	0.236	17%
15	0.223	45.1	0.255	14%	45.3	0.255	14%	45.3	0.3	0.261	17%

these scenarios in the first column, and reports the expected throughput R, optimal bleed–feed time t_b^* and the optimal start amount b_2^* for the second cultivation under relevant strategies. Bold entries represent the base case.

In Table 3.4, we observe that the expected throughput R increases as m' increases for all strategies. We obtain this behavior because, for high m', we can produce higher biomass amounts without failure risk (risk of entering the stationary phase). This leads to higher expected yield and throughput. The additional benefit obtained from JBO decreases as critical biomass level m' increases. The underlying reason can be explained as follows: Recall that b_2 is fixed at $b_2 = 1$ gram under BO. In JBO, b_2^* is increasing in m' and getting closer to $b_2 = 1$. Thus, BO and JBO perform similar as m' increases. We note that except from the scenario $m' = 1$, the improvement percentages of the scenarios are close for a given strategy ($\%I$ ranges between $10 - 14\%$ for BO, and $17 - 21\%$ for JBO). This is because the throughput already increases in m' under CP. Hence, practitioners should keep in mind that BO brings more benefit when m' is high, and JBO brings more benefit when m' is low, although both strategies improve the throughput as m' increases. Consistent with results from Section 3.4.1, Table 3.4 indicates that NBP implements the bleed–feed slightly earlier than BO and JBO. Nevertheless, $\%I$ obtained from NBP and BO strategies are similar, especially for high-risk batches (i.e., higher m' values).

Table 3.4 shows that the optimal bleed–feed time t_b^* increases in m'. This is because the risk of entering the stationary phase starts later when the critical biomass level m' gets higher. Hence, the system can collect higher amounts of biomass without

Table 3.5: Sensitivity on maximum biomass that can be obtained H.

	CP	**NP**			**BO**			**JBO**			
H	R	t'	$R(t')$	$\%I$	t_b^*	$R(t_b^*)$	$\%I$	t_b^*	b_2^*	$R(t_b^*, b_2^*)$	$\%I$
12	0.134	36.6	0.161	20%	36.8	0.161	20%	36.8	0.2	0.168	25%
15	0.144	36.6	0.167	16%	37.0	0.168	17%	37.0	0.2	0.175	21%
20	**0.156**	**36.6**	**0.176**	**12%**	**37.3**	**0.177**	**13%**	**37.2**	**0.2**	**0.183**	**17%**
25	0.167	36.6	0.183	10%	37.5	0.184	11%	37.5	0.3	0.190	14%
30	0.176	36.6	0.190	8%	37.7	0.191	8%	37.6	0.3	0.197	12%
35	0.185	36.6	0.195	6%	37.9	0.197	7%	37.8	0.3	0.203	10%
40	0.193	36.6	0.201	4%	38.1	0.203	5%	38.0	0.4	0.208	8%
45	0.201	36.6	0.206	3%	38.2	0.209	4%	38.1	0.4	0.213	6%
50	0.208	36.6	0.211	2%	38.4	0.214	3%	38.3	0.4	0.218	5%
55	0.215	36.6	0.216	0%	38.5	0.219	2%	38.4	0.4	0.223	4%

risking the bleed–feed. Also, observe that b_2^* increases in m'. The underlying intuition is related to the complex inter-dependency between b_2^*, m' and t_b^*. Notice that the optimal policy tends to bleed–feed earlier at lower values of m'. This also implies that we reach lower biomass amounts at time t_b^* when m' is low. However, we aim to obtain as much biomass as possible from both cultivations. To obtain more from the first cultivation (although t_b^* is low), we tend to extract more biomass from the first cultivation during bleed–feed. For the second cultivation, this leads to lower starting amounts b_2^* for lower m' values.

3.5.3.2 Sensitivity on Maximum Biomass Level

The maximum biomass amount H that can be obtained from a cell culture could be finite because of limited cell viability. Hence, we investigate the following scenarios: *(i) base case*, $H = 20$ grams, *(ii) lower levels of maximum biomass*, $H = \{12, 15\}$ grams, and *(iii) higher levels of maximum biomass*, $H = \{25, 30, 35, 40, 45, 50, 55\}$ grams. We refer to the cases with lower H as "high-risk" batches (as their risk of entering the stationary phase is higher). Table 3.5 presents the results.

Observe from Table 3.5 that the throughput increases in H for all scenarios. The reason is that the expected yield increases when the batch can reach higher biomass values H. We also observe that $\%I$ decreases both in BO and JBO as H increases. This is because the throughput R in CP is already high when H is high. Besides,

the biomass yield obtained from the second cultivation when the bleed–feed is successful is similar to the expected yield obtained from the first cultivation under CP (as all scenarios have the same growth conditions for similar time duration). For these reasons, $\%I$ is lower for higher H values. This indicates that the business case for bleed–feed is stronger when the maximum biomass level H is small (i.e., when cells have a low production capacity).

We observe from Table 3.5 that the optimal bleed–feed time t_b^* increases as the maximum possible biomass amount H increases. The reason can be explained as follows: For higher H values, the risk of entering the stationary phase is lower. Hence, we can bleed–feed later without increasing the risk of failure. Observe also that b_2^* increases as H gets higher under JBO. This is because when H is lower, a smaller amount of initial biomass b_2 would be sufficient to obtain the maximum possible yield from that batch. For practitioners these results indicate that both the bleed–feed time t_b^* and the starting amount b_2^* should be higher when H increases. Lastly, we observe from Table 3.5 that NBP and BO provide similar improvements $\%I$, as their suggested bleed–feed times are close, especially for high-risk batches.

3.5.4 Sensitivity on Setup Duration

The setup time needed for cleaning the bioreactor and transferring the medium and the seed culture into the bioreactor can vary across different bioreactor sizes. Hence, we consider the following cases for the setup duration: *(i) base case*, $s = 8$ hours, *(ii) shorter setups*, $s = \{0, 2, 4, 6\}$ hours, and *(iii) longer setups*, $s = \{10, 12, 14\}$ hours. These scenarios are shown in the first column in Table 3.6. The expected throughput, optimal bleed–feed time and the staring amount for the second cultivation are also presented in Table 3.6 for relevant strategies. Bold entries represent the base case.

In Table 3.6, we observe that $\%I$ ranges between %9 and %16 for BO, and %13 and %20 for JBO when the setup duration changes from 0 to 14 hours. In the extreme case where the bioreactor has no setup ($s = 0$), the benefit of bleed–feed is still %9 for BO, and %13 for JBO. This insight is interesting because it means that the percentage improvement $\%I$ obtained through bleed–feed is not only a result of producing higher biomass yield per single setup, but also of decreased processing time with bleed–feed, i.e., fermentation processing time (excluding setup times) for

Table 3.6: Sensitivity on setup duration s.

	CP	**BO**			**JBO**			
s	R	t_b^*	$R(t_b^*)$	$\%I$	t_b^*	b_2^*	$R(t_b^*, b_2^*)$	$\%I$
0	0.174	37.3	0.190	9%	37.2	0.2	0.197	13%
2	0.169	37.3	0.186	10%	37.2	0.2	0.193	14%
4	0.165	37.3	0.183	11%	37.2	0.2	0.190	15%
6	0.160	37.3	0.180	12%	37.2	0.2	0.186	16%
8	**0.156**	**37.3**	**0.177**	**13%**	**37.2**	**0.2**	**0.183**	**17%**
10	0.153	37.3	0.174	14%	37.2	0.2	0.180	18%
12	0.149	37.3	0.171	15%	37.2	0.2	0.177	19%
14	0.145	37.3	0.168	16%	37.2	0.2	0.174	20%

two cultivations takes $(t_b + t_h)$ with bleed–feed and $(t_h + t_h)$ without bleed–feed (note that the harvest time $t_h \geq t_b$ because the batch is harvested in the stationary phase, whereas bleed–feed is performed in the exponential growth phase). Hence, the benefits of bleed–feed comes from a combination of the reduced processing and setup times and increased levels of biomass production per setup.

Notice from Table 3.6 that expected throughput R decreases as setup duration s increases in all strategies. This is because the setup duration does not affect the expected yield but only prolongs the expected cycle length. For this reason, optimal bleed–feed time t_b^* (both for BO and JBO) and the starting amount b_2^* (for JBO) are robust to setup time s. In addition, we observe that the benefits ($\%I$) of bleed–feed increases as the setup duration s increases (under both BO and JBO).

3.6. Conclusion

Setups are needed before a fermentation process to clean and sterilize the bioreactor. These setups are time consuming as they can take up to ten hours Sharma (2019). Therefore, increasing the fermentation throughput is a critical problem to improve efficiency. To address this problem, we consider a novel approach for eliminating bioreactor setups: bleed–feed.

Bleed–feed enables to skip intermediary bioreactor setups by replenishing some amount of the culture by fresh medium, instead of harvesting the batch. It is a novel

method for prolonging the cell growth in batch fermentation. However, the timing of bleed–feed is important for a successful implementation. Bleed–feed can only be performed in the exponential growth phase of fermentation. As the duration of the exponential growth phase is random, there is a trade-off between implementing bleed–feed too soon versus too late. In addition, the starting biomass amount of the second cultivation (after bleed–feed) affects the expected fermentation yield and throughput. In this work, we formulate the critical trade-offs associated with bleed–feed decisions. We build a stochastic optimization model using renewal reward theory, and determine an optimal bleed–feed time and starting biomass amount to maximize the expected throughput. Our model links the biological dynamics of fermentation with operational trade-offs to support optimal decision-making.

We explore the structural properties of the optimization problem. We generate insights on optimal policies and assess the impact of risks. We show that the throughput function is convex from the start of the fermentation until the critical biomass time under a sufficient condition. Using this result, we discuss the settings under which bleed–feed is not optimal, and understand that the optimal bleed–feed time is at or after the critical biomass time. Based on an industry case study obtained from MSD Animal Health, we present a comprehensive numerical analysis and analyze the potential impact of implementing bleed–feed on current practice. Our numerical analysis shows that bleed–feed can bring benefits. By jointly optimizing the bleed–feed time and amount, our case study (base case) shows that the expected throughput can increase by 17% compared to current practice. We also observe that bleed–feed has a stronger business case for fast-growing cells, high-risk cultures or long setups.

3.A. Proofs

Proof of Lemma 3.1. Take two policies: $\pi(t_b, b_2)$ and $\pi(t', b_2)$, where $0 \leq t_b \leq t'$, for all b_2. We compare the expected yield under these policies and show $\mathbb{E}[Y(t_b, b_2)] \leq \mathbb{E}[Y(t', b_2)]$ for $0 \leq t_b \leq t'$. From the fact that $g(t_b|b_i) = 0$ for $t_b \leq t'$, we have:

$$\mathbb{E}[Y(t_b, b_2)] = b_1 e^{\mu t_b} + \mathbb{E}[Z(t_h, b_2)] - b_2 \leq b_1 e^{\mu t'} + \mathbb{E}[Z(t_h, b_2)] - b_2 = \mathbb{E}[Y(t', b_2)],$$

which concludes the proof. □

Proof of Proposition 3.1. Consider a bleed–feed policy $\pi(t_b, b_2)$, where $0 \leq t_b \leq t'$ for a fixed b_2. Under the policy $\pi(t_b, b_2)$, we prove convexity of the throughput function by showing that $\frac{\partial^2 R(t_b,b_2)}{\partial t_b^2} > 0$. Since $g(t_b|b_i) = 0$ for $t_b \leq t'$, we write $R(t_b, b_2)$ as:

$$R(t_b, b_2) = \frac{b_1 e^{\mu t_b} + \mathbb{E}[Z(t_h, b_2)] - b_2}{s + t_b + t_h}. \tag{3.9}$$

Hence,

$$\frac{\partial^2 R(t_b, b_2)}{\partial t_b^2} = \frac{\mu^2 b_1 e^{\mu t_b}}{s + t_b + t_h} - \frac{2\mu b_1 e^{\mu t_b}}{(s + t_b + t_h)^2} + \frac{2b_1 e^{\mu t_b}}{(s + t_b + t_h)^3} + \frac{2\mathbb{E}[Z(t_h, b_2)] - 2b_2}{(s + t_b + t_h)^3}. \tag{3.10}$$

We now show that if (3.6) holds, then $\frac{\partial^2 R(t_b,b_2)}{\partial t_b^2} > 0$. Rearranging (3.6) we have that:

$$0 > \frac{1}{s + t_h} - \frac{\mu}{2}.$$

Multiplying both sides of the inequality by μ and rearranging the terms we obtain:

$$\begin{aligned} 0 &> \frac{\mu}{s + t_b + t_h} - \frac{\mu^2}{2} && (3.11)\\ &> \frac{\mu}{s + t_b + t_h} - \frac{1}{(s + t_b + t_h)^2} - \frac{\mu^2}{2}, && (3.12) \end{aligned}$$

where (3.11) follows since $\frac{\mu}{2} > \frac{1}{s+t_h} \geq \frac{1}{s+t_b+t_h}$ for $t_b \geq 0$, and (3.12) follows from the fact that $\frac{1}{(s+t_b+t_h)^2} > 0$. Multiplying both sides of (3.12) by $\frac{2b_1 e^{\mu t_b}}{s+t_b+t_h}$ we obtain:

$$\begin{aligned} 0 &> \frac{2\mu b_1 e^{\mu t_b}}{(s + t_b + t_h)^2} - \frac{2b_1 e^{\mu t_b}}{(s + t_b + t_h)^3} - \frac{\mu^2 b_1 e^{\mu t_b}}{s + t_b + t_h} \\ &> \frac{2\mu b_1 e^{\mu t_b}}{(s + t_b + t_h)^2} - \frac{2b_1 e^{\mu t_b}}{(s + t_b + t_h)^3} - \frac{\mu^2 b_1 e^{\mu t_b}}{s + t_b + t_h} - \frac{2\mathbb{E}[Z(t_h, b_2)] - 2b_2}{(s + t_b + t_h)^3}, && (3.13) \end{aligned}$$

where (3.13) follows from $\frac{2\mathbb{E}[Z(t_h,b_2)]-2b_2}{(s+t_b+t_h)^3} > 0$. Rearranging (3.13) we obtain:

$$\frac{\partial^2 R(t_b,b_2)}{\partial t_b^2} = \frac{\mu^2 b_1 e^{\mu t_b}}{s+t_b+t_h} - \frac{2\mu b_1 e^{\mu t_b}}{(s+t_b+t_h)^2} + \frac{2b_1 e^{\mu t_b}}{(s+t_b+t_h)^3} + \frac{2\mathbb{E}[Z(t_h,b_2)]-2b_2}{(s+t_b+t_h)^3} > 0, \tag{3.14}$$

which completes the proof. □

Proof of Proposition 3.2. Take a linearly increasing rate function $\nu(m) = c\,m$ for $c > 0$ (i.e., $\nu(m(t,b_2)) = c\,m(t,b_2) = c\,b_2 e^{\mu t}$). We prove concavity of $\mathbb{E}[Z(t_h,b_2)] - b_2$ in b_2 by showing that $\frac{\partial^2(\mathbb{E}[Z(t_h,b_2)]-b_2)}{\partial b_2^2} < 0$. Using $\nu(m(t,b_2)) = c\,m(t,b_2) = c\,b_2 e^{\mu t}$, we have:

$$\begin{aligned}\mathbb{E}[Z(t_h,b_2)] - b_2 &= \int_0^{t_h} b_2 e^{\mu t_2}\, g(t_2|b_2) dt_2 + (1 - G(t_h|b_2))\, b_2 e^{\mu t_h} - b_2 \\ &= -b_2 + b_2 e^{-\frac{c\,b_2(-1+e^{\mu t_h})}{\mu} + \mu t_h} + \frac{b_2(c - c\,e^{\frac{c\,b_2 - c\,b_2 e^{\mu t_h} + \mu^2 t_h}{\mu}}) + \mu - e^{-\frac{c\,b_2(-1+\mu t_h)}{\mu}}\mu}{c}.\end{aligned}$$

Then,

$$\frac{\partial^2(\mathbb{E}[Z(t_h,b_2)]-b_2)}{\partial b_2^2} = -\frac{c\,e^{-\frac{c\,b_2(-1+e^{\mu t_h})}{\mu}}(-1+e^{\mu t_h})^2}{\mu} < 0,$$

which completes the proof. □

Proof of Proposition 3.3. Take two batches as batch A and B with identical b_1 and μ, with the rate function of entering the stationary phase for batch B dominating A. Let G^j denote the distribution function of time to enter stationary phase for batch $j = \{A,B\}$ and T_i^j denote the random time to enter stationary phase for batch $j = \{A,B\}$; T_i^A being distributed according to G^A, and T_i^B according to G^B, for cultivation $i = \{1,2\}$. Then, t_i^j denotes the realization of random time to enter stationary phase for batch $j = \{A,B\}$ in cultivation $i = \{1,2\}$. Take a bleed–feed policy $\pi(t_b,b_2)$. $R^j(t_b,b_2)$ denotes the throughput and $\mathbb{E}[Y^j(t_b,b_2)]$ the expected yield under bleed–feed policy $\pi(t_b,b_2)$ for batch $j = \{A,B\}$. From Equation (3.3),

the expected yield for batch j under policy $\pi(t_b, b_2)$ is given as:

$$\mathbb{E}[Y^j(t_b, b_2)] = \mathbb{E}[Z^j(t_b, b_1)] + (1 - G^j(t_b|b_1)) \left[\mathbb{E}[Z^j(t_h, b_2)] - b_2\right].$$

Because the rate function of entering the stationary phase for batch B dominates that of A, the random time to enter stationary phase for batch A is stochastically larger than that of batch B, $T_i^A \succeq T_i^B$. By coupling (Proposition 9.2.2 from Ross (1996)), we have $t_i^A > t_i^B$ for every realization of T_i^A and T_i^B (considering a given cultivation i). Thus, for the yield in the batch from the second cultivation we can say that $Z^A(t_h, b_2) \geq Z^B(t_h, b_2)$ for each realization, so $\mathbb{E}[Z^A(t_h, b_2)] \geq \mathbb{E}[Z^B(t_h, b_2)]$ by Proposition 9.1.2 from Ross (1996). Similarly, we can say that $\mathbb{E}[Z^A(t_b, b_1)] \geq \mathbb{E}[Z^B(t_b, b_1)]$. By definition of stochastic ordering, $1 - G^A(t_b|b_1) > 1 - G^B(t_b|b_1)$ holds. Thus, $\mathbb{E}[Y^A(t_b, b_2)] \geq \mathbb{E}[Y^B(t_b, b_2)]$. If we divide both sides by the cycle length under the bleed–feed policy $\pi(t_b, b_2)$ we obtain:

$$R^A(t_b, b_2) = \frac{\mathbb{E}[Y^A(t_b, b_2)]}{s + t_b + t_h} \geq \frac{\mathbb{E}[Y^B(t_b, b_2)]}{s + t_b + t_h} = R^B(t_b, b_2),$$

which completes the proof. □

3.B. Establishing the Transition Rate Function from Industry Data

We explain a procedure to obtain the rate function from industry data. Let $\nu(m)$ denote the rate of entering the stationary phase, and $F(m)$ denote the (long-run) fraction of batches that enter the stationary phase at a biomass of at most m, and $f(m)$ is the corresponding density, i.e., $f(m) = F'(m)$. If Δ is a small time interval, then the probability that a batch will enter the stationary phase at biomass between m and $m(1 + \mu\Delta)$ (recall that the growth is exponential), given that at time t the batch has m units biomass satisfies

$$f(m)\mu\, m\Delta = \nu(m)\Delta(1 - F(m)).$$

Hence,

$$\frac{f(m)}{1-F(m)} = \frac{\nu(m)}{\mu\, m}.$$

The function $F(m)$ can be directly estimated from the industry data, m discretized with stepsize δ. If we then approximate $f(m) \approx F((m+1)\delta) - F(m\delta)$, we obtain as estimate for the stationary phase function

$$\frac{F((m+1)\delta) - F(m\delta)}{1-F(m\delta)} \approx \frac{\nu(m\delta)}{\mu m}$$

or rewritten,

$$\nu(m\delta) \approx \mu m \frac{F((m+1)\delta) - F(m\delta)}{1-F(m\delta)} \text{ for } m = 0, \delta, 2\delta \ldots.$$

This rate function is used to establish the probability of entering the stationary phase, as explained in Section 3.3.2.1.

4

Optimal Bleed–Feed Decisions under Practical Constraints

4.1. Introduction

In this chapter, we extend our renewal model from Chapter 3. Different from Chapter 3, we now take *accumulation of waste* in the batch and the corresponding purification costs into account, and we find the optimal time to bleed–feed to maximize the *expected fermentation profit*. In addition, this chapter considers *practically relevant constraints* on bleed–feed time to ensure that bleed–feed happens when operators are available in the company, and that we implement bleed–feed successfully with a certain probability.

Recall that biomanufacturing operations consists of upstream processing (USP) and downstream processing (DSP). Upstream processing is the first step where the cells are grown. USP includes operations such as preparation of seed culture and medium, fermentation process and harvest. Downstream processing refers to purification and finishing operations. In DSP, biomass is separated from the impurities in the batch and prepared for storage until its delivery. We focus on upstream fermentation processes in this chapter.

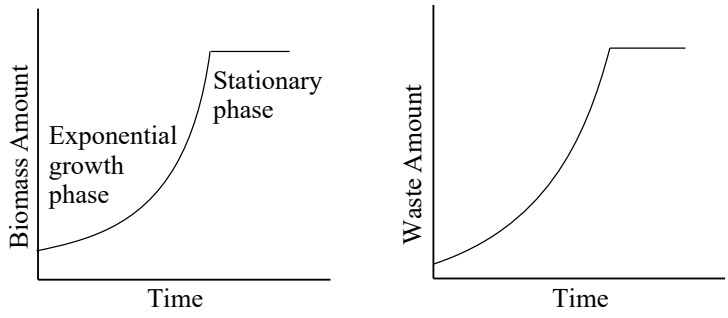

(a) Biomass growth. *(b)* Waste accumulation.

Figure 4.1: Biomass growth (a) and waste accumulation (b) over time without bleed–feed.

Fermentation typically take place in a bioreactor which is a stainless-steel vessel, providing a controlled environment for cell growth. Fermentation starts with a bioreactor setup, where the bioreactor is cleaned and sterilized and seed culture (initial biomass) with a suitable medium is placed into the bioreactor. The seed culture uses the medium to grow. The growth follows a specific pattern as shown in Figure 4.1(a). Observe that the fermentation starts with a small amount of initial biomass. This biomass uses the medium and reproduce. This phase is the *exponential growth phase*. In the batch production, medium is added only once, at the beginning of the fermentation process. As the biomass amount increases in the exponential growth phase, it consumes the limited amount of medium and nutrients deplete in the batch. As a result, the cell growth stops and the cells enter to the *stationary phase*. Commonly, the batch is harvested in the stationary phase.

Along with biomass growth, byproducts (also called as impurities, waste) accumulate in the batch as a result of metabolic activities of cells during fermentation. Ammonia and lactate are examples of byproducts. Inspired by industry data, Figure 4.1(b) illustrates accumulation of waste over time. Waste accumulation deteriorates the culture environment by increasing the toxicity in the batch. Hence, excessive amount of byproducts inhibits cell growth and decreases the batch quality. After harvesting the batch, the output of the fermentation process, i.e., homogeneous mixture of biomass and byproducts, is transferred to the downstream processing for purification.

Following the harvest, the bioreactor is set up for the new fermentation process.

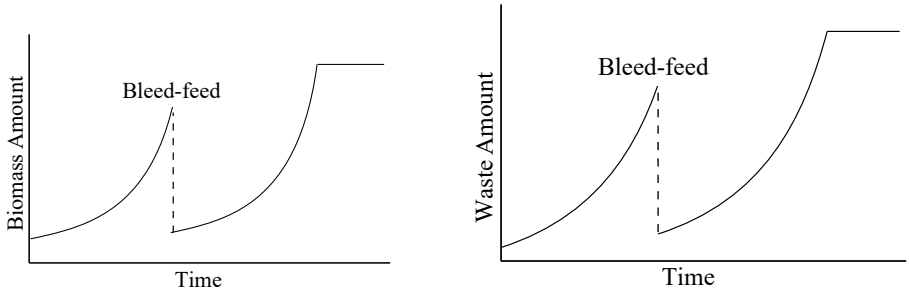

(a) Biomass growth with bleed-feed. *(b)* Waste accumulation with bleed-feed.

Figure 4.2: Biomass growth (a) and waste accumulation (b) over time with bleed–feed.

These setups are time consuming and expensive. For instance, a bioreactor setup can take up to ten hours (Sharma, 2019; Yang and Sha, 2019). In addition, the consumables and reagents used in cleaning and sterilization in each setup constitute around 16% of the total fermentation costs (Oyebolu et al., 2019; Mahal et al., 2021). This results in long bioreactor occupation time and less fermentation profit obtained per time unit. Hence, there is a strong business case for biomanufacturers to eliminate some of the setups. For this purpose, *bleed–feed* is a promising technique. The main dynamics of bleed–feed are demonstrated in Figure 4.2. When bleed–feed is implemented, some predetermined fraction of the culture in the batch is extracted (bleed), and fresh medium is added to the bioreactor (feed). Then the remaining biomass in the culture acts as a seed culture and the growth continues (Figure 4.2(a)). Hence, bleed–feed enables practitioners to skip an intermediary setup and produce two cultivations from a batch. The batch is harvested when the second cultivation reaches its predetermined harvest time.

Although a promising technique to increase fermentation profit, determining the bleed–feed time is not straightforward. We can bleed–feed only in the exponential growth phase for a successful implementation. Otherwise, the biomass growth stops before the next cultivation and the technique does not work. However, the exponential growth phase duration is stochastic due to the inherent randomness of biological systems. Also, the amount of byproducts accumulated in fermentation has an important effect on purification workload in the downstream processing (Farid, 2007; Gronemeyer et al., 2014). For instance, a batch with high impurity levels may require multiple steps of certain purification operations and inspection steps to ensure batch quality, therefore increasing the costs. In Figure 4.2(b) the

remaining waste also continues to accumulate after the bleed–feed, leading to waste from two cultivations. In this setting, if we are "too early" to bleed–feed, we may not receive the highest yield, and hence the highest revenue from the first cultivation. In addition, more impurity will accumulate in the batch as a result of producing two cultivations, and purification cost will be higher. Contrarily, if we are "too late", the bleed–feed opportunity is lost and we harvest the batch with one cultivation. This means that we obtain the revenue corresponding to one cultivation only. Yet, the impurity amount and the purification cost will also be less in this case (as it will be associated to one cultivation only). Managing this trade-off and understanding how the cost parameters affect the bleed–feed decisions are important aspects for increasing the expected profit per time unit with bleed–feed.

In addition, bleed–feed implementation requires operators to take certain actions (such as initiating the medium transfer and extracting certain fraction from the batch). However, in a biomanufacturing company working in shifts, no operators are available during certain time periods. In this case, it is crucial to ensure that bleed–feed is implemented during a shift.[1] Also, practitioners might tolerate some certain probabilities of bleed–feed failure only. For instance, they might not want to take the risk of missing the bleed–feed and adjust their bleed–feed time in a risk-averse manner. Such restrictions limit the time that bleed–feed can be implemented, and the benefits obtained from it compared to flexible cases. Hence, we formulate our research questions as follows:

- When to implement bleed–feed to maximize the expected profit per time unit from a fermentation, considering the impurity level in the batch?
- How to ensure that bleed–feed takes place during a shift, and that bleed–feed is implemented successfully with a certain probability level?
- How is the benefit obtained from bleed–feed affected by the shift and the chance constraints? What is the value of flexibility (i.e., having no restrictions on bleed–feed time) in bleed–feed decisions? Under which settings adopting bleed–feed is not desirable?

In order to answer these questions, we extend our renewal model from Chapter 3.

[1] This does not need to hold for the harvest time. Bioreactors can be adjusted so that at a specific time the culture is frozen. This stops any metabolic activities in the culture, enabling the operators harvest the batch later if harvest time does not take place in a shift.

We determine the optimal bleed–feed time to maximize the expected profit per time unit under shift and chance constraints. We present a numerical analysis to demonstrate the use of our model, and to investigate the value of flexibility when adopting bleed–feed under practically relevant restrictions.

Fermentation profit per unit time has been considered in life sciences literature. Jia et al. (2007) built mass balance equations and kinetic models to identify key parameters in evaluating fermentation profit per time unit. Yuan et al. (2009) developed predictive models to find scheduling approaches to maximize profit of a batch over its production time. However, these studies focus on chemical and biological dynamics of fermentation. We combine the biological dynamics of fermentation with operational trade-offs of bleed-feed, and propose a generic model that can be extended to other industries. Martagan et al. (2016) developed an MDP model to improve fermentation profit. In addition to yield production and its revenue, they also model waste accumulation and associated purification cost. However, they determine condition-based harvest policies, and they did not address the bleed–feed problem. Koca et al. (2021b) presents the first attempt for modeling bleed–feed (Chapter 2). They built an MDP model to determine condition-based bleed–feed policies to maximize batch yield and assumed a fixed initial biomass amount for the second cultivation. Next, Koca et al. (2021a) developed a renewal model to optimize the bleed–feed time and the initial biomass amount for the second cultivation jointly (Chapter 3). They generate time-based bleed-feed policies to optimize the throughput (expected batch yield per time unit). However, none of these studies consider the fermentation profit, waste accumulation, and costs associated to purification. In this chapter, we extend the renewal model from Koca et al. (2021a). We model the waste accumulation, and its effects on the exponential growth phase duration. We consider the costs and revenues associated to fermentation process to find optimal bleed–feed time to maximize the fermentation profit per time unit. In addition, practical constraints have not been taken account in the previous studies. We include a shift constraint in our model to ensure that the bleed–feed is implemented when operators are available. We also include a chance constraint to capture practitioner's risk-averse behavior. We investigate the value of flexibility in decision making, by relaxing these constraints. We note that Koca et al. (2021b) and Koca et al. (2021a) considered risk-averse strategies in bleed–feed implementation. Having a chance constraint is different for the following reasons: *(i)* If we also consider a shift restriction on

bleed–feed time, the risk-averse strategy from these studies might be infeasible. By having a change constraint (rather than considering a risk-averse strategy) we can capture risk-averse behavior under shift restrictions. *(ii)* With a chance constraint, we can consider different levels of tolerating the risk of bleed–feed failure.

Our work contributes to both life sciences and operations research. Bleed–feed problem is a new and relevant problem for biomanufacturing, with high potential of improving efficiency. We develop an analytical model that combines biological dynamics of living systems and operational trade-offs of bleed–feed. This study is the first in finding the optimal bleed–feed time that maximizes the fermentation profit, considering practically relevant restrictions on the bleed–feed time and effects of waste accumulation on exponential growth phase duration. We present a generic model that can be adopted in other industries with fermentation processes. We demonstrate the use of our model with a numerical analysis. We investigate the value of flexibility in bleed–feed decisions by relaxing the constraints and generate insights on the bleed–feed implementation for different production configurations. Our numerical analysis revealed that it is not necessarily better to bleed–feed earlier if bleed–feed time does not take place in a shift, and chance constraints have more impact for low-risk batches. In addition, we observe that bleed–feed does not bring benefit for batches with fast waste accumulation, or if the bleed–feed time has both the shift and the chance constraint.

The remainder of the chapter is organized as follows. In Section 4.2 we formulate the renewal model. We present the numerical analysis in Section 4.3. Section 4.4 concludes the chapter.

4.2. Model Formulation

We formulate a renewal model to find the optimal bleed–feed time t_b to maximize the expected fermentation profit per time unit $J(t_b)$. A fermentation cycle starts with a bioreactor setup and continues until the batch is harvested. Recall that bleed–feed can only be implemented in the exponential growth phase. If at the pre-determined bleed–feed time t_b the culture is still in the exponential growth phase, the bleed–feed is successful. Then, we extract a fraction ψ from the batch mixture, add fresh medium in the bioreactor and let the remaining biomass grow.

This way we produce two cultivations from one setup. The second cultivation (after the bleed–feed) is harvested after a fixed cultivation time t_h. Then, fermentation profit captures the revenue obtained from the biomass produced in the batch, the purification cost of waste accumulated during the two cultivations, and the direct costs of bleed–feed and harvest operations. If the batch is not in the exponential growth phase at time t_b, then bleed–feed fails and the batch is harvested only with one cultivation. This means that we obtain revenue and incur purification costs from one culture, and we incur the direct harvest cost.

Our renewal model captures the trade-offs on the bleed–feed time, and the complex biological dynamics of fermentation (i.e., the impact of biomass and waste amount on the exponential growth phase duration). In addition, we include practically relevant constraints in our optimization problem, to ensure that *(i)* bleed–feed is implemented during a shift, and *(ii)* with a certain probability the bleed–feed implementation is successful. We first elaborate on the expected length of a fermentation cycle (Section 4.2.1) and expected profit obtained in a fermentation cycle (Section 4.2.2) to establish our objective function and build our optimization model (Section 4.2.3). Table 4.1 summarizes the notation we used in the model.

4.2.1 Length of a Fermentation Cycle

Each fermentation cycle starts with a bioreactor setup. Setup activities (i.e., cleaning, sterilization, medium and seed culture transfer) are standardized, and their duration is known in advance. We let s denote the fixed duration of a bioreactor setup.

Our model generates a time-based bleed–feed policy, meaning that we define a fixed bleed–feed time t_b and do not change our decision during fermentation. In practice, biomanufacturers prefer adopting time-based policies, because of production planning restrictions. For example, there is a no-wait constraint such that the batch needs to immediately continue with subsequent purification operations after harvest. In such settings, time-based policies are easier to implement. We note that the bleed–feed time takes relatively short time (i.e., only 1-2 minutes) with respect to the overall fermentation time (i.e., several days or weeks until the first bleed–feed), and it is negligible.

Consistent with current good manufacturing practices (CGMPs), we harvest the

Table 4.1: Notation used in the renewal model.

η	Waste accumulation rate.
μ	Biomass growth rate.
ψ	Fraction of the batch mixture to be extracted during bleed–feed.
ω_i	Initial waste amount for the ith cultivation.
b_i	Initial biomass amount for the ith cultivation.
c_b	Bleed–feed cost.
$c_p(w)$	Purification cost incurred from w units of waste.
c_h	Harvest cost.
$g(t\|b,\omega)$	Probability density function of time to enter stationary phase at the ith cultivation given b units of initial biomass and ω units of initial waste.
$G(t\|b,\omega)$	Cumulative distribution function of the time to enter stationary phase given b units of initial biomass and ω units of initial waste.
$J(t_b)$	Expected profit per unit time obtained from a fermentation when bleed–feed is implemented at time t_b.
$m(t,b)$	Biomass growth during the exponential growth phase by time t, when the fermentation starts with b units biomass.
$P(t_b)$	Random profit obtained from a fermentation cycle if bleed–feed is implemented at time t_b.
$r(m)$	Revenue obtained from m units biomass amount.
s	Bioreactor setup duration.
t_b	Time to bleed–feed.
T_i	Random time to enter the stationary phase at the ith cultivation.
t_i	Realization of the exponential growth phase's duration for the ith cultivation.
t_h	Time to harvest a cultivation.
$w(t,\omega)$	Waste accumulation during the exponential growth phase of the biomass by time t, when the initial waste amount is ω units.

second cultivation (after bleed–feed) at a fixed cultivation time t_h. If we decide to implement bleed–feed at time t_b, this implies that the bioreactor is occupied for $t_b + t_h$ time units (t_b for the first, and t_h for the second cultivation). Therefore, the fermentation cycle length when we bleed–feed at time t_b is deterministic, and given as $s + t_b + t_h$.

4.2.2 Expected Profit Obtained in a Fermentation Cycle

In a fermentation process biomass accumulates in the batch along with byproducts. Then, output of a cultivation is a homogeneous mixture of biomass and waste. When we stop the cultivation (either with harvest or bleed–feed), we earn revenue associated to the final biomass level, and incur purification cost related to the waste amount. In addition, we incur a direct cost of stopping the cultivation. Hence, fermentation profit depends on the relationship between biomass and waste accumulation, their complex relationship with exponential growth phase duration, and related revenues and costs. Our renewal model captures these parameters to establish expected fermentation profit.

We use the term b_i to denote the initial biomass amount for cultivation $i \in \{1, 2\}$, where $i = 1$ represents the first cultivation (before bleed–feed) and $i = 2$ represents the second cultivation (after bleed–feed). Fermentation process starts with a certain biomass amount, denoted as b_1. Every time we start a batch, there is also a small amount of impurities in the seed culture, accumulated during preculture activities. We denote this initial waste amount as ω_1. Initial waste ω_1 is usually close to zero. During bleed–feed, we extract a known fraction $\psi \in (0, 1)$ of the batch mixture. Hence, the remaining fraction $1 - \psi$ of the biomass and impurities produced in the first cultivation until the bleed–feed time t_b correspond to the start amount for the second one (i.e., b_2 and ω_2, respectively).

Let the random variable T_i (with realization t_i) denote the time to enter the stationary phase in cultivation i. The random variable T_i has probability density function $g(t_i|b_i, \omega_i)$, and distribution function $G(t_i|b_i, \omega_i) = P(T_i \leq t_i|b_i, \omega_i)$ in cultivation i. Note that the probability of entering the stationary phase depends on the initial biomass amount b_i and the initial waste amount ω_i. More specifically, a batch with higher initial biomass and waste is likely to have a shorter exponential growth phase. The underlying intuition of this behavior can be explained as follows: a batch with a higher biomass amount consumes the limited amount of medium faster. As a result, the nutrients deplete, and the cells lose viability earlier. In addition, impurities deteriorate the culture environment and increase the toxicity in the batch. Then, the growth inhibition is likely to occur faster, and the cells enter the stationary phase. By modeling this relationship, our model captures the random exponential growth duration and its complex underlying biological relationships

with the biomass and the impurity levels.[2]

We let the function $m(t, b)$ represent the biomass growth by time t, when the fermentation starts at time $t = 0$ with b units biomass. We note that $m(t, b)$ is valid as long as the batch is in the exponential growth phase. Based on well-known fermentation models in chemical engineering, the biomass accumulation by time $t \geq 0$ is given as (Doran, 1995):

$$m(t, b) = be^{\mu t}, \tag{4.1}$$

where μ denotes the cell growth rate and b the initial biomass level. The growth continues until the batch enters the stationary phase.

Along with the biomass growth, byproducts accumulate as a result of metabolic activities of the cells during a fermentation. This implies that when biomass growth stops, waste accumulation also stops. We let the function $w(t, \omega)$ represent the byproduct accumulation by time t, when the fermentation starts at time $t = 0$ with ω units impurity. Then, we present the byproduct accumulation by time $t \geq 0$ while the biomass is in the exponential growth phase as:

$$w(t, \omega) = \omega e^{\eta t}, \tag{4.2}$$

where η is the waste accumulation rate and ω is the initial waste amount. For some cell cultures, empirical evidence exists showing that waste and yield production are independent processes, evolving over time (Ozturk et al., 1997; Tsao et al., 2005; Xing et al., 2010). Hence, we use different growth rates for biomass growth and waste accumulation.

We note that, the final biomass and the waste amounts in the batch are random, because the exponential growth phase duration is random. Until the realized time t_i, the biomass and waste accumulate as shown in Equations (4.1)-(4.2) in cultivation i. At time t_i the batch enters to the stationary phase for the cultivation i. Then, the biomass and waste accumulations stop.

When a cultivation is stopped (either by harvest or bleed–feed), we obtain the

[2] A way to estimate the probability distribution to stationary phase from the industry data could be to use the rate function as explained in Section 3.3.2.1 in Chapter 3, which is established in Section 3.B based on biomass amount m. Note that this time we should generate the *joint* rate function of entering the stationary phase depending both on biomass amount m, and the waste amount w.

fermentation output, i.e., mixture of the biomass and the waste (if we harvest we extract the entire batch, and if we bleed–feed we extract a fraction). We obtain revenue $r(m)$, if m units biomass is achieved in the cultivation. The amount of waste products affects the purification operations and workload in downstream processing. A batch with a high amount of waste product would require more steps in downstream processing and inspection steps to meet purity requirements, hence increasing the purification cost (Farid, 2007; Gronemeyer et al., 2014). Then, we incur purification cost $c_p(w)$ with respect to w units of waste products at the end of a cultivation. The purification costs include raw material costs, equipment costs, labor costs, costs of quality assurance and control activities, and clean room costs. Finally, we incur fixed costs for implementing bleed–feed c_b, and harvest c_h. Bleed–feed cost c_b captures the cost of medium preparation and costs of other bleed–feed related activities such as transfer of medium into the batch and transfer of culture out of the batch. Harvest cost c_h captures the cost of cleaning, sterilization and setup of a new batch (including costs related to preculture preparation, medium preparation, transfer of medium and culture into the bioreactor, and transferring the culture out of the bioreactor). Thus, we have $c_p < c_h$. Then, the profit obtained from a cultivation that is harvested with m units biomass and w units waste is $r(m) - c_p(w) - c_h$. If the cultivation is stopped by bleed–feed with m units biomass and w units waste the profit is $r(m) - c_p(w) - c_b$.

We let $P(t_b)$ denote the random profit obtained from a fermentation cycle when the bleed–feed is implemented at time t_b, and $\mathbb{E}[P(t_b)]$ its expectation.[3] The fermentation profit is random because the final biomass and waste amounts in the batch are random, and we produce the second cultivation only if bleed–feed is successful at time t_b. Then, $\mathbb{E}[P(t_b)]$ can be formulated as:

$$\mathbb{E}[P(t_b)] = \mathbb{E}[P_1(t_b)] + (1 - G(t_b|b_1, \omega_1))\, \mathbb{E}[P_2(t_b)]. \tag{4.3}$$

In Equation (4.3), $\mathbb{E}[P_1(t_b)]$ represents the expected profit from the first, and $\mathbb{E}[P_2(t_b)]$ from the second cultivation, when we implement bleed–feed at time t_b. The term $1 - G(t_b|b_1, \omega_1)$ represent the probability of a successful bleed–feed. This

[3]The profit obtained from the fermentation also depends on the initial biomass amount b_1 and the waste amount ω_1, since they affect the random time to enter to the stationary phase. Therefore, the expected profit from a fermentation cycle could be denoted as $\mathbb{E}[P(t_b)|b_1, \omega_1]$. We note that these parameters are known for every problem case, and they are no decision variables. Hence, for notational simplicity we decide to leave out the terms b_1 and ω_1 in the profit function.

means that second cultivation profit is obtained only if the bleed–feed is successful. Using the discussions above, the expected profit from the first cultivation $\mathbb{E}[P_1(t_b)]$ can be written as:

$$\begin{aligned}\mathbb{E}[P_1(t_b)] = &\int_0^{t_b} \left[r(b_1 e^{\mu t_1}) - c_p(\omega_1 e^{\eta t_1}) - c_h\right] g(t_1|b_1,\omega_1)dt_1 \\ &+ (1 - G(t_b|b_1,\omega_1)) \left[r(\psi b_1 e^{\mu t_b}) - c_p(\psi\omega_1 e^{\eta t_b}) - c_b\right]. \end{aligned} \tag{4.4}$$

The first summand in Equation (4.4) represents the case when the bleed–feed fails, i.e., $t_1 \leq t_b$. In this case the biomass amount will be $b_1 e^{\mu t_1}$, and the waste accumulates to $\omega_1 e^{\eta t_1}$. Hence, we obtain revenue $r(b_1 e^{\mu t_1})$, and incur purification cost $c_p(\omega_1 e^{\eta t_1})$. We harvest the batch as the bleed–feed fails, thus incurring harvest cost c_h. The second summand represents the profit obtained from the first cultivation when the bleed–feed is successful i.e., $t_1 > t_b$. In this case we extract fraction ψ from the batch, leading to a mixture of $\psi\, b_1 e^{\mu t_b}$ units biomass and $\psi\, \omega_1 e^{\eta t_b}$ units waste. As a result, we obtain $r(\psi\, b_1 e^{\mu t_b})$ revenue, and incur purification cost $c_p(\psi\, \omega_1 e^{\eta t_b})$, and bleed–feed cost c_b. In case bleed–feed is successful, we produce the second cultivation, and obtain expected profit $\mathbb{E}[P_2(t_b)]$ given as:

$$\begin{aligned}\mathbb{E}[P_2(t_b)] = &\int_0^{t_h} \Big[r((1-\psi)b_1 e^{\mu(t_b+t_2)}) - c_p((1-\psi)\omega_1 e^{\eta(t_b+t_2)}) - c_h\Big] \\ &\qquad \times g(t_2|(1-\psi)b_1 e^{\mu t_b}, (1-\psi)\omega_1 e^{\eta t_b})dt_2 \\ &+ (1 - G(t_2|(1-\psi)b_1 e^{\mu t_b}, (1-\psi)\omega_1 e^{\eta t_b})) \\ &\qquad \times \Big[r((1-\psi)b_1 e^{\mu(t_b+t_h)}) - c_p((1-\psi)\omega_1 e^{\eta(t_b+t_h)}) - c_h\Big]. \end{aligned} \tag{4.5}$$

In the second cultivation, the remaining fraction of biomass $(1-\psi)b_1 e^{\mu t_b}$ acts as a seed culture and continue growing in the exponential growth phase. Similarly, remaining waste $(1-\psi)\omega_1 e^{\eta t_b}$ continues to accumulate. Then, the first summand of Equation (4.5) captures the expected profit obtained from the second cultivation when the exponential growth phase ends before the harvest time, i.e., $t_2 \leq t_h$. In this case the profit becomes $r((1-\psi)b_1 e^{\mu(t_b+t_2)}) - c_p((1-\psi)\omega_1 e^{\eta(t_b+t_2)}) - c_h$. If the exponential growth does not end before the harvest time t_h, i.e., $t_2 > t_h$, then the harvest time t_h limits the biomass and waste accumulations. Then, the profit is $r((1-\psi)b_1 e^{\mu(t_b+t_h)}) - c_p((1-\psi)\omega_1 e^{\eta(t_b+t_h)}) - c_h$, as given in the second summand of Equation (4.5).

4.2.3 The Objective Function and the Optimization Model

We now present our optimization model to determine the optimal bleed–feed time t_b to maximize the expected profit per time unit $J(t_b)$. From the discussions of Section 4.2.1 and 4.2.2, we present our objective function as:

$$J(t_b) = \frac{\mathbb{E}[P_1(t_b)] + (1 - G(t_b|b_1, \omega_1))\mathbb{E}[P_2(t_b)]}{s + t_b + t_h}. \tag{4.6}$$

Then, we solve the following optimization problem:

$$\begin{aligned} \max \quad & J(t_b) \\ \text{s.t.} \quad & 0 \leq t_b \leq t_h, && (4.7)\\ & d_k \leq t_b + s \leq d_k + l, && (4.8)\\ & 1 - G(t_b|b_1, \omega_1) \geq q, && (4.9)\\ & a \geq k \geq 0, \quad k \text{ integer}. \end{aligned}$$

In the optimization problem, the first constraint sets a boundary on the bleed–feed time t_b. In practice, the harvest time t_h represents a prespecified time on the cultivation time. Hence, the constraint (4.7) ensures that the bleed–feed time t_b does not exceed this cultivation time t_h.

In addition, implementing bleed–feed requires operator interaction. Hence, we include constraint (4.8) to ensure that the bleed–feed happens in a shift, when operators are available. Recall that every fermentation process starts with a setup. In (4.8), we begin the first shift with a setup at time 0. A shift captures the time period in which operators are present in the company, and it continues for l hours $0 < l \leq 24$, after which no operators are present for $24 - l$ hours. This pattern repeats every 24 hours. See Figure 4.3 for an illustration of this pattern. The term d_k denotes the start time of the kth shift since time 0 ($d_k = 24k$ hours, for $a \geq k \geq 0$, and integer k, where $k = 0$ captures the first shift of the fermentation). The term a limits the number of shifts until bleed–feed, due to cell viability and production planning restrictions.[4] Then, the time until bleed–feed since time 0, i.e., $t_b + s$, should be in the time period that kth shift takes place, i.e., $[d_k, d_k + l]$ for $a \geq k \geq 0$, and integer k. In this case we also determine the value of k in our problem, representing on which

[4]In MSD AH weekly production schedules (also called as rhythm wheels) are applied. The limit a can ensure that these schedules work smoothly with bleed–feed.

shift bleed–feed must be performed to meet the requirement of operator availability.

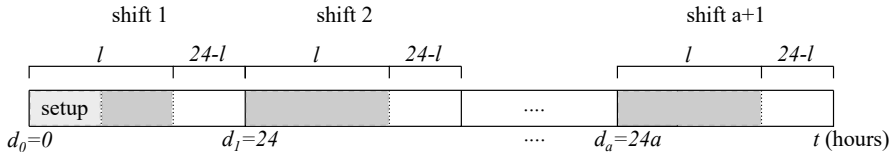

Figure 4.3: Illustration of the shift pattern. Gray areas represent shifts of l hours, and white areas represent the times no operator is present at the company.

Finally, constraint (4.9) ensures bleed–feed is implemented successfully with a certain probability level. We let $q \in [0,1]$ be the probability level the biomanufacturer wants to achieve. Recall that the bleed–feed is successful when the realized time of the exponential growth phase for the first cultivation is after the bleed–feed time, i.e., $t_1 > t_b$. Then, constraint (4.9) ensures that the probability of success is greater than q. If $q = 1$ the optimization problem captures a risk-averse behavior, where the biomanufacturer wants each bleed–feed implementation to be successful.

Our optimization problem takes these practically relevant constraints into account to generate the optimal bleed–feed time that maximizes the expected profit per time unit. We note that constraint (4.7) is valid for all settings. However, constraints (4.8) and (4.9) might not always be necessary. For instance, a biomanufacturing company working full time (i.e., 24 hours a day) has available operators the entire day. Or a biomanufacturer might tolerate the risk of missing the bleed–feed as long as the fermentation profit per time unit is improved. In the numerical analysis, we investigate different cases by relaxing one or both of these (shift and the chance) constraints to understand the impact of such restrictions and the value of flexibility on the bleed–feed time.

4.3. Numerical Analysis

In this section, we present numerical analysis to *(i)* demonstrate the effect of bleed–feed on the expected profit per time unit, and *(ii)* investigate the value of flexibility on the performance of bleed–feed. We determine the base case parameters combining literature study and fermentation data obtained from MSD AH. We

present sensitivity analysis on the shift duration and the desired level probability of successful bleed–feed implementation for the base case in Section 4.3.1. In addition, we perform sensitivity analysis on critical process parameters; the waste accumulation rate in Section 4.3.2, and revenue in Section 4.3.3.[5]

We establish the base case parameters as follows: The fermentation starts with $b_1 = 1$ gram biomass. The biomass growth rate is $\mu = 0.06$ cell divisions per hour. Waste accumulation is modeled based on literature (Jang and Barford, 2000; Doran, 1995; Ozturk et al., 1992). The initial waste amount at the beginning of the fermentation is $\omega_1 = 0.006$ grams. Waste products accumulate with rate $\eta = 0.07$ per hour. The probability density function to enter to the stationary phase is established from the rate based on fermentation dynamics obtained from fermentation literature (Omasa et al., 1992; Ozturk et al., 1992). Figure 4.4 depicts the probability density function and the cumulative distribution function for the time to enter the stationary phase used as base case, given that $b_1 = 1$ and $\omega_1 = 0.006$ grams. The harvest time of a cultivation (i.e., fermentation processing time without bleed–feed) is $t_h = 72$ hours, and setup duration is $s = 8$ hours in our numerical analysis. In accordance with regulations and industry implementation, we extract 90% of the batch mixture during bleed–feed, and let the remaining 10% continue the fermentation in the second cultivation. Thus, $\psi = 0.9$. Finally, we determine the cost parameters from literature (Martagan et al., 2016; Farid, 2007), and expert opinion based on industry data. From m grams biomass we obtain $r(m) = 1.3\,m$ revenue, and for purification cost we have $c_p(w) = 0.13\,w$ as a result of purifying w grams waste products. Direct cost of harvesting the batch is $c_h = 5$ and implementing bleed–feed is $c_b = 1$. We refer to this setting as the *base case* in our numerical analysis. We note that the parameters presented in this section are scaled.

To establish benchmark and assess the value of flexibility on bleed–feed decisions, we consider the following cases in our numerical analysis:

No Bleed–feed (NoB) harvests the batch at time t_h, without implementing bleed–feed. This case represents the common industry practice since bleed–feed has not been widely adopted yet. We consider this case to understand when implementing bleed–feed is not desirable.

Bleed–feed optimization (BO) relaxes both the shift and the chance constraints in our

[5]We also performed sensitivity on the biomass growth rate and the purification cost, and obtained similar insights. For brevity, we focus only on sensitivity on the waste accumulation rate and revenue.

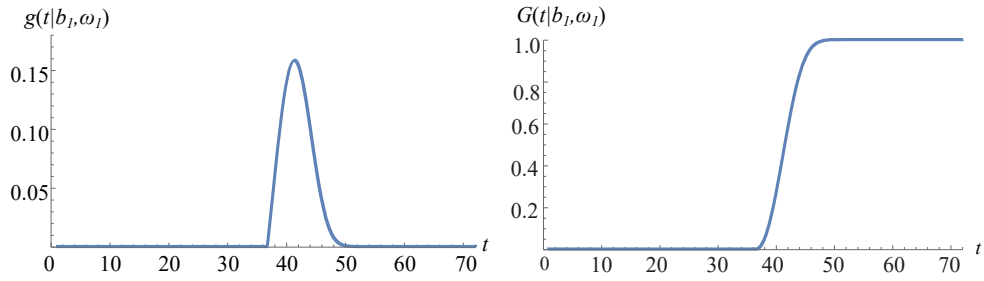

Figure 4.4: The probability density function $g(t|b_1, \omega_1)$ and the cumulative distribution function $G(t|b_1, \omega_1)$ to enter the stationary phase in the base case ($b_1 = 1$ and $\omega_1 = 0.006$).

renewal model, and generates the optimal bleed–feed time to maximize the profit per time unit. This case represents the *most flexible* case (assumes 24 hours operator availability, and desired probability level of successful bleed–feed to be greater that zero, i.e., $l = 24$ hours and $q = 0$). We use BO as a benchmark to assess the percentage decrease in the bleed–feed performance when there are restrictions on the bleed–feed time.

Risk-averse bleed–feed optimization (BO_{RA}) captures the case where all bleed–feed implementations need to be successful and no risk of failure is tolerated. In this case we relax the shift constraint, set $q = 1$ to represent risk-averse behavior of the biomanufacturer and find the optimal bleed–feed time to maximize the profit per time unit.

Bleed–feed optimization with shift (BO_S) assumes a shift of eight hours (i.e., $l = 8$ hours), and generates the optimal time to implement the bleed–feed to maximize the profit per time unit. In this case we relax the chance constraint.

Risk-averse bleed–feed optimization with shift (BO_{RA+S}) assumes risk-averse behavior (i.e., $q = 1$) and a shift of eight hours (i.e., $l = 8$ hours), to generate the optimal bleed–feed time to maximize the profit per time unit. BO_{RA+S} is our *least flexible* case.

In our numerical analysis, we compare the (absolute values of) profit per time unit if bleed–feed is not implemented (NoB), with the other cases with bleed–feed implementation (BO, BO_{RA}, BO_S, BO_{RA+S}) to observe under which settings bleed–feed technique is not an attractive option. In addition, we calculate the percentage

Table 4.2: Base case results.

NoB	**BO**		**BO$_{RA}$**			**BO$_{S}$**			**BO$_{RA+S}$**		
J	t_b^*	$J(t_b^*)$	t_b^*	$J(t_b^*)$	D%	t_b^*	$J(t_b^*)$	D%	t_b^*	$J(t_b^*)$	D%
0.138	37.6	0.155	36.6	0.153	1%	40	0.142	8%	24	0.118	24%

decrease D% in the expected profit per time unit if we have restrictions on the bleed–feed time (BO$_{RA}$, BO$_{S}$, BO$_{RA+S}$), rather than having the most flexible case BO. This way we investigate the effects of constraints on the bleed–feed decisions.

4.3.1 Base Case Results

In this section we present the results for the base case. In addition, we perform sensitivity analysis on the duration of the shift l, and the probability of successful bleed–feed implementation q that we want to satisfy to understand the effects of shift and chance constraints on the optimal policies and performances of the cases.

Table 4.2 shows the results for the base case. We observe that the profit per time unit is $J = 0.138$ if we do not implement bleed–feed (NoB). If we implement bleed–feed with no restrictions on the bleed–feed time (BO), it is optimal to bleed–feed at time $t_b^* = 37.6$. In the risk-averse case BO$_{RA}$, optimal bleed–feed time is $t_b^* = 36.6$, slightly earlier than that of BO. The performance of bleed–feed decreases by 1% as a result of having the chance constraint with $q = 1$. If we have the shift constraint only (BO$_{S}$), the optimal bleed–feed time is $t_b^* = 40$, corresponding to the beginning of the third shift. In this case the performance of bleed–feed drops by 8% compared to the most flexible case. If we have both the chance and the shift constraints on the bleed–feed time (BO$_{RA+S}$), the optimal bleed–feed time becomes $t_b^* = 24$, corresponding to the end of the second shift. This case restricts the bleed–feed time so much that the system bleed–feeds too early. This results in 24% decrease on the bleed–feed performance compared to BO. Observe also that this case results in less profit per time unit $J(t_b^*)$ than NoB, meaning that adopting bleed–feed is not desirable.

We note that the performances of the cases with shift constraint (BO$_{S}$ and BO$_{RA+S}$) are sensitive to problem parameters such as the shift duration, and how close the optimal bleed–feed time from BO is, to any of these shift. To explain this further, we plot the expected profit per time unit $J(t_b)$ as a function of the bleed–feed time

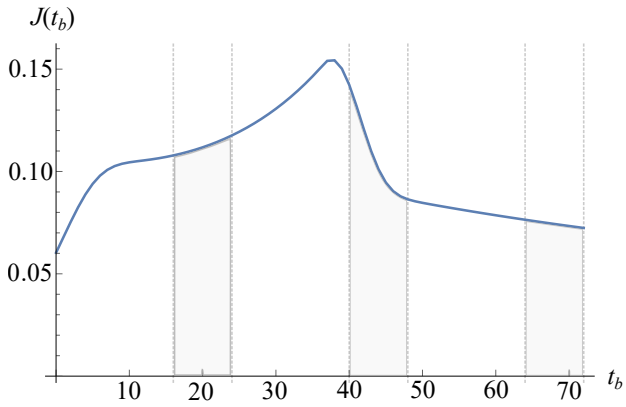

Figure 4.5: Base case profit per time unit $J(t_b)$ versus t_b for BO. Shaded areas correspond to shifts of $l = 8$ hours.

t_b for BO in Figure 4.5. The shaded areas represent the time corresponding to the shifts of $l = 8$ hours (in our base case the first shift is spent with setup and hence not included in Figure 4.5).

Observe in Figure 4.5 that the optimal bleed–feed time is at $t_b^* = 37.6$, and bleed–feeding earlier or later results in less profit per time unit $J(t_b)$. We see a steep decrease in $J(t_b)$ after $t_b^* = 37.6$, since it becomes more likely to miss the bleed–feed opportunity. Still, observe in Table 4.2 that when we have a shift constraint we bleed–feed later ($t_b^* = 40$ in BO_S). This is counter intuitive to common industry belief that we would always bleed–feed earlier if optimal time in the most flexible case is not feasible, because of the steep decrease in the profit per time unit. However, observe from Figure 4.5 that the optimal bleed–feed time is much closer to the next shift (starting at time 40) than the previous one (ending at time 24). Hence, implementing the bleed–feed at the beginning of the next shift results in a higher $J(t_b)$. Note that if the shifts would be longer, or the optimal bleed–feed time would be earlier (due to different production settings) then it could be favorable to bleed–feed earlier. For practitioners this implies that implementing the bleed–feed earlier is not necessarily optimal if the bleed–feed time does not take place in a shift.

We now present a sensitivity analysis on the shift duration l that is imposed by our shift constraint in (4.8) for the base case. We consider the following scenarios: $l = \{8, 10, 12, 14, 16, 18, 20, 22\}$ hours. These scenarios are given in the first column of Table 4.3. Column BO represents the most flexible case, and column BO_l

represents the case with shift duration l, when the chance constraint is relaxed ($BO_{l=8}$ is equivalent to BO_S). We report the optimal bleed–feed time t_b^* and the optimal profit per time unit $J(t_b^*)$ for each case. Column $D\%$ shows the percentage decrease in expected profit per time unit if we have shift constraint on the bleed–feed time with duration l. Observe from Table 4.3 that until $l = 18$, optimal bleed–feed time is at $t_b^* = 40$ for BO_l. After $l = 18$, it becomes optimal to bleed–feed earlier (than BO). Performance of BO_l approaches to BO (i.e., $D\%$ decreases) in l. When $l = 22$, the optimal time for the most flexible case BO and the case with the shift constraint BO_l is equal. This is because the optimal bleed–feed time from BO takes place in a shift when $l = 22$.

Table 4.3: Sensitivity on the shift duration l for the base case.

	BO		**BO$_l$**		
l	t_b^*	$J(t_b^*)$	t_b^*	$J(t_b^*)$	$D\%$
8	37.6	0.155	40	0.142	8.0%
10	37.6	0.155	40	0.142	8.0%
12	37.6	0.155	40	0.142	8.0%
14	37.6	0.155	40	0.142	8.0%
16	37.6	0.155	40	0.142	8.0%
18	37.6	0.155	34	0.143	7.7%
20	37.6	0.155	36	0.150	2.9%
22	37.6	0.155	37.6	0.155	0.0%

Now, we focus on a sensitivity analysis on the probability level of successful bleed–feed that the practitioners want to achieve q, captured by Constraint (4.9). We consider the following scenarios: $q = \{1, 0.99, 0.98, 0.97, 0.96, 0.95\}$. These scenarios are shown in the first column of Table 4.4. We present the results for the base case, and for a lower risk batch (the probability of entering to the stationary phase is lower at the same cultivation time). We illustrate the probability density and cumulative distribution functions of the lower risk batch (together with the base case) in Figure 4.6 in Appendix 4.A. For each of these risk scenarios, column BO represents the most flexible case, and column BO_q represents the case with probability level q, when the shift constraint is relaxed ($BO_{q=1}$ is equivalent to BO_{RA}). We report the optimal bleed–feed time t_b^* and the optimal profit per time unit $J(t_b^*)$ for each case. Column $D\%$ shows the percentage decrease in expected profit per time unit if we have a chance constraint with probability level q, rather

Table 4.4: Sensitivity on the probability of successful bleed–feed q for the base case and a case with lower risk (of entering to the stationary phase).

	Base Case					**Lower Risk**				
	BO		**BO$_q$**			**BO**		**BO$_q$**		
q	t_b^*	$J(t_b^*)$	t_b^*	$J(t_b^*)$	D%	t_b^*	$J(t_b^*)$	t_b^*	$J(t_b^*)$	D%
1	37.6	0.155	36.6	0.153	1.3%	40.4	0.213	36.6	0.205	3.5%
0.99	37.6	0.155	37.3	0.155	0.1%	40.4	0.213	38.3	0.210	1.2%
0.98	37.6	0.155	37.5	0.155	0.0%	40.4	0.213	38.9	0.212	0.6%
0.97	37.6	0.155	37.6	0.155	0.0%	40.4	0.213	39.4	0.212	0.3%
0.96	37.6	0.155	37.6	0.155	0.0%	40.4	0.213	39.8	0.213	0.1%
0.95	37.6	0.155	37.6	0.155	0.0%	40.4	0.213	40.2	0.213	0.0%

than having the most flexible case BO (for the corresponding risk scenario). Observe from Table 4.4 that as the probability of success level q decreases, D% decreases, meaning that BO$_q$ performs closer to BO. When we become more tolerant to failure (lower q) the optimal bleed–feed time t_b^* becomes later, and profit per time unit $J(t_b^*)$ increases. Note that our base case setting is rather robust to the changes in the probability level q. This is mainly because in our specific base case the probability of entering to the stationary phase increases suddenly (see Figure 4.4). As a result, t_b^* from BO has a quite high successful bleed–feed probability, and the chance constraint does not affect the bleed–feed decisions much. In the case with lower risk, we can observe the impact of the chance constraint better. Practitioners should keep this behavior in mind when they set their tolerance levels.

4.3.2 Sensitivity on the Waste Accumulation Rate

The waste accumulation rate η can differ for cell cultures based on the cell characteristics, medium and equipment used. Hence, we consider the following scenarios for waste accumulation: *base case* $\eta = 0.07$, *slow accumulation* $\eta = \{0.055, 0.06, 0.065\}$, and *fast accumulation* $\eta = \{0.075, 0.08, 0.085, 0.09\}$. Table 4.5 presents these scenarios in the first column, and reports the profit per time unit J and optimal bleed–feed time t_b^* for relevant cases. Columns D% demonstrate the percentage decrease in the cases with restrictions on the bleed–feed time (BO$_{\text{RA}}$, BO$_{\text{S}}$ and BO$_{\text{RA+S}}$) compared to the case with no constraints (BO). Bold entries represent the base case.

Table 4.5: Sensitivity on the waste accumulation rate η.

	NoB	**BO**		**BO$_{RA}$**			**BO$_{S}$**			**BO$_{RA+S}$**		
η	J	t_b^*	$J(t_b^*)$	t_b^*	$J(t_b^*)$	$D\%$	t_b^*	$J(t_b^*)$	$D\%$	t_b^*	$J(t_b^*)$	$D\%$
0.055	0.210	42.1	0.266	41.4	0.265	1%	42.1	0.266	0%	41.4	0.265	1%
0.06	0.181	40.4	0.220	39.7	0.218	1%	40.4	0.220	0%	24	0.177	19%
0.065	0.158	38.9	0.184	38.1	0.182	1%	40	0.181	2%	24	0.143	22%
0.07	**0.138**	**37.6**	**0.155**	**36.6**	**0.153**	**1%**	**40**	**0.142**	**8%**	**24**	**0.118**	**24%**
0.075	0.121	36.3	0.132	35.3	0.129	2%	40	0.110	16%	24	0.098	26%
0.08	0.106	35.2	0.112	34.0	0.109	2%	40	0.085	24%	24	0.081	28%
0.085	0.094	34.2	0.095	32.8	0.093	3%	40	0.068	28%	24	0.067	29%
0.09	0.083	33.2	0.080	31.7	0.078	3%	40	0.057	29%	24	0.056	31%

Observe in Table 4.5 that the optimal bleed–feed time t_b^* decreases as the accumulation rate η increases. If waste accumulates too fast, environment deteriorates, and the batch becomes more likely to enter stationary phase. Thus, we implement bleed–feed early to avoid missing the bleed–feed opportunity. If waste accumulation rate increases, profit per time unit J decreases for all cases. This is because *(i)* we produce more waste and incur higher purification costs, and *(ii)* the biomass growth will stop earlier due to growth inhibition leading to less revenue. If η is too high ($\eta = 0.09$), bleed–feed is not an attractive option as we obtain less profit per time unit J in BO than NoB. These results indicate that practitioners should adjust their bleed–feed policies based on waste accumulation rate.

In Table 4.5, we see that percentage decrease $D\%$ ranges between $1 - 3\%$ if we have risk-averse behavior BO_{RA}, between $0 - 29\%$ for the case with shift BO_{S}, and between $1 - 31\%$ for the case with both risk-averse behavior and shift $\text{BO}_{\text{RA+S}}$. In BO_{RA}, $D\%$ is lower if waste accumulates slower, meaning that BO_{RA} performs closer to BO for batches with slow waste accumulation. This is because for high η, profit per time unit J in BO is already low. Observe that for small accumulation rates, i.e., $\eta \leq 0.06$, BO is equal to the case with a shift constraint BO_{S} (and BO_{RA} is equal to $\text{BO}_{\text{RA+S}}$). The reason is that, the optimal bleed–feed time takes place in a shift in these scenarios. As η increases, the optimal bleed–feed time decreases to $t_b^* = 40$ for BO_{S} in our example. Yet, especially for scenarios with high η, implementing bleed–feed at $t_b^* = 40$ (from BO_{S}), and $t_b^* = 24$ from ($\text{BO}_{\text{RA+S}}$) result in similar profit per time unit J, and performance decrease $D\%$. This is because the optimal bleed–feed time of BO is far away from both the previous shift and the

Table 4.6: Sensitivity on the factor in the revenue function ϕ_r.

		NoB	**BO**		**BO$_{RA}$**			**BO$_{S}$**			**BO$_{RA+S}$**		
ϕ_r	ϕ_p/ϕ_r	J	t_b^*	$J(t_b^*)$	t_b^*	$J(t_b^*)$	$D\%$	t_b^*	$J(t_b^*)$	$D\%$	t_b^*	$J(t_b^*)$	$D\%$
1.9	0.07	0.230	37.5	0.250	36.6	0.248	1%	40	0.231	8%	24	0.199	20%
1.7	0.08	0.199	37.5	0.218	36.6	0.216	1%	40	0.201	8%	24	0.172	21%
1.5	0.09	0.168	37.5	0.187	36.6	0.184	1%	40	0.172	8%	24	0.145	22%
1.3	**0.10**	**0.138**	**37.6**	**0.155**	**36.6**	**0.153**	**1%**	**40**	**0.142**	**8%**	**24**	**0.118**	**24%**
1.1	0.12	0.107	37.6	0.123	36.6	0.121	1%	40	0.113	8%	24	0.090	26%
0.9	0.14	0.076	37.7	0.091	36.6	0.090	2%	40	0.084	8%	24	0.063	31%
0.7	0.19	0.045	37.7	0.059	36.6	0.058	2%	40	0.054	9%	24	0.036	39%

next shift. In these scenarios, bleed–feeding is not an attractive option if we have shift restrictions. Also observe that in BO$_{RA+S}$, implementing bleed–feed does not increase J compared to NoB in any scenario (except from the scenario $\eta = 0.055$), meaning that implementing bleed–feed is not desirable in the least flexible case.

4.3.3 Sensitivity on Revenue

Revenue obtained from unit biomass might differ based on the industry and the final product (cell cultures), since revenue margins can change. Hence, we perform sensitivity analysis on the factor in the revenue function, denoted as ϕ_r. Recall in the base case we have $r(m) = 1.3\,m$, hence, $\phi_r = 1.3$. We also consider the following scenarios: *lower revenue* $\phi_r = \{0.7, 0.9, 1.1\}$ and *higher revenue* $\phi_r = \{1.5, 1.7, 1.9\}$. Table 4.6 presents these scenarios in the first column, and reports the profit per time unit J and optimal bleed–feed time t_b^* for relevant cases. Columns $D\%$ demonstrate the percentage reduction in the cases with restrictions on the bleed–feed time (BO$_{RA}$, BO$_S$ and BO$_{RA+S}$) compared to the case with no constraints (BO). Besides the revenue obtained from biomass, fermentation profit also takes the purification cost into account. We let ϕ_p denote the factor in the purification cost function ($c_p(w) = \phi_p\, w$ with $\phi_p = 0.13$ in the base case). We also conducted sensitivity analysis on ϕ_p, and obtained similar insights. Hence, we present the sensitivity on revenue alone for brevity, and we interpret our results based on the ratio ϕ_p/ϕ_r given in the second column of Table 4.6. Bold entries represent the base case.

Observe from Table 4.6 that as ϕ_p/ϕ_r increases, fermentation profit per time unit J decreases for all cases. In BO, the optimal bleed–feed time t_b^* slightly increases

in ϕ_p/ϕ_r. This is because the system is willing to take more risk in bleed–feed to earn more, when the system gets less revenue compared to the costs incurred. This implies that practitioners should adjust their bleed–feed decisions based on ϕ_p/ϕ_r. Observe also that the optimal bleed–feed time is robust in the cases with constraints (BO_{RA}, BO_S and BO_{RA+S}). This is intuitive, as the biological characteristics of the system remain unchanged, and the change in optimal bleed–feed time in BO is very small among scenarios. The percentage decrease $D\%$ ranges between $1-2\%$ in BO_{RA}, $8-9\%$ in BO_S, and $20-39\%$ in BO_{RA+S}. We observe that $D\%$ increases in ϕ_p/ϕ_r for all cases, meaning that the performance gets worse as ϕ_p/ϕ_r increases. This can be explained as follows: The optimal bleed–feed times from BO and BO_{RA} become more distant for higher ϕ_p/ϕ_r. This results in worse performance for BO_{RA} compared to BO for high ϕ_p/ϕ_r. In BO_S we bleed–feed later (at $t_b^* = 40$) and increase failure risk, and earn less from the extra time bioreactor is occupied since revenue is lower. Hence, $D\%$ increases in ϕ_p/ϕ_r. In BO_{RA+S}, implementing bleed–feed too early (at $t_b^* = 24$) means that we give up on the extra biomass that could be achieved due to exponential growth, while we earn less revenue from the biomass produced due to lower revenue. Thus, $D\%$ increases in ϕ_p/ϕ_r. Finally, observe that no bleed–feed case NoB results in higher profit per time unit J than BO_{RA+S}, implying that implementing bleed–feed is not optimal.

4.4. Conclusion

Bleed–feed enables biomanufacturers to skip intermediary setups by replenishing some percentage of the culture with medium, instead of harvesting the batch. However, the time of bleed–feed is crucial for a successful implementation. Bleed–feed is successful, only if it is performed in the exponential growth phase of the fermentation. Since the exponential growth phase duration is random, finding the optimal bleed–feed time is not straightforward. Implementing it too early, or too late results in suboptimal fermentation profit per time unit. In addition, bleed–feed implementation requires operator interaction, meaning that it can only be implemented when operators are present in the company. Also, biomanufacturers might tolerate different probabilities of bleed–feed failure. For instance, they might want to implement bleed–feed ensuring that it is always successful. Such constraints restrict the time bleed–feed can be implemented, and its potential benefits. In this

work, we extend our renewal model from Chapter 3, and determine the optimal bleed–feed time to maximize the fermentation profit per time unit. Our model links the biological dynamics of fermentation with operational trade-offs of bleed–feed decisions, and our optimization problem includes practically relevant constraints to capture restrictions on the bleed–feed time.

We present a numerical analysis inspired from literature and fermentation data from MSD AH. By relaxing the constraints, we consider different cases to investigate the value of flexibility in bleed–feed decisions. We perform sensitivity analysis on the critical process parameters to generate insights on the bleed–feed with constraints under different production configurations. Our numerical analysis reveals that it is not necessarily better to bleed–feed earlier if bleed–feed time is not during a shift, and chance constraint has more impact for low-risk batches. We observe that in our example the risk-averse case usually performs the best, and the least flexible case is the worst, compared to the most flexible case. We also see that if we have a shift constraint and risk-averse approach, bleed–feed is not desirable.

4.A. Low-Risk Batch

Figure 4.6 demonstrates the probability density function and cumulative distribution function of the base case (solid line) and the batch with lower risk of entering the stationary phase (dashed line) of Table 4.4, for $b_1 = 1$ and $\omega_1 = 0.006$.

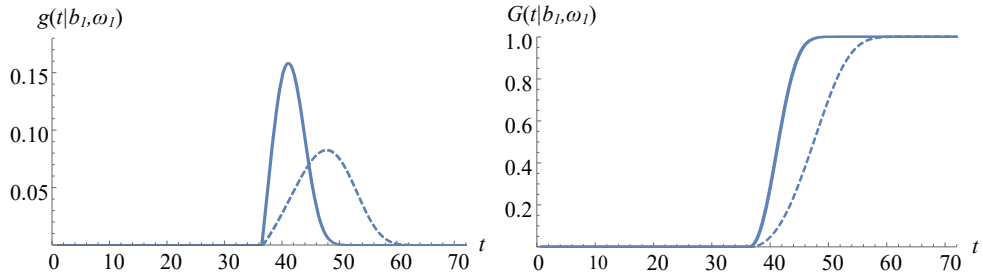

Figure 4.6: The probability density functions $g(t|b_1, \omega_1)$ and the cumulative distribution functions $G(t|b_1, \omega_1)$ to enter the stationary phase in the base case (solid line) and the case with a lower risk (dashed line) for $b_1 = 1$ and $\omega_1 = 0.006$.

5

Operations Research Improves Biomanufacturing Efficiency at MSD Animal Health

5.1. Introduction

Animals have important roles in our daily lives. They can be our companions, such as service animals and domestic pets. Some of them contribute to our food supply with milk, eggs, and meat. Caring for them is critical to improve the health and welfare of not only animals but also humans. For example, there are several *zoonotic* diseases that are naturally transmitted between animals and humans. A recent report published by the World Health Organization estimates that 61% of all human diseases are zoonotic in nature (World Health Organization, 2019). This emphasizes the critical role of the pharmaceutical industry in maintaining the health and welfare of animals as well as humans.

Recent advances in *biomanufacturing* have led to innovative medicines for animals and humans. The active ingredients of these medicines are generated by novel biomanufacturing methods. These methods can successfully re-engineer and use living organisms (e.g., bacteria and viruses) during the production process.

The resulting active ingredients are highly complex and unique. For example, a biopharmaceutical molecule might contain 25,000 atoms whereas an aspirin molecule consists of only 21 atoms (McKinsey & Company, 2014). This complexity leads to several challenges related to the predictability, stability, and batch-to-batch variability in biomanufacturing operations.

Regulatory requirements for the biomanufacturing of animal health products are equally stringent compared with those for human health and might also require additional studies to ensure food safety. Most importantly, unlike human drugs that are often subsidized, animal owners are responsible for paying the full price for these drugs. Subsequently, this restricts the acceptable prices in the animal health industry. For example, from a farmer's perspective, the price of a vaccine should be justifiable compared with the actual value of (or revenue obtained from) a healthy animal. From a biomanufacturer's perspective, this leads to smaller margins for covering the risks and costs and creates a strong incentive to improve biomanufacturing efficiency.

Increasing market demand is another critical reason for improving biomanufacturing efficiency. As such, recent market analyses anticipate that the total demand for animal products will double in developing countries by 2030, and the global demand for companion animals will grow exponentially during the same period (Food and Agriculture Organization of the United Nations, 2018; Grand View Research, 2018). To stay competitive, biomanufacturers around the world are looking for novel methodologies and opportunities to reduce costs and lead times. "Our target is to double our output in the next five years" says Bram van Ravenstein, Associate Director at MSD AH, "We cannot rely only on capacity expansions to achieve this target. We also need to get the best use of our existing capacity by optimizing our production processes."

Operations research (OR) methodologies have benefited several industries by reducing costs and lead times. However, the applications of OR methodologies to biomanufacturing are still premature. This is mainly because, to date, the scientific capability to produce these drugs was one of the main competitive advantages. However, with growing competition, there is an increasing need for a data-driven, OR-based transformation to reduce biomanufacturing costs and lead times.

In this chapter, we develop a portfolio of optimization models and decision support

tools for biomanufacturing operations.[1] To generate these models, we adopted a systematic approach that combines life sciences research with various OR methodologies. The project has been conducted through a three years of close collaboration between Eindhoven University of Technology (TU/e) and Merck Sharp & Dohme Animal Health (MSD AH) in Boxmeer, the Netherlands. MSD AH's facility in Boxmeer is one of the world's leading biomanufacturing centers. Hereafter, we use the term MSD AH to refer to the Production Department of the Boxmeer facility. Although we focus on MSD AH's operations, the true impact of this work extends to other biomanufacturing companies (including human health applications). The project outcomes have been shared with a broader biomanufacturing community through working group sessions (Nederlandse Biotechnologische Vereniging, 2018) and social media (MSD, 2019).

5.2. Overview of Biomanufacturing Operations

Figure 5.1 illustrates a generic biomanufacturing process flow. Biomanufacturing operations typically consist of upstream processing (USP) and downstream processing (DSP) activities. USP starts with preculture. In this step, a working seed (i.e., a small volume of inactive cells, such as 5 ml) is fed with a medium. This enables the working seed cells to divide, grow, and get ready for fermentation. Next, the preculture is transferred into a bioreactor to conduct a fermentation operation. Bioreactors are typically stainless-steel vessels or flasks that provide a highly controlled environment to facilitate cell growth. Depending on the specific application, bioreactors can significantly vary in size, e.g., 1 to 1500 L. In the fermentation, the cells are fed with a medium to help them grow and produce the desired end products (e.g., antigens, proteins, antibodies, etc.). The output of fermentation is a batch mixture consisting of the desired end products and unwanted impurities (e.g., byproducts, dead cells, etc.). Hereafter, we use the term antigen to refer to the desired end products in our specific problem setting.

Production steps after fermentation are referred to as DSP. The main aim of DSP is to purify the fermentation output. More specifically, the antigens are separated from unwanted impurities, so that the batch can be stored safely and remains stable until it is shipped to customers. Centrifugation, chromatography, and filtration

[1] A brief video on this project is available at `https://youtu.be/79B7OBuvRkY`.

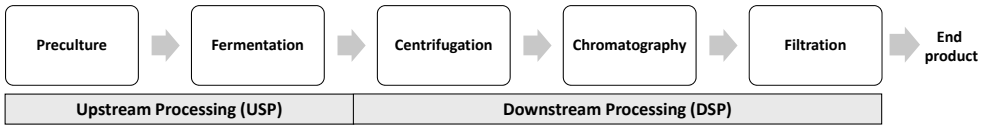

Figure 5.1: A general overview of biomanufacturing operations.

are common examples of DSP activities. Depending on the characteristics of the cell culture, production requirements, and regulations, different combinations of DSP operations are applied in different orders. After DSP operations, the end product is stored to be shipped to customers. Among all USP and DSP operations, fermentation is the bottleneck of our production setting at MSD AH. This is also the main step in the complete process where the antigens are actually being made by living organisms.

5.2.1 Fermentation Operations

During the fermentation process, the cell growth follows a specific pattern, as illustrated in Figure 5.2. Typically, six different growth phases occur during a batch fermentation process. First, the cells go through the lag phase. During the lag phase, cells adapt to their new environment, and hence do not undergo any growth. Growth starts in the acceleration phase and continues through the exponential growth phase where it reaches a maximum for that batch. When the nutrients are depleted in the medium, the cell growth slows down and enters the deceleration phase. Next, the culture enters a stationary phase in which the cell growth stops. In the death phase, the cells lose viability and die. During the fermentation process, the cells produce the antigens as they grow. Therefore, a common industry practice is to harvest the batch at the deceleration or stationary phase, as the fermentation operating costs do not typically outweigh the incremental gains in production yield obtained during these growth phases.

Although the fermentation process is highly controlled, the time spent in each growth phase and the rate at which the cells grow can be highly variable in practice. This is mainly because of the complex biological and chemical dynamics of fermentation processes. From a practical perspective, this leads to significant batch-to-batch variability in terms of processing times, production yields, and costs. These

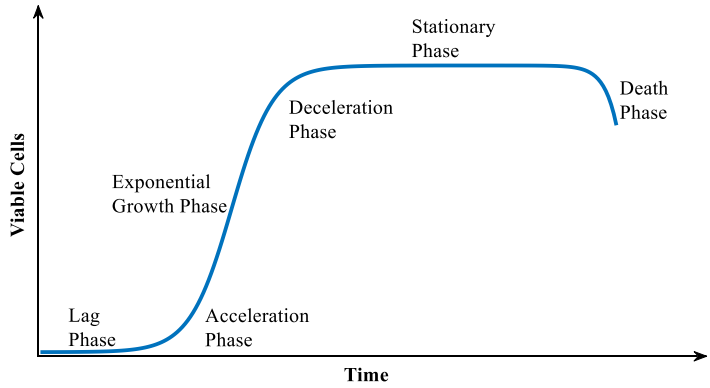

Figure 5.2: Typical phases of cell growth during fermentation.

operational challenges have led to three main process improvement opportunities at MSD AH, namely, the bleed–feed problem, the yield optimization problem, and the rhythm wheel problem. We elaborate on each of these problems in the following sections.

5.2.2 The Bleed–Feed Problem

The bioreactor needs to be cleaned and sterilized after each use. In practice, these changeovers often require several expensive resources, such as buffers, mediums, special equipment, and highly skilled labor. In addition, these changeovers are time consuming, as up to one-third of the total fermentation operating time can often be spent on cleaning and sterilization activities. Therefore, there is a significant business case in the industry to reduce bioreactor changeovers.

To reduce the number of changeovers, MSD AH developed a new replenishment technique named *bleed–feed*. Bleed–feed is also a novel technique in the life science literature, especially in the context of batch fermentation processes. With this technique, instead of harvesting the entire batch at the stationary phase, some fraction of the cell culture is extracted during the exponential growth phase (bleed) and a special medium is added (feed). Subsequently, the remaining cell culture acts as a seed for a new fermentation run and continues to grow at the exponential growth phase. Therefore, if the bleed–feed is performed successfully, it enables the changeover activities and the lag phase of the subsequent batch to be skipped. From

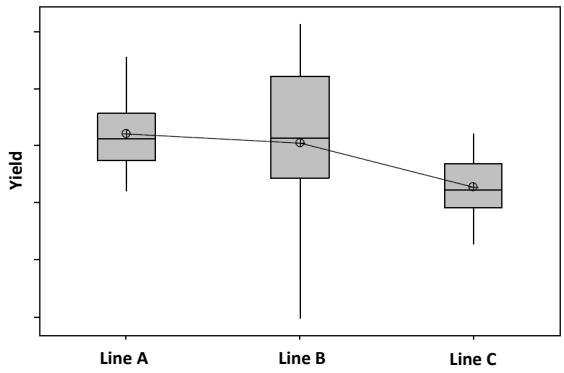

Figure 5.3: A box plot to compare the average production yield of Lines A, B, and C.

a practical standpoint, if performed successfully, the bleed–feed technique provides a significant opportunity to reduce fermentation costs and lead times.

As a critical constraint, the bleed–feed can only be performed in the exponential growth phase. Otherwise, the technique does not work, and the entire batch needs to be harvested. In this setting, identifying the best bleed–feed time is challenging because the time when the exponential growth phase stops is unknown beforehand (i.e., the duration of each cell growth phase is stochastic). This implies that if the bleed–feed is carried out *too early*, then we might not achieve the maximum yield from that batch. In contrast, if it is performed *too late*, then the batch needs to be harvested and the bioreactor needs to be set up for the next batch. This leads to the bleed–feed problem, which aims to optimize this trade-off. To identify the optimal bleed–feed time, a formal decision-support tool is needed.

5.2.3 The Yield Optimization Problem

Once a bioreactor is set up for fermentation, a natural incentive is to achieve the highest possible production yield from that batch. However, the fermentation process is highly unpredictable, and several factors affect the production outcomes. This is illustrated in Figure 5.3, which is also the business case for the yield optimization problem. The box plot in Figure 5.3 shows the mean and variability of annual production yield obtained from three production lines (Line A, B, and C) at MSD AH. These production lines conducted the same fermentation process

using an identical recipe (i.e., the cell paste, physicochemical parameters, buffers, and all other critical control parameters were identical across these production lines). However, Line C consistently produced lower production yields, as shown in Figure 5.3.

The only difference between these three production lines was the bioreactor type used. Interestingly, Line C was using a new bioreactor with latest technology. Further investigation showed that this new bioreactor had a different mixing mechanism, leading to a different type of flow inside this bioreactor. This implied that a controllable input parameter needed to be adjusted to achieve the best performance from Line C. (The specific name of this parameter is confidential. Hereafter, we refer to it as the critical process parameter.)

However, finding the best configuration for the critical process parameter was a challenging problem in practice. First, there were no information in the literature to estimate how production yield (of that specific cell culture) would change as a function of this critical process parameter under this new bioreactor technology. Therefore, MSD AH needed to conduct several experiments to understand this relationship. However, it was not possible to conduct these experiments at the laboratory scale because of resource limitations and potential scalability issues. This implied that experiments needed to be conducted at the industry scale. Subsequently, this has led to an optimal learning problem, where the relationship between the critical process parameter and yield needed to be quantified under a limited number of experiments. Note that each of these experiments were expensive as they were conducted at the industry scale. In addition, the yield obtained from each experiment would be subject to an inherent randomness owing to biological dynamics. Therefore, a smart experimental design mechanism was needed to identify the best parameter configuration at a limited number of bioreactor runs.

5.2.4 The Rhythm Wheel: Production and Capacity Planning Problems

Production planning can often be challenging in biomanufacturing practice owing to several factors. For example, the use of living cells causes batch-to-batch variability in yield and processing times. In addition, each antigen has unique production requirements. More specifically, the production process of each antigen needs to

abide by a unique recipe indicating the specific production configurations and associated resources (i.e., media, seed cells, buffers, equipment, etc.). This recipe can impose constraints on production planning decisions, i.e., not every antigen is permitted to be produced on every process line. Similar constraints are also applicable for equipment selection decisions. Equipment such as bioreactors might vary in size and technology. Subsequently, processing times of antigens may depend on the type of equipment being used. Some equipment also requires further sterilization steps in addition to the standard cleaning process performed after each batch. All these factors translate into differences in processing and set-up times for each possible equipment–antigen pair.

The production process involves several inter-dependent operations to be completed. For example, the manufacturing process for one antigen (from working seed to end product) might involve up to $3,000$ inter-dependent production steps (i.e., including buffer and media preparation, documentation, setups, cleaning, control, etc). In this setting, a sub-optimal performance in one production step has a magnifying impact on the subsequent operations. In addition, bio-safety requirements introduce "no-wait" constraints between different production steps. If an antigen waits as work-in-progress, its quality deteriorates rapidly and the entire batch needs to be scrapped. The no-wait constraint adds an additional layer of challenge, as it requires a rigorous production plan and a smooth flow of all products throughout the system.

Biomanufacturers face with *capacity planning* challenges. One of the key factors is the shared use of resources, such as equipment, operators, and utilities. For example, specialized equipment (e.g., bioreactors with a unique mixing and aeration technology) can often be limited in number, and shared between different process lines. Similarly, highly skilled scientists can be assigned to multiple process lines. The workforce consists of scientists with different skill sets. Some tasks, such as operating a chromatography technique, can be performed by highly skilled scientists only. Therefore, allocation of antigens to shared resources and specialized scientists might make production and capacity planning decisions even harder. Another critical factor is associated with unpredictable and non-stationary demand (i.e., in our context, non-stationarity means that monthly demand is not constant and changes over time. This could be associated with several factors, such as, seasonality, surge in demand due to an unforeseen disease spreading among

animals, etc.). This implies that production and capacity plans should be flexible enough to quickly respond to changing market needs.

To address these challenges, MSD AH tested several commercially available software packages to support production and capacity planning decisions. However, existing software packages were not fully equipped to address all of the complexities and unique features of their production system. Consequently, MSD AH relied on past experience and domain knowledge. Production plans were generated manually by the most experienced planners, and revised on a weekly basis. However, there was a strong need for an automated and rigorous framework to achieve better system control and predictability.

5.3. Operations Research Tools Provide Solutions

A portfolio of OR tools have been developed over three years of collaboration with a multidisciplinary team of researchers from MSD AH and Eindhoven University of Technology. Figure 5.4 presents a summary of the OR tools in terms of their input, output, and the OR methods used.

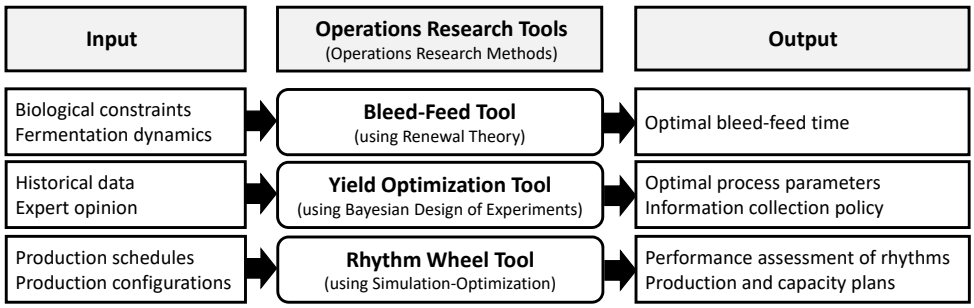

Figure 5.4: Summary of the tools developed in this project.

The bleed–feed and yield optimization tools address the challenges faced in USP activities. Both of them aim to improve fermentation processes in terms of increased throughput and reduced lead times. The rhythm wheel tool addresses production and capacity planning challenges and captures both USP and DSP activities. In this context, the term *rhythm wheel* refers to cyclic production plans. These tools are developed based on a variety of OR methods, such as renewal theory, Bayesian

design of experiments, and simulation-optimization. In this chapter, we elaborate on each of the tools, and discuss the implementation process at MSD AH.

5.3.1 Relevant Literature and Contributions

There is a large body of work in the field of chemical and biological engineering. For brevity, we focus on relevant studies in the field of Operations Research and Management Science (OR/MS).

To date, applications of OR/MS methodologies in biomanufacturing have received little attention. In the context of fermentation modeling and control, there are only a few studies related to our work (the bleed–feed tool). For example, Martagan et al. (2016) present a Markov decision process model to optimize bioreactor harvesting decisions but do not consider bleed–feed decisions. In a similar context, Xie et al. (2020) provide a Bayesian Network to capture the inter-dependence between process parameters and quality attributes. Structural characteristics of the optimal bleed–feed policies are analyzed in Koca et al. (2021a). However, Koca et al. (2021a) focus on the mathematical analysis of optimal polices, and do not discuss the implementation and integration of the three developed tools at MSD AH.

The yield optimization tool builds on the well-known theory of optimal learning and Bayesian design of experiments. In this context, our work presents a real-world application of the theory described in Powell (2010); Gelman et al. (2013); Frazier (2014, 2018).

The rhythm wheel tool is closely related to the field of production planning and scheduling in OR/MS. In this context, several studies address common industry challenges. For example, Limon and Krishnamurthy (2020) use Queuing Theory to address a resource allocation problem in protein purification. Petrides and Siletti (2004) discuss the benefits of process simulation in biopharmaceutical plants. Similarly, Leachman et al. (2014) develop an optimization-based production planning tool for the biotechnology industry. However, existing studies and commercially available software did not fully address the specific needs of MSD AH. The rhythm wheel tool presented in our work uses the well-known theory of simulation-based optimization, and addresses the specific needs and challenges of MSD AH.

5.3.2 The Bleed–Feed Tool

The bleed–feed tool determines an optimal bleed–feed time for a batch to maximize the long-run expected yield obtained per unit time. The tool uses renewal theory, and combines cell-level dynamics (i.e., cell growth phases and yield accumulation mechanisms) with manufacturing-level dynamics (i.e., harvest risks and yield trade-offs) to support decision making.

The input to the renewal model is related to the underlying dynamics of the fermentation process, such as the initial amount of pre-culture, biomass accumulation rate, set-up time, and parameters of the probability distributions related to the duration of the cell growth phases. The tool determines an optimal time to perform the bleed–feed operation to maximize the expected reward, namely expected throughput (i.e., expected yield obtained per unit time). To optimize the expected throughput of the system, the renewal model captures the expected yield and the expected cycle time as a function of the bleed–feed time. In this setting, a renewal cycle starts with a new setup. To calculate the expected yield of a renewal cycle, we developed a stochastic model that captures how the antigens accumulate over time during fermentation. This stochastic model is established based on Monod-type equations obtained from the biological and chemical engineering literature (Monod, 1949; Doran, 1995).

To calculate the expected cycle time, the renewal model considers the complex interaction between the bleed–feed time and the randomness in the duration of the exponential growth phase. Note that the bleed–feed operation can be performed only during the exponential growth phase. However, the time when the exponential growth phase ends is stochastic. This has complex implications on the expected yield and cycle time of a renewal cycle. More specifically, if the bleed–feed is performed after the exponential growth stops, then the bleed–feed is *unsuccessful* and the batch is harvested. In the model, this implies the end of a renewal cycle. Whereas, if the bleed–feed is *successful*, then the exponential growth phase is prolonged and the cells continue to grow for another round without any set-ups. This means that the existing renewal cycle continues, and hence the expected yield and cycle times continue to evolve accordingly. Therefore, the renewal model considers the random evolution of the yield and cycle time as a function of the bleed–feed time and identifies an optimal policy to maximize the resulting

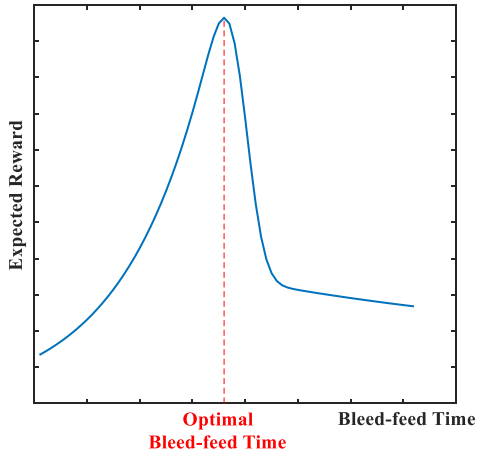

Figure 5.5: Example output of the bleed–feed tool.

throughput. We refer to Appendix 5.A for more information on the mathematical model.

The tool is developed in MATLAB® software. An integration with MS Excel is also provided for a user-friendly interface. Users enter the input parameters into an Excel file. Then, the renewal model runs automatically and calculates the optimal bleed–feed time. As an output, the tool reports an optimal bleed–feed time and its corresponding long-run expected throughput. In addition, the tool reports a plot that shows how the expected throughput changes as a function of the bleed–feed time. For example, Figure 5.5 represents an example output of the tool for a case study at MSD AH. In this case study, two years of production data have been analyzed for a specific antigen to identify model inputs. In this figure, we see that there is a unique optimal bleed–feed time (indicated with the dotted line). We can also observe that the model indeed captures the trade-off between yield and bleed–feed risks: performing the bleed–feed operation *too soon* leads to a sub-optimal throughput (i.e., the left-hand side of the optimal bleed–feed time) because of the lower yield collected from a bioreactor run; whereas, performing it *too late* also yields a sub-optimal throughput (i.e., the right-hand side of the optimal bleed–feed time), mainly because of the increased risk of missing the bleed–feed opportunity and incurring set-up costs for the subsequent batch.

Prior to the bleed–feed tool, there were no tools or models available in common

practice to assist with the bleed–feed decision. This decision was mainly made based on expert opinion and domain knowledge. The bleed–feed tool provides a data-driven and quantifiable approach to understand the system risks and optimize bleed–feed decisions.

5.3.3 The Yield Optimization Tool

The yield optimization tool builds a methodological approach for MSD AH to identify the best possible process configuration using a limited (and predetermined) number of experiments. First, we start by explaining our modeling assumptions. In our specific case study, we did not have full knowledge of the expected batch yield as a function of the critical process parameter. Therefore, we assumed a generic setting in which the expected yield was not necessarily monotone or concave in the critical process parameter. The yield obtained at each experiment was assumed to be normally distributed, with a mean and variance that depend on the critical process parameter. We validated this normality assumption through statistical analysis of a two years of production data. We also assumed an independent and identically distributed noise for each experiment, as the bioreactor was sterilized, and the system was reconfigured after each use.

The main goal of the project was to achieve the highest possible batch yield by adjusting the value of the critical process parameter. However, we had a limited budget for conducting experiments, and hence our central research problem was to smartly design an information collection policy in such a way that it would eventually lead us to an optimal value of the critical process parameter. To address this problem, we adapted a Bayesian approach, and modeled the uncertainty in the yield function by using a Gaussian process prior, which is commonly used to model continuous functions in Bayesian spatial statistics (we refer to Murphy (2012) for details on Gaussian processes). In our setting, the starting Gaussian process prior was determined based on expert opinion and domain knowledge. Then, we built a dynamic programming (DP) model with the objective of finding the best information collection policy that maximizes the expected yield. Following the literature on Bayesian methods for simulation optimization, we used the knowledge-gradient (KG) policy to build a one-step ahead approximation to the optimal policy (Powell and Ryzhov, 2012; Frazier, 2018). The main idea of KG policy is to compare the myopic value of what we learn from sampling different

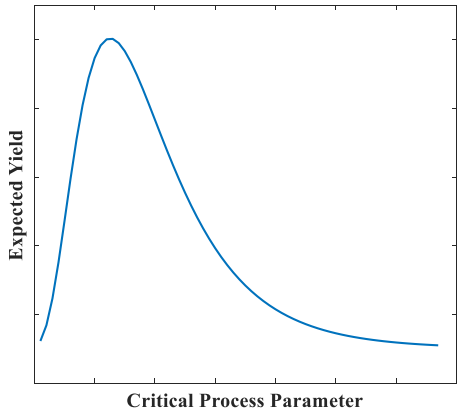

Figure 5.6: Example output of the yield optimization tool.

choices of the critical process parameter. Based on this information, KG policy suggests a specific value to be tested in such a way that the expected difference in value between our current knowledge on the prior distribution and our one-step lookahead knowledge on prior distribution is maximized (see Appendix 5.B for details on the mathematical model, and Frazier (2018) for a recent review on Bayesian optimization).

The output of the yield optimization tool is an information collection policy and an estimate of the best value of the critical process parameter that maximizes the expected yield. Figure 5.6 illustrates an example output of the tool. This figure plots our final belief on the expected yield as a function of the critical process parameter (we note that the original result is scaled to protect confidentiality). In this case study, eight real-world experiments were conducted to build this function. We observed that the end result is a monotone and concave function. The tool was developed using MATLAB® software, and open-source packages on KG heuristic and Bayesian learning were used to complement it. The tool provided a formal and rigorous approach to MSD AH for optimally designing experiments to support process improvement projects.

5.3.4 The Rhythm Wheel: Production and Capacity Planning Tool

The rhythm wheel tool addresses production and capacity planning problems of biomanufacturers. The tool is designed to help MSD AH assess the feasibility of a weekly production schedule and create smart schedules with higher throughput and lower lead times than the current practice. In addition, the tool is used to evaluate and justify capacity planning decisions at MSD AH.

The rhythm wheel tool consists of three steps: *simulation*, *optimization*, and *visualization*. The *simulation* model is developed with the Arena software and contains more than 8000 inter-dependent production steps for 48 different products with their unique routing on 25 pieces of equipment. The simulation model contains three main components: (1) a planning component in which a specific production rhythm is defined; (2) USP activities with a detailed process flow of pre-culture and fermentation operations; and (3) DSP activities with a detailed process flow of purification operations. The simulation model also captures several critical production constraints, such as bill of materials, precedence requirements, and the no-wait constraint in the system.

The main input to the simulation model includes a list of equipment and constraints on their availability (i.e., some processes cannot operate overnight as close monitoring might be needed), a list of available operators and their corresponding skill sets, routing information for each antigen, bill of materials, antigen-specific production steps and their corresponding processing times (i.e., distribution, mean and standard deviation of each operation), and a production rhythm to be evaluated. However, we note that further details of the simulation model (i.e., process flow diagrams, bill-of-materials, information on processing times and steps) are not disclosed to protect confidentiality. After the simulation model was built, it was linked to a simple MS Excel file to provide a user-friendly interface. This allowed the user to easily edit and change model inputs without interfacing with the details of the simulation model. For example, the user can input a specific rhythm to the Excel user interface by entering the names of antigens to be produced and their corresponding start time at the main fermentation operation. The simulation model retrieves this information and matches it with antigen-specific USP and DSP operations to run the simulation model. As an output, the rhythm wheel tool presents critical performance parameters (e.g., throughput,

utilization, and manufacturing lead times) obtained through a long-run (e.g., two years) simulation of the model.

After the simulation step, the tool uses a Tabu search algorithm in the *optimization* step to create smart schedules. The objective of the optimization step is to maximize throughput. For this purpose, the optimization model searches over feasible rhythms by changing the order and the start time of antigens in the main fermentation step. For a rhythm to be feasible, it should *(i)* have zero waiting times between biological processes (from pre-culture to main culture, or from USP to DSP), *(ii)* maintain the equipment utilization below a predefined threshold level (e.g., 90% utilization), and *(iii)* comply with production constraints (i.e., some resources are not available during night shifts, some operations must be performed by specific equipment or scientists, etc.). Considering these constraints, the tool determines when and on which process line the antigens should be produced. In case the planner is interested in evaluating (but not optimizing) the performance of a specific rhythm, she can skip the optimization and proceed with the visualization step.

After the optimization step, the tool *visualizes* the results in a dashboard. The dashboard reports the performance of a given rhythm (i.e., equipment utilization, throughput, and waiting times) in a way that is visually appealing and easy to understand for users. For example, equipment utilization and waiting times are presented in the form of a simple bar chart. If the equipment utilization exceeds 90% (utilization constraint) or waiting times are greater than zero (no-wait constraint) for a process line, then the schedule is clearly undesired.

Prior to the rhythm wheel tool, MSD AH relied on past experience and spreadsheet calculations to support production and capacity planning decisions, and the corresponding system performance could be assessed only through real-world implementation. The rhythm wheel tool provided a rigorous and reliable approach for predicting and better controlling the production system.

5.4. Implementation

Throughout the collaboration, MSD AH provided strong expertise on the life-science-related aspects of the project, and Eindhoven University of Technology

(TU/e) brought in expertise on OR. In this way, we encouraged an active collaboration leading to a smooth and successful implementation of the developed tools in daily operations. In compliance with common practice at MSD AH, we adopted the plan–do–check–act (PDCA) cycle to execute the project. The PDCA cycle is an iterative method for continuous improvement. Based on this approach, we describe the main steps of the project as follows.

1. **Plan:** The project was planned and monitored through regular meetings and brainstorming sessions at MSD AH. We conducted these meetings on a daily or weekly basis, depending on the specific needs of the project. Every three to four months, we provided an update presentation to a larger audience at MSD AH (including potential end users from various departments). In these meetings, we formulated specific objectives and reviewed the progress leading to the development of OR tools.

2. **Do:** This step corresponds to *data collection*, analysis, and development of OR tools.

3. **Check:** We *validated* the developed models and assumptions through expert opinions, historical data, and either laboratory- or industry-scale experiments. We also conducted numerical (sensitivity) analysis to check the robustness of the tool output and the quality of solutions.

4. **Act:** Based on the results obtained from the steps above, we identified improvement opportunities. We performed *tool enhancements* by revising the models, assumptions, and adding new features. To ensure a smooth implementation of the tools in daily operations, we *automated* their input and output and developed user-friendly interfaces.

A multi-disciplinary team of researchers were involved in the execution of the project. The core team at MSD AH consisted of three people and the extended team involved around ten researchers from various departments (i.e., including upper and middle management, process improvement engineers, and scientists working on daily production processes in clean rooms). The TU/e team consisted of two faculties, one Ph.D. student, and four Master's students. The students worked full-time on the project while supervisors from TU/e and MSD AH provided daily guidance. No formal "maintenance contract" was signed between TU/e and MSD

AH for the work done. However, it is envisioned that the developed tools will be maintained and enhanced over time through continued collaboration. For example, currently, MSD AH is sponsoring two new Ph.D. students (for four years) and around two Master's students per semester to sustain a longer-term collaboration.

In the following, we elaborate on the implementation process, and describe the challenges and opportunities raised throughout the process. First, we focus on the implementation of the bleed–feed tool and yield optimization tool, then elaborate on the rhythm wheel tool.

5.4.1 Implementation of the Bleed–Feed Tool and Yield Optimization Tool

In this section, we discuss the implementation of the bleed–feed and yield optimization tools together, because both of these tools focus on fermentation, and their implementation steps are similar.

Data collection. Fermentation is a highly controlled process where several physicochemical parameters (e.g., temperature, pH, etc.) are monitored and documented for regulatory purposes. Throughout the project, such process data were useful in modeling and analyzing the fermentation dynamics. For example, for the bleed–feed tool, antigen-related information (initial biomass amount and resulting yield) were obtained from historical data. However, in some cases, available process data were limited, and did not have sufficient information to justify our model assumptions. Therefore, several test runs were conducted at the laboratory or industry scale to collect the required information. For example, for the bleed–feed tool, the cell growth behavior after the bleed–feed operation was not fully known. Expert opinion indicated that the duration of the exponential growth phase would be prolonged with bleed–feed, and this behavior was later validated through laboratory-scale experiments. In some other cases, required data were not available but could be inferred from process measurements. For example, the duration of cell growth phases was not available. However, by detecting some pattern changes in certain physicochemical parameters, each cell growth phase duration was calculated. Such data were preprocessed manually, and then converted into a digital format.

For the yield optimization tool, the relationship between the critical process

parameter and yield was unknown, and hence industry-scale experiments were performed to understand this relationship. These experiments were conducted during the Christmas break. This time period was most suited to conduct such large-scale experiments, as most productions line were not active. This also meant that some operators agreed to work during this holiday break to perform the test runs. For some laboratory- or industry-scale experiments, additional sensors needed to be installed to measure the required parameters. As a hands-on approach, internship students from Eindhoven University of Technology were trained to independently operate these sensors and collect data.

Validation. The developed models and assumptions were validated through historical data, test runs, and expert opinions. Relevant papers from the life-science literature were also used to validate model assumptions on cell growth. What-if analysis was conducted to test the robustness of proposed solution. Then, the proposed policies were tested through laboratory- or industry-scale experiments. Results of these test runs were continuously monitored and discussed through regular meetings. For the yield optimization tool, the post-implementation process played a vital role in validation. After the new configuration of the critical process parameter was implemented, results of the industry-scale production runs were closely monitored for several months; the mean and variance of the batch yield were analyzed to ensure the quality and stability of the new production configuration.

Automation and tool enhancements. The input and output of the tools were automated through spreadsheet models. Simple user interfaces were developed at MS Excel to help scientists use the tools without interacting with the underlying optimization model. Through regular meetings with potential end users, we made several enhancements to the tools. For example, the objective of the bleed–feed tool was initially defined as to maximize the average profit. However, sensitivity analysis of the tool output revealed that the optimal bleed–feed time was very sensitive to the cost parameters. Therefore, we revised the objective function as to maximize the throughput. The solution obtained from the revised objective was more robust, and easier to adopt in practice. A critical feature we added to the bleed–feed tool was a module allowing the user to optimize the harvesting time. We decided to add this feature, after we observed that the current harvest policy was sub-optimal for the corresponding case study. Based on the user's preference, the enhanced version of the tool can optimize the bleed–feed time alone, harvesting

time alone, or jointly optimize both of them. Similarly, the yield optimization tool was initially developed to predict the expected yield as a function of one critical process parameter. As an enhancement, the model was extended to capture dependencies over multiple process parameters. This enhancement could be useful for future implementations at other process lines.

5.4.2 Implementation of the Rhythm Wheel Tool

Data collection. Biomanufacturing is a highly regulated environment where all processes are closely monitored and documented. This implies that relevant data were mostly available. However, finding the correct data from the appropriate resource in the correct format was not straightforward. During the project, we needed to track down process data from different resources and then matched them to ensure compatibility with the rhythm wheel tool. For example, ten years of USP data (on processing times and production parameters) were recorded for regulatory purposes. These USP data were stored in separate Excel spreadsheets for each antigen. We extracted relevant information from these spreadsheets and combined them into one master file. However, this master file did not include DSP data. Unlike USP data, DSP data were not available in a digital format. Therefore, we needed to pre-process and digitalize this information. We knew that every item of DSP equipment was continuously monitored through a batch monitoring software. This software kept track of all process parameters for each batch produced in the past two years. However, the software was designed to view the screen only, without allowing data to be stored digitally on an external drive. Therefore, we took screen shots of these data, and then printed and scanned them through an optical character recognition software to obtain a digital data set. There were a few minor cases in which equipment was not connected to this batch monitoring software. For such cases, we collected the required data in the field, by retrieving the corresponding information from the memory of the equipment itself.

Validation. The simulation model was validated through comparison against historical production data, what-if experiments, and expert opinion. For example, random snapshots were selected from historical production data and corresponding rhythms were mirrored to the simulation model. Subsequently, the output of the simulation model and the performance metrics obtained in real-world were compared in terms of lead time, utilization, and throughput. On average, the

simulation model performed with 95–98% accuracy compared with the real-world performance results. In addition, we conducted several sensitivity analyses (on distributions and parameters of processing times, batch sizes, capacity constraints, specific rhythms, etc.) to test the robustness of the model output. Several meetings were held with operators and production planners to validate the process flows, bill-of-materials, production constraints, processing times, etc.

Automation and tool enhancements. Input and output of the tool are automated via a user-friendly interface, such that users with no simulation-optimization background could easily use the tool. For this purpose, the simulation model interacts with an MS Excel file. Users enter the required information (i.e., products to be produced, operator availability, etc.) into the Excel spreadsheet. In less than twenty seconds, the tool reports the results in terms of simple and understandable visuals, such as plots and tables. Through several iterations, we made multiple enhancements to the simulation model to make sure that we created a digital twin of the Boxmeer facility. These enhancements included adding or removing dependencies and production constraints, adjusting process parameters, etc. The most significant tool enhancement was related to the optimization part. Initially, the project objective was to develop a simulation model for performance evaluation. The development of the optimization part arose naturally during the process as a new module to enhance the simulation model.

Implementation highlights. When the rhythm wheel tool was first implemented, it showed that one extra batch could have been produced each week, without any capacity expansions. After we discovered it, the visualization step of the tool provided an effective means of communicating this insight with stakeholders. For example, it showed that one extra batch per week would not necessarily lead to higher congestion in the system. This encouraged an open and clear discussion on what could be done and how, and prevented any possible resistance to change. Subsequently, the proposed solution was successfully implemented and led to one extra batch per week.

The rhythm wheel tool has also been successfully used to evaluate process improvement opportunities. For example, in one specific case study, the process improvement team realized that increasing the fermentation time of a specific antigen would improve the batch yield. However, the simulation model revealed that the potential gains in yield would not outweigh the corresponding increase in

fermentation time and would lead to a lower throughput on average. In this setting, the tool provided a rigorous approach for translating a process-level change (i.e., fermentation time and yield) into a system-level metric (i.e., throughput), which would not have been possible otherwise.

Such success stories inspired several follow-up projects. For example, MSD AH is in the process of implementing these ideas at two other facilities, in two other countries. Similarly, the bleed-feed and yield optimization tools were initially developed for one production line but their success encouraged follow-up implementations at two other production lines in the Boxmeer facility.

5.5. Impact

The OR tools have been used in daily operations at MSD AH since August 2017. The OR tools have been implemented in multiple different production lines and directly affected the business metrics: In total, the project resulted in roughly €50 million additional revenue per year.[2] More specifically, we achieved an increase of 45% in annual production yield on one of the production lines, resulting in an additional revenue of €12 million per year. On a second production line, we achieved an increase of 50% in yield, leading to €18 million per year. On a third production line, we achieved an additional revenue of €2.5 million per year. On average, the implementation of the bleed–feed tool resulted in an 85% improvement in batch yield per setup (based on one bleed–feed). The rhythm wheel tool allowed one extra batch to be produced per week, without making any investments on additional resources, leading to an additional €18 million per year. As a joint impact of all the OR tools, the production outcome increased by 97% without expanding the existing capacity. As a side benefit, the systematic application of a data-driven, OR-based approach enabled a better standardization of daily operations, resulting in 20% reduction in the standard deviation of the annual production yield.

In addition to the financial benefits, the OR tools provided several non-quantified benefits:

[2]We quantified the impact in terms of additional 'revenue' (and not 'cost' reduction). This is because we found that this approach was more intuitive and easier to present within MSD. For example, the yield optimization tool increased the yield obtained from each batch while the total production cost (per batch) remained the same.

1. Reduced CO_2 reduction through increased production yield per batch.

2. Better response to market needs: The animal health industry is currently experiencing large deficiencies in meeting the market demand worldwide. Every extra unit produced has a significant contribution in responding to market needs. In particular, in the context of animal health, the facility in Boxmeer is a leading biomanufacturing hub serving the entire world. Therefore, increasing the production yield at this facility can have substantial social implications in terms of improved availability and accessibility of these drugs.

3. Creation of new jobs: MSD AH created four new job positions in the Boxmeer facility for industrial engineers. As Oscar Repping, the Executive Director at MSD AH states, the company recognizes OR as an important skill set to consider during future hiring processes. Currently, MSD AH is in the process of sponsoring new PhD students at Eindhoven University of Technology.

4. Rigorous assessment of production capabilities: The rhythm wheel tool allowed a formal and quantitative assessment of manufacturing capabilities and production schedules. More specifically, the tools helped MSD AH translate the complex dynamics of the underlying biological processes into business metrics, such as throughput, lead times, and costs. This also resulted in an improved understanding of the system dynamics within the facility.

5. Increased flexibility: The use of OR tools helped to increase the yield without additional resource investment. The increased batch yield freed up significant production capacity, leading to higher flexibility within the facility. In addition, the OR tools provided flexibility of designing several process improvement ideas and allowed them to be evaluated through what-if analysis (e.g., purchase of equipment) before implementing them in real life.

6. Data-driven decision making; change in the mindset: MSD AH experienced a systematically increased use of a data-driven, OR-based approach. Prior to the OR tools, process data were collected for documentation purposes, but were not actively analyzed for optimization projects. The project encouraged making the best use of historical process data. In addition, the idea of integrating the underlying biology with manufacturing system dynamics and financial trade-offs was new for most scientists, and they all embraced it.

We note that the developed tools are flexible to address common industry challenges and can be easily adjusted to other production lines or facilities. For example, MSD AH is currently in the process of implementing these tools on additional production lines within the Boxmeer facility. The longer-term vision is to encourage systematic use of these tools at other facilities worldwide.

5.6. Conclusions

Biopharmaceuticals are highly innovative, and complex compared with conventional drugs. Their production process relies on growing cell cultures and using live organisms to generate active ingredients. However, the use of live organisms during production creates challenges that are unlike those in any other industries. For example, most biomanufacturers encounter issues related to predictability, stability, and high levels of batch-to-batch variability. Whereas, with the growing market demand and increasing competition, the competitive advantage in the industry is shifting from the scientific expertise to finding new ways of achieving higher efficiency.

To address these challenges, a multidisciplinary team of researchers collaborated over three years to develop a portfolio of optimization models and decision support tools. These tools were aimed at improving biomanufacturing efficiency using a variety of operations research methodologies, including stochastic optimization, Bayesian design of experiments, and simulation-optimization. The developed models link the underlying biology and chemistry of biomanufacturing processes with financial trade-offs and business risks. The research has been conducted in close collaboration with MSD AH. Industry implementation at MSD AH had a significant impact with up to 50% increase in batch yield and an additional revenue of €50 million per year.

To date, several industries have benefited from OR to improve efficiency and reduce costs. However, the applications of OR have not been widely adopted in the biomanufacturing practice yet. This project is one of the first examples that shows and quantifies how OR can benefit the biomanufacturing industry. Our project is generalizable to other biomanufacturing companies. For example, the developed OR tools (e.g., mathematical models presented in Appendix 5.A and 5.B) are generic

and can be easily applicable to other biomanufacturing companies. The effort in this project builds on the existing work in the OR literature, as it presents a systematic application of the well-known OR methodologies (i.e., renewal reward theory, machine learning, and simulation-based optimization) in an innovative context of biomanufacturing. As more companies such as MSD AH embrace operations research, we believe that this will significantly help the industry provide faster and more affordable access to new treatments.[3]

5.A. Mathematical Model of the Bleed-Feed Tool

A fermentation cycle starts with a set-up and involves the fermentation process (including bleed-feed). A new cycle starts each time a batch is harvested. Let t_b denote the time when the bleed-feed is performed in a fermentation cycle. We let $\mathbb{E}[Y(t_b)]$ denote the expected yield obtained in a fermentation cycle and $\mathbb{E}[L(t_b)]$ be the expected length of a fermentation cycle when the bleed-feed is performed at time t_b. Subsequently, we let $R(t_b)$ be the expected yield obtained per unit time when the bleed-feed is done at t_b. Using the renewal reward theory, we get

$$R(t_b) = \frac{\mathbb{E}[Y(t_b)]}{\mathbb{E}[L(t_b)]}. \tag{5.1}$$

First, we focus on the term $\mathbb{E}[L(t_b)]$ in Equation (5.1). We let T_e denote a random time when the exponential growth phase ends. The random variable T_e has the probability density function $g(\cdot)$ and realization t_e. In addition, t_h denotes the harvesting time (i.e., the processing time of fermentation without bleed–feed), and s is the duration of a bioreactor setup. Therefore, the expected length of a fermentation cycle when we bleed-feed at time t_b is

$$\mathbb{E}[L(t_b)] = s + \int_0^{t_b} t_b\, g(t_e)dt_e + \int_{t_b}^{\infty} (t_b + t_h)g(t_e)dt_e. \tag{5.2}$$

Equation (5.2) indicates that the processing time is equal to the bleed–feed time t_b when the exponential growth phase stops before the bleed–feed time t_b. Otherwise, the processing time is $t_b + t_h$.

[3]MSD AH's notes on conclusions are presented in Appendix 5.C.

Next, we focus on the term $\mathbb{E}[Y(t_b)]$ in Equation (5.1). Fermentation starts with a pre-defined biomass (yield) amount b_1. In alignment with the literature, we use the function $b_1 e^{\mu t}$ to capture the total amount of biomass that accumulates by time t, where $t \leq t_e$ and the term μ denotes a constant accumulation rate (Doran, 1995). Next, we let $\psi \in (0,1)$ represent the fraction of biomass to be extracted during bleed-feed (i.e., the remaining fraction $1-\psi$ continues growing inside the bioreactor after we bleed-feed). Therefore, the expected yield obtained in a fermentation cycle when we bleed-feed at t_b is

$$\begin{aligned}\mathbb{E}[Y(t_b)] = &\int_0^{t_b} b_1 e^{\mu t_e} g(t_e) dt_e \\ &+ \int_{t_b}^{t_h} [\psi b_1 e^{\mu t_b} + (1-\psi) b_1 e^{\mu(t_b+t_e)}] g(t_e) dt_e \\ &+ \int_{t_h}^{\infty} [\psi b_1 e^{\mu t_b} + (1-\psi) b_1 e^{\mu(t_b+t_h)}] g(t_e) dt_e.\end{aligned} \tag{5.3}$$

Using Equations (5.1)-(5.3), the optimal bleed-feed time t_b^* is given by $\underset{t_b}{\operatorname{argmax}}\, R(t_b)$.

5.B. Mathematical Model of the Yield Optimization Tool

In our problem setting, we have k alternative options to configure the critical process parameter, where k is assumed to be finite and countable. We let $\mu_x \in \mathbb{R}$ represent the underlying value of alternative x, which is unknown to the decision-maker and learned through real-world (industry-scale) experiments. To model the uncertainty in underlying value μ_x of option x, we use a Bayesian approach. Specifically, we assign a probability distribution that describes the uncertainty in μ_x. Following Powell (2010); Gelman et al. (2013) and Frazier (2014), before we start collecting any information, we assume that our prior distribution of belief about μ_x is normally distributed with mean μ_x^0 and precision β_x^0. Let W_x^n denote the output of the experiment n representing the realized yield value. It is considered that the precision of this measurement is given by β_e. In our problem setting, the precision is fixed and known.

In total, only N experiments can be conducted because of resource limitations and

budget constraints on experimentation. When we select an alternative $x_{n+1} = x$ at the $(n+1)$th experiment, we observe $W_x^{n+1} \sim \text{Normal}(\mu_x, 1/\beta_\epsilon)$. Given that our current belief about unknown μ_x is captured with normal prior belief having parameters μ_x^n and β_x^n (at the end of nth experiment), Bayes theorem can be used to show that the updated mean and precision of the posterior belief on μ_x can be computed using $\mu_x^{n+1} = (\beta_x^n \mu_x^n + \beta_\epsilon w_x^{n+1})/(\beta_x^n + \beta_\epsilon)$ and $\beta_x^{n+1} = \beta_x^n + \beta_\epsilon$ (Gelman et al., 2013). Furthermore, since the prior belief of μ_x is normally distributed, its posterior belief is also normally distributed.

Repeating the updating procedure, we subsequently collect samples $x_1, \ldots, x_N$, $w_1, \ldots, w_N$ after a total of N experiments. Based on these samples, if we choose the alternative x, we get the conditional expected reward $E[\mu_x | x_1, \ldots, x_N, w_1, \ldots, w_N] = \mu_{N,x}$. Therefore, our objective is to identify the alternative which has the highest conditional expected reward; i.e., $\text{argmax}_x \, \mu_{N,x}$ with the corresponding value $\max_x \mu_{N,x}$. The question then becomes how collect the samples (i.e., choose the alternatives $x_1, \ldots, x_N$) such that the conditional expected reward is maximized. We answer this question by adopting the knowledge gradient approach for offline learning Powell (2010); Gelman et al. (2013). Specifically, we first compute the expected value of measuring the option x, i.e.,

$$\mathbb{E}[V^{n+1}(S^{n+1}(x)) - V^n(S^n) | S^n], \tag{5.4}$$

where $S^n = \{(\mu_x^n, \beta_x^n) : x = 1, \ldots, k\}$ is the current state of knowledge, $S^{n+1}(x)$ is the updated state of knowledge after choosing option x and observing W_x^{n+1}, and $V^n(S^n)$ denotes $\max_{x' \in \{1,\ldots,k\}} \mu_{x'}^n$ (i.e., the value of being in the knowledge state S^n). The term in (5.4) is referred as the knowledge gradient as it represents the marginal value of information from measuring the option x. For a more detailed description of how to calculate the knowledge gradient, see (Powell, 2010; Gelman et al., 2013; Frazier, 2014, 2018).

5.C. Notes of MSD AH on Conclusions

This project serves to our motto "*Invent. Impact. Inspire.*" Our motto represents a mechanism for value creation through continuous improvement. By combining knowledge from the life sciences and OR, we have built a variety of optimization

models and decision support tools to improve biomanufacturing efficiency (*Invent*). The project achieved a significant impact with up to 50% increase in batch yield and €50 million additional revenue each year. As a combined effect of all the OR tools, the production output at the Boxmeer facility increased by 97%, without any additional investment in capacity (*Impact*). The results inspired several follow-up projects both nationally and internationally (*Inspire*). For example, the Boxmeer facility is currently collaborating with two other facilities in two other countries to help them use the OR tools. Furthermore, new initiatives are encouraged for knowledge transfer to the human health department in the Netherlands.

In the future, such projects can help animals and humans get cheaper and faster access to new treatments. As Oscar Repping, Executive Director at MSD AH states, "We [the industry] will benefit from OR, as such, we will avoid investments, we will become more predictive, leading to cost reduction, leading to more capacity on our production lines, meaning that we can make this world a better place."

6

Conclusion

Biopharmaceuticals are revolutionary and complex compared to conventional drugs, due to the use of living cells in their production processes. Therefore, biomanufacturers face challenges that are different than those in any other industry. In this thesis we develop analytical models to improve biomanufacturing efficiency. We focus on a novel technique: bleed–feed. Bleed–feed is promising in skipping intermediary setups, but its optimal implementation involves unique trade-offs and challenges. We combine the biological dynamics of fermentation and the operational trade-offs of bleed–feed, and present stochastic optimization models to find optimal bleed–feed policies for different contexts. We generate managerial insights and inform practitioners about the potential of bleed–feed implementation. Our work is one of the limited attempts to demonstrate how OR can complement life sciences. To the best of our knowledge, we are the first to address the bleed–feed problem and to present successful industry scale implementation of bleed–feed for batch fermentation.

In this section we present our findings and discuss their practical implications. We first elaborate on our main results from each chapter (Section 6.1), and then conclude the thesis with directions for future research (Section 6.2).

6.1. Main Results

Main Results from Chapter 2. In Chapter 2, we assume the batch condition is monitored regularly, and we aim to the obtain as much yield as possible from a batch with bleed–feed under regulatory requirements. We search for: (RQ1) the optimal condition-based bleed–feed policies to maximize the expected total biomass obtained from a batch, (RQ2) the effects of regulatory limitations on bleed–feed (i.e., maximum number of bleed–feeds permitted on a batch), and (RQ3) the room for improvement with bleed–feed.

We build a finite-horizon, discrete time MDP model to maximize the total expected batch yield (RQ1). We analyze the structural characteristics of the optimal policies and show that the optimal bleed–feed policies have three-way control limit structure on the cultivation age, cell growth rate, and the bleed–feed count under mild conditions. This structure continues to hold if we aim to maximize the batch profit. Control limit policies are intuitive and easy to implement in practice. In addition, we present a sufficient condition under which a risk-averse heuristic is optimal. We characterize the value function as a function of the regulatory restrictions on bleed–feed number and show that marginal benefit of an additional bleed–feed decreases and converges to the critical biomass level (RQ2). Our base model assumes that the number of bleed–feeds performed on the batch does not affect the transition probabilities to the stationary phase. This assumption is valid if we do not exceed the maximum bleed–feed number permitted by the regulations. We relax this assumption in a model extension and show that three-way control limit structure continues to hold under sufficient conditions. We also perform analytical sensitivity analyses and generate insights about impact of batch risk and cell growth rate on the expected total biomass and the optimal bleed–feed time. In addition, we perform a case study from MSD AH to demonstrate the impact of bleed–feed under different production settings (RQ3). We observe an 137% increase in total biomass production from one setup with two bleed–feed implementations (in the base case). Sensitivity analyses on system risks and the critical biomass level reveal that low risk batches and cultures with high critical biomass levels benefit more from bleed–feed implementation. We observe that implementing bleed–feed is better for all production settings compared to no bleed–feed.

Our MDP model is simple and captures the biological dynamics of fermentation

and operational trade-offs of bleed–feed. Hence, we could derive most of the managerial insights from analytical results. Our analytical results contribute both to OR literature and practice. Insights from this chapter are useful when the focus is maximizing the batch yield and the processing time is less important (e.g., if certain demand must be met), and for implementing multiple bleed–feeds. However, the MDP model assumes the batch state is monitored. This may not be the case in companies due to unavailability of sensors and operators. For this reason, implementation of this model might be harder (or less attractive) compared to time-based models.

Main Results from Chapter 3. In Chapter 2 we observe that the expected total biomass obtained from a batch increases with bleed–feed. However, bleed–feed increases the fermentation processing time as well. In addition, time-based policies are also attractive for practitioners due to production planning restrictions. Thus, in Chapter 3 we generate time-based bleed–feed policies to maximize throughput (RQ4). Industry data indicated that the initial biomass amount for the second cultivation affects the throughput. Hence, we optimize the bleed–feed time and the initial biomass amount for the second cultivation jointly and investigate the additional benefit of the joint optimization (RQ5). We explore the production settings that benefit the most from bleed–feed, or when adopting bleed–feed is not desirable (RQ6).

We build a renewal model to jointly optimize the bleed–feed time and the initial biomass amount for the second cultivation, to maximize fermentation throughput (RQ4 and RQ5). We explore the structural properties of the optimization problem to generate insights on optimal policies and assess the impact of batch risks on throughput (RQ6). We present a sufficient condition under which the throughput function is convex for a specific range of bleed–feed time. Using this result, we discuss the settings where implementing bleed–feed is not beneficial. We show that the expected yield obtained from the second cultivation is concave in the initial biomass amount for the second cultivation for a special case. In addition, we show that a higher risk batch reaches a lower throughput. We enhance the managerial insights with a case study from MSD AH. In this case study we consider several strategies to understand the benefits of optimizing the bleed–feed time and the replenishment amount jointly (RQ5). We quantify the potential benefits of bleed–feed implementation under different production settings (RQ6). Our numerical

analysis shows that the expected throughput can be improved by 17% with bleed–feed and bleed–feed brings the most benefit for fast-growing cells. We see that even if we have no setup time the throughput increases with bleed–feed, although the improvement percentage is lower for these scenarios. Different from Chapter 2, in this chapter implementing bleed–feed is not beneficial under certain settings. For instance, bleed–feed is not an attractive option for slow-growing cell cultures. This is because extra biomass produced does not outweigh the increased processing time.

We note that our analytical results are limited in this chapter, due to the complex behavior of the reward function. This is because the probability distribution of entering to the stationary phase is a complex function (recall that we characterize the distribution of the exponential growth phase duration as a function of the biomass level using the rate function established from the industry data). Since our reward function depends on these rate and probability functions, analyzing its structure was not straightforward. Still, our analytical results contribute to OR literature and provide a better understanding on bleed–feed.

Insights from Chapter 3 can be useful when increasing the yield per setup is not our only concern, and the increased processing time with bleed–feed is also considered. In this model the bleed–feed time is determined in advance, meaning that the system does not have to be monitored. Hence, this model can be easier to adopt under production planning restrictions and can be attractive to practitioners. We also generate insights on optimizing the start amount for the second cultivation together with bleed–feed time. In practice start amount can be changed by adjusting the amount extracted from the batch during bleed–feed. However, this might not be easy, since it requires special adjustments to be done at the bleed–feed time, and operators' presence. For instance, it may be more practical to extract a fraction (as in Chapter 4 and 5). However, extracting a fraction complicates the reward function more, and for tractability we assume that we optimize the initial amount. We believe that our insights remain the same for wither case. Also, this model assumes full operator availability and does not consider constraints on the bleed–feed time. Hence, the optimal bleed–feed generated by the model time might not be feasible under certain settings.

Main Results from Chapter 4. In Chapter 4, we take relevant restrictions on the bleed–feed time into account. We also model the impurity accumulation in the

batch, along with the biomass growth. We find the optimal bleed–feed time to maximize the fermentation profit per time unit (RQ7), ensure operators are available during the bleed–feed time and capture the risk-behavior of the biomanufacturer (RQ8), and investigate the value of flexibility in bleed–feed decisions (RQ9).

We extend our renewal model from Chapter 3 to find the bleed–feed time that optimizes the fermentation profit per time unit, including practically relevant constraints in the optimization model (RQ7 and RQ8). The constraints capture the restrictions on the bleed–feed time related to operator availability to perform bleed–feed and the biomanufacturer's risk behavior. In this model we also include waste accumulation, costs related to its purification and its effect on the exponential growth phase duration. We perform a numerical analysis to generate managerial insights. We consider different cases by relaxing the constraints, so that we investigate the value of flexibility in bleed–feed decisions (RQ9). Our results indicate that it is not necessarily better to implement bleed–feed earlier if bleed–feed time is not in a shift, and chance constraints have more impact for low-risk batches. We assess effects of restrictions on the bleed–feed time under different production configurations. We observe that if revenue is higher compared to the purification cost, then the risk-averse case performs closer to the most flexible case. We observe cases where bleed–feed is worse than no bleed–feed. If we have both the shift and the chance constraints, or if the waste accumulation is fast, then bleed–feed is not an attractive option.

We note that this model is less tractable than the one from Chapter 3, because it captures the waste accumulation, takes constraints on the bleed–feed time into account, and assumes that we extract a fraction from the batch. Thus, our insights from this chapter are based on a numerical analysis. We also note that real-world data on waste accumulation was not available and we rely on literature review and expert opinion to model waste. Yet, this chapter provides a framework for modeling the effects of waste accumulation in the bleed–feed decisions for maximizing the profit. When the waste accumulation is significant and/or waste decreases batch quality dramatically, this framework can be useful. Also, companies working with shifts, or practitioners when determining their risk behavior can benefit from the insights generated in this chapter. This model assumes a fraction is extracted from the batch. This may be more practical compared to the model from Chapter 3. In line with industry application, we assume this fraction is given, and we do not

optimize it. We believe Chapter 3 captures the optimization of the replenishment amount, and the insights do not change for this model.

Main Results from Chapter 5. In Chapter 5, we collaborate with MSD AH, and present a portfolio of operations research tools to improve biomanufacturing efficiency. More specifically, we introduce: *(i) bleed–feed tool*, by using renewal reward theory to determine optimal bleed–feed time to optimize the fermentation throughput, *(ii) yield optimization tool*, by using Bayesian design of experiments to provide a methodological approach for determining the best fermentation configurations under limited number of experiments, and *(iii) rhythm wheel tool*, by using simulation-optimization to assess the feasibility of a weekly production schedule and create smart schedules to increase throughput and lower the lead times. We elaborate on the development of these tools and their implementation at MSD AH. These tools are currently in use at MSD AH. Thanks to these tools, MSD AH had a significant impact with up to 50% increase in the batch yield, and an additional revenue of €50 million per year. The rhythm wheel tool allowed one extra batch production per week. Bleed–feed tool resulted in 85% increase in the batch yield per setup (using one bleed–feed).

We note that the tools are developed specifically for MSD AH, and the results are based on MSD AH implementation. Still, the tools are flexible to address common industry challenges, and they can be extended to other process lines and companies. The results can motivate other companies to use OR methods to improve their processes. The proposed models and their insights can be used as a starting point and the tools can be adapted based on the special needs of different companies/process lines. For example, the renewal model presented in this chapter is a modified version of Chapter 3 and 4. Modifications ensure that the model fits the needs of MSD AH and is easy to implement in real life. Yet, as shown in Chapter 3 and 4, we can easily extend our model for different contexts.

Overall Results. Our chapters capture different objectives and base cases; thus, it is not straightforward to compare their numerical results. Still, we obtain several insights based on our overall bleed–feed analyses. First, we observe that bleed–feed is promising. We emphasize that a bleed–feed does not produce a full batch but produces slightly less to avoid missing the bleed–feed opportunity. Still, significant improvement in the expected batch yield is achieved with bleed–feed (Chapter 2).

Benefits drop when we include processing time in the objective by considering throughput (Chapter 3) or profit per time unit optimization (Chapter 4). This is because bleed–feed also increases the fermentation processing time as the bioreactor is occupied longer. In Chapter 3 and 4 we observe certain scenarios (i.e., batches with slow growth, low initial biomass or fast waste accumulation) does not benefit from bleed–feed.

Chapter 2 and 3 show that the optimal policy implements bleed–feed later than the risk-averse policy, if bleed–feed is desirable. However, when we have restrictions on the bleed–feed time in Chapter 4, shift constraints might force the system to bleed–feed earlier than the risk-averse policy. We observe in each chapter that if critical biomass is higher, or if we have batches that exhibit higher probabilities of entering the stationary phase in the critical biomass level, risk-averse strategy performs closer to optimal. We note that risk-averse policy assumes critical biomass level to be greater than the initial biomass amount of the fermentation. This might not always be the case, and the culture can have the risk of entering to the stationary phase since the start of fermentation. Then, the risk-averse policy does not implement bleed–feed, while, as we observe, the optimal policy does. Although in this case bleed–feed brings lower benefits (recall that for batches with higher critical biomass bleed–feed has a stronger business case).

Having restrictions on the bleed–feed time can reduce its benefits up to 24% in the base case compared to the flexible case. This case represents the most restrictive case where the bleed–feed time is forced to be too early. Then, we see that bleed–feed is not an attractive option. Note that it is also possible for the optimal bleed–feed time from the flexible case to be during a shift (as in Chapter 5). Thus, a shift constraint might have no effects on implementation or impact of bleed–feed. Hence, this result is highly sensitive to the process parameters. Our constraints guarantee to meet these restrictions, and provide an understanding on how optimal bleed–feed time is affected by them.

6.2. Directions for Future Research

In this thesis we assume availability of sufficiently large data to make inferences about fermentation systems. This might not be the case for all products and

companies. For instance, since bleed–feed is a new technology, in the early stages of this research no bleed–feed data was available. Our preliminary models relied on literature review, expert opinion, fermentation data (without bleed–feed) and some laboratory scale experiments. This is also the reason for our renewal models and industry implementation to focus on single bleed–feed implementation. When bleed–feed implementations started in MSD AH, we could validate our assumptions with industry data. However, this data is still limited. Companies should collect fermentation data with and without bleed–feed. Especially the cell growth rate, and transitioning to the stationary phase based on biomass level should be observed after each bleed–feed to capture the effects of bleed–feed on each cultivation. Our models could be revisited if evidence is found from additional data. Such modifications would especially be important for Chapter 2, as the MDP model implements multiple bleed–feeds. This is because determining the optimal bleed–feed time in different cultivations (under multiple bleed–feeds) would require a good understanding on them. Our renewal models could be extended to capture multiple bleed–feeds. Also, Chapter 4 captures the waste and its effects on profit and exponential growth phase. Due to lack of industry data on waste, our models in Chapter 4 rely on literature review and expert opinion. Future work could collect more data on waste accumulation. If needed, our model from Chapter 4 should be modified. Also, future studies could train machine learning models to support bleed–feed decisions under limited data.

Chapter 4 takes operator availability into account, but it does not consider the scheduling aspect in detail. Future research can relax the assumption of setups starting at the beginning of a shift. Then, we can decide when to start the fermentation process to maximize the fermentation throughput (or profit per time unit) ensuring that bleed–feed takes place in a shift. Another direction for future research could focus on production planning. The demand, holding and shortage costs could be considered. Subsequently, start time of the fermentation, bleed–feed and harvest times and production amount (e.g., which bioreactor size to use) could be determined. Depending on the cost parameters and demand, harvesting early, or not implementing bleed–feed could be optimal. Fermentation of other products can also be taken into account to make plant-wise production planning decisions. This could be done by incorporating the bleed–feed technique in the rhythm wheel tool.

Although we increase the bioreactor time with bleed–feed, we do not consider reliability of the bioreactor. If the bioreactor fails, the batch might fail suddenly or contamination may accumulate in the batch. This contamination may deteriorate the batch quality and lead to batch failure. Chapter 4 captures the waste and its effects on profit and exponential growth phase. Also, the model extension provided in Chapter 2 might provide insight for these aspects, as we assume batch failures become more likely as we bleed–feed. Yet, these models capture the failure of bleed–feed implementation (as a result of transitioning to the stationary phase), and do not exclusively model the bioreactor reliability. Future research can model the trade-off between producing more with bleed–feed and risking to scrap the entire batch due to increased bioreactor time. This extension would be useful especially for products and industries where contamination significantly deteriorates the product quality or when bioreactor is less reliable. Future work could extend our MDP model, so that contamination of the batch is also monitored. Specification limit for the highest allowable waste could be considered to capture batch failure.

Note that implementation of bleed–feed to a batch fermentation does not require investments for switching to different fermentation modes. A cost/benefit analysis could be performed to compare switching to a continuous system (continuous, fed-batch or perfusion mode of fermentation) versus implementing bleed–feed in the existing batch fermentation.

Finally, we propose analytical models in this thesis, that are generic and can be extended to different companies. Implementation of the decision support tools (presented in Chapter 5) in other MSD plants and process lines are ongoing. Bleed–feed could also be implemented in single use bioreactor systems, where setup time is significantly reduced for a batch. Our numerical analysis from Chapter 3 suggests that bleed–feed still brings benefits for lower setup times. Another extension could focus on implementing "bleed" into fed-batch fermentation systems. Insight from our work could be combined with growth dynamics of fed-batch fermentation, and bleed policies could be investigated. It could also be interesting to explore applications of bleed–feed in other industries involving fermentation processes, or working with living cells (i.e., food processing). The proposed models might be directly applicable to certain settings. In this case, first the process parameters should be determined through an analysis of fermentation data, then the optimal bleed–feed policies can be found using our models. Or the models

might need modifications before being implemented to other industries, since our understanding of bleed–feed in this thesis is based on animal health industry. For instance, human health industry is known to be more sensitive to waste accumulation. A more comprehensive waste accumulation model (than the one presented in Chapter 4) might be needed for human health applications. Similarly, cell growth dynamics can vary among different industries, due to the use of different type of cells, medium and equipment. For instance, bleed–feed might affect the cell growth rate, or the batch might not have to be harvested if cells enter to the stationary phase. Hence, fermentation dynamics should be observed to understand the cell growth behavior. If necessary, our models can be modified before being implemented in real life.

Bibliography

M.-L. Allain, E. Henry, and M. Kyle. Competition and the efficiency of markets for technology. *Management Science*, 62(4):1000–1019, 2016.

A. Arora, A. Gambardella, L. Magazzini, and F. Pammolli. A breath of fresh air? Firm type, scale, scope, and selection effects in drug development. *Management Science*, 55(10):1638–1653, 2009.

X. Bei, X. Zhu, and D. W. Coit. A risk-averse stochastic program for integrated system design and preventive maintenance planning. *European Journal of Operational Research*, 276(2):536–548, 2019.

H. Ben-Ameur, M. Breton, and P. L'Ecuyer. A dynamic programming procedure for pricing American-style Asian options. *Management Science*, 48(5):625–643, 2002.

S. Bhattacharya, V. Gaba, and S. Hasija. A comparison of milestone-based and buyout options contracts for coordinating R&D partnerships. *Management Science*, 61(5):963–978, 2015.

T. Boone, R. Ganeshan, Y. Guo, and J. K. Ord. The impact of imperfect processes on production run times. *Decision Sciences*, 31(4):773–787, 2000.

S. Çetinkaya and C.-Y. Lee. Stock replenishment and shipment scheduling for vendor-managed inventory systems. *Management Science*, 46(2):217–232, 2000.

H.-C. Chang and C.-H. Ho. Exact closed-form solutions for "optimal inventory model for items with imperfect quality and shortage backordering". *Omega*, 38 (3-4):233–237, 2010.

H. N. Chang, N.-J. Kim, J. Kang, C. M. Jeong, J.-d.-r. Choi, Q. Fei, B. J. Kim, S. Kwon, S. Y. L. Lee, and J. Kim. Multi-stage high cell continuous fermentation for high productivity and titer. *Bioprocess and Biosystems Engineering*, 34(4):419–431, 2011.

J. J. S. Cheema, N. V. Sankpal, S. S. Tambe, and B. D. Kulkarni. Genetic programming assisted stochastic optimization strategies for optimization of glucose to gluconic acid fermentation. *Biotechnology Progress*, 18(6):1356–1365, 2002.

H. Cherkaoui, K. T. Huynh, and A. Grall. Quantitative assessments of performance and robustness of maintenance policies for stochastically deteriorating production systems. *International Journal of Production Research*, 56 (3):1089–1108, 2018.

Y. Chow, S. Moriguti, H. Robbins, and S. M. Samuels. Optimal selection based on relative rank (the "secretary problem"). *Israel Journal of Mathematics*, 2(2):81–90, 1964.

D. F. Ciocan and V. V. Mišić. Interpretable optimal stopping. *Management Science*, 2020.

P. F. Colletti, Y. Goyal, A. M. Varman, X. Feng, B. Wu, and Y. J. Tang. Evaluating factors that influence microbial synthesis yields by linear regression with numerical and ordinal variables. *Biotechnology and Bioengineering*, 108(4):893–901, 2011.

J. C. Cox, S. A. Ross, and M. Rubinstein. Option pricing: A simplified approach. *Journal of Financial Economics*, 7(3):229–263, 1979.

P. Crama, B. D. Reyck, and Z. Degraeve. Milestone payments or royalties? Contract design for R&D licensing. *Operations Research*, 56(6):1539–1552, 2008.

C. Cunha, J. Glassey, G. Montague, S. Albert, and P. Mohan. An assessment of seed quality and its influence on productivity estimation in an industrial antibiotic fermentation. *Biotechnology and Bioengineering*, 78(6):658–669, 2002.

M. C. D'anjou and A. J. Daugulis. A rational approach to improving productivity

in recombinant Pichia pastoris fermentation. *Biotechnology and Bioengineering*, 72 (1):1–11, 2001.

I. David and U. Yechiali. A time-dependent stopping problem with application to live organ transplants. *Operations Research*, 33(3):491–504, 1985.

S. Dayanik, C. Goulding, and H. V. Poor. Bayesian sequential change diagnosis. *Mathematics of Operations Research*, 33(2):475–496, 2008.

B. De Jonge and P. A. Scarf. A review on maintenance optimization. *European Journal of Operational Research*, 285(3):805–824, 2019.

C. Derman, G. J. Lieberman, and S. M. Ross. On the use of replacements to extend system life. *Operations Research*, 32(3):616–627, 1984.

P. M. Doran. *Bioprocess Engineering Principles*. Elsevier, 1995.

Eppendorf. Perfusion - Making the Most out of Your Working Volume, 2017. URL `https://handling-solutions.eppendorf.com/cell-handling/bioprocess/processes-and-applications/detailview/news/perfusion-making-the-most-out-of-your-working-volume/`.

EURO. The research project was a finalist of 2019 EURO Excellence in Practice Award, 2019.

European Commission. The research project was one of the three finalists of 2020 MSCA2020.HR Awards. The competition was among all disciplines to acknowledge the most influential projects under Horizon 2020 program of European Commission, 2020. URL `https://msca2020.hr/msca-awards/`.

S. S. Farid. Process economics of industrial monoclonal antibody manufacture. *Journal of Chromatography B*, 848(1):8–18, 2007.

Food and Agriculture Organization of the United Nations. Livestock production, 2018. URL `http://www.fao.org/3/y4252e/y4252e07.htm`. Date accessed June 20, 2019.

P. I. Frazier. Optimal learning: An overview. 2014. URL `https://people.orie.cornell.edu/pfrazier/Presentations/2014.06.TsinghuaIE_GuestLecture.pdf`.

P. I. Frazier. A tutorial on bayesian optimization. *arXiv preprint arXiv:1807.02811*,

2018. URL https://arxiv.org/abs/1807.02811.

A. Gelman, J. B. Carlin, H. S. Stern, D. B. Dunson, A. Vehtari, and D. B. Rubin. *Bayesian Data Analysis*. Chapman and Hall/CRC, 2013.

Grand View Research. Animal health market size, share and trends analysis report, 2018. URL https://www.grandviewresearch.com/industry-analysis/animal-health-market. Date accessed June 20, 2019.

P. Gronemeyer, R. Ditz, and J. Strube. Trends in upstream and downstream process development for antibody manufacturing. *Bioengineering*, 1(4):188–212, 2014.

M. W. Handlogten, A. Lee-O'Brien, G. Roy, S. V. Levitskaya, R. Venkat, S. Singh, and S. Ahuja. Intracellular response to process optimization and impact on productivity and product aggregates for a high-titer CHO cell process. *Biotechnology and Bioengineering*, 115(1):126–138, 2018.

M. Hermosilla. Rushed innovation: Evidence from drug licensing. *Management Science*, Articles in Advance:1–22, 2020.

Z. G. Icten, S. M. Shechter, L. M. Maillart, and M. Nagarajan. Optimal management of a limited number of replacements under Markovian deterioration. *IIE Transactions*, 45(2):206–214, 2013.

IFORS News. Innovative applications of operations research: Reducing costs and lead times in biomanufacturing, 2020. URL https://www.ifors.org/newsletter/ifors-news-march-2020.pdf.

IMPACT. Operational research improves biomanufacturing efficiency, 2020. URL https://www.theorsociety.com/publications/magazines/impact-magazine/.

INFORMS. The research project was a finalist of 2019 INFORMS Decision Analysis Society Excellence in Practice Award, 2019.

B. Jabarivelisdeh and S. Waldherr. Optimization of bioprocess productivity based on metabolic-genetic network models with bilevel dynamic programming. *Biotechnology and Bioengineering*, 115(7):1829–1841, 2018.

J. D. Jang and J. P. Barford. An unstructured kinetic model of macromolecular metabolism in batch and fed-batch cultures of hybridoma cells producing monoclonal antibody. *Biochemical Engineering Journal*, 4(2):153–168, 2000.

L. Jia, N. Luo, and J. Yuan. A model-based estimation of the profit function for the continuous fermentation of baker's yeast. *Chemical Engineering and Processing: Process Intensification*, 46(11):1215–1222, 2007.

V. Kachrimanidou, A. Vlysidis, N. Kopsahelis, and I. K. Kookos. Increasing the volumetric productivity of fermentative ethanol production using a fed-batch vacuferm process. *Biomass Conversion and Biorefinery*, pages 1–8, 2020.

E. Kakes. Supplement: Continuous Processing's Benefits within Biopharma's Reach, 2018. URL `https://www.genengnews.com/magazine/324/supplement-continuous-processings-benefits-within-biopharmas-reach/`.

P. Kaminsky and Y. Wang. Analytical models for biopharmaceutical operations and supply chain management: a survey of research literature. *Pharmaceutical Bioprocessing*, 3(1):61–73, 2015.

M. D. Kapadi and R. D. Gudi. Optimal control of fed-batch fermentation involving multiple feeds using differential evolution. *Process Biochemistry*, 39(11):1709–1721, 2004.

C. Karamatsoukis and E. Kyriakidis. Optimal maintenance of a production-inventory system with idle periods. *European Journal of Operational Research*, 196 (2):744–751, 2009.

Y. Koca, T. Martagan, and I. Adan. Optimizing the fermentation throughput in biomanufacturing with bleed–feed. *International Journal of Production Research*, Ahead-of-print:1–20, 2021a.

Y. Koca, T. Martagan, I. Adan, L. Maillart, and B. van Ravenstein. Increasing biomanufacturing yield with bleed-feed: Optimal policies and insights. *Invited for minor revision at Manufacturing & Service Operations Management*, 2021b. URL `https://papers.ssrn.com/sol3/papers.cfm?abstract_id=3659907`.

R. C. Leachman, L. Johnston, S. Li, and Z. Shen. An automated planning engine for biopharmaceutical production. *European Journal of Operational Research*, 238(1): 327–338, 2014.

D. Li, L. Qian, Q. Jin, and T. Tan. Reinforcement learning control with adaptive gain for a Saccharomyces cerevisiae fermentation process. *Applied Soft Computing*, 11 (8):4488–4495, 2011.

Y. Limon and A. Krishnamurthy. Resource allocation strategies for protein purification operations. *IISE Transactions*, 52(9):945–960, 2020.

A. Low. Single-use versus stainless-steel bioreactors. 2020. URL `https://www.pall.com/en/biotech/blog/single-use-stainless-steel-bioreactor.html`.

B. Maddah and M. Y. Jaber. Economic order quantity for items with imperfect quality: Revisited. *International Journal of Production Economics*, 112(2):808–815, 2008.

H. Mahal, H. Branton, and S. Farid. End-to-end continuous bioprocessing: Impact on facility design, cost of goods, and cost of development for monoclonal antibodies. *Biotechnology and Bioengineering*, 2021.

T. Martagan, A. Krishnamurthy, and C. T. Maravelias. Optimal condition-based harvesting policies for biomanufacturing operations with failure risks. *IIE Transactions*, 48(5):440–461, 2016.

T. Martagan, A. Krishnamurthy, and P. A. Leland. Managing trade-offs in protein manufacturing: How much to waste? *Manufacturing & Service Operations Management*, 22(2):330–345, 2019.

T. Martagan, Y. Koca, I. Adan, B. van Ravenstein, M. Baaijens, and O. Repping. Operations research improves biomanufacturing efficiency at msd animal health. *INFORMS Journal on Applied Analytics*, 51(2):150–163, 2021.

McKinsey & Company. From sciences to operations. 2014. URL `https://www.mckinsey.com/~/media/mckinsey/dotcom/client_service/pharma%20and%20medical%20products/pmp%20new/pdfs/from_science_to_operations-intro.ashx`.

McKinsey & Company. Rapid growth in biopharma: Challenges and opportunities, 2014. URL `https://www.mckinsey.com/industries/pharmaceuticals-and-medical-products/our-insights/rapid-growth-in-biopharma`. Date accessed October 25, 2021.

McKinsey & Company. Operations as a competitive advantage in biotechnology. 2019. URL `https://www.mckinsey.com/industries/pharmaceuticals-and-medical-products/our-insights/operations-as-a-competitive-advantage-in-biotechnology`.

J. Monod. The growth of bacterial cultures. *Annual Review of Microbiology*, 3(1): 371–394, 1949.

Mordor Intelligence. Biopharmaceuticals Market - Growth, Trends, COVID-19 Impact, and Forecasts (2021 - 2026), 2020. URL https://www.mordorintelligence.com/industry-reports/global-biopharmaceuticals-market-industry. Date accessed October, 2021.

S. Moreira, T. M. Klueter, and S. Tasselli. Competition, technology licensing-in, and innovation. *Organization Science*, 31(4):1012–1036, 2020.

MSD. Operations research improves biomanufacturing efficiency, 2019. URL https://www.youtube.com/watch?v=79B7OBuvRkY&feature=youtu.be. Date accessed June 25, 2019.

M. Muldowney. Continuous vs. batch production, 2018. URL https://www.contractpharma.com/issues/2018-04-01/view_features/continuous-vs-batch-production/.

K. P. Murphy. *Machine Learning, A Probabilistic Perspective*. The MIT Press, Cambridge, Massachusetts, 2012.

S. Mutturi and G. Lidén. Model-based estimation of optimal temperature profile during simultaneous saccharification and fermentation of Arundo donax. *Biotechnology and Bioengineering*, 111(5):866–875, 2014.

S. C. Nakanishi, L. B. Soares, L. E. Biazi, V. M. Nascimento, A. C. Costa, G. J. M. Rocha, and J. L. Ienczak. Fermentation strategy for second generation ethanol production from sugarcane bagasse hydrolyzate by Spathaspora passalidarum and Scheffersomyces stipitis. *Biotechnology and Bioengineering*, 114(10):2211–2221, 2017.

Nederlandse Biotechnologische Vereniging. Computers and bioprocess development, 2018. URL https://nbv.kncv.nl/en/activities/nbv-detail-page/411/computers-bioprocess-development/about. Date accessed March 28, 2018.

S. Oh and Ö. Özer. Characterizing the structure of optimal stopping policies. *Production and Operations Management*, 25(11):1820–1838, 2016.

T. Omasa, K.-I. Higashiyama, S. Shioya, and K.-i. Suga. Effects of lactate concentration on hybridoma culture in lactate-controlled fed-batch operation.

Biotechnology and Bioengineering, 39(5):556–564, 1992.

F. B. Oyebolu, R. Allmendinger, S. S. Farid, and J. Branke. Dynamic scheduling of multi-product continuous biopharmaceutical facilities: A hyper-heuristic framework. *Computers & Chemical Engineering*, 125:71–88, 2019.

S. Ozturk, J. Thrift, J. Blackie, and D. Naveh. Real-time monitoring and control of glucose and lactate concentrations in a mammalian cell perfusion reactor. *Biotechnology and Bioengineering*, 53(4):372–378, 1997.

S. S. Ozturk, M. R. Riley, and B. O. Palsson. Effects of ammonia and lactate on hybridoma growth, metabolism, and antibody production. *Biotechnology and Bioengineering*, 39(4):418–431, 1992.

G. Patel, M. D. Patil, S. Soni, T. P. Khobragade, Y. Chisti, and U. C. Banerjee. Production of mycophenolic acid by Penicillium brevicompactum—a comparison of two methods of optimization. *Biotechnology Reports*, 11:77–85, 2016.

C. V. Peroni, N. S. Kaisare, and J. H. Lee. Optimal control of a fed-batch bioreactor using simulation-based approximate dynamic programming. *IEEE Transactions on Control Systems Technology*, 13(5):786–790, 2005.

D. Petrides and C. Siletti. The role of process simulation and scheduling tools in the development and manufacturing of biopharmaceuticals. In *Proceedings of the 2004 Winter Simulation Conference*, volume 2, pages 2046–2051, 2004.

J. Pollock, S. V. Ho, and S. S. Farid. Fed-batch and perfusion culture processes: economic, environmental, and operational feasibility under uncertainty. *Biotechnology and Bioengineering*, 110(1):206–219, 2013.

W. B. Powell. *The Knowledge Gradient for Optimal Learning*. 2010. URL `https://castlelab.princeton.edu/html/Papers/Powell-EORMS-OptimalLearningFebruary172010.pdf`.

W. B. Powell and I. O. Ryzhov. *Optimal Learning*, volume 841. John Wiley & Sons, 2012.

A. Rao. Strategic research and development investment decisions in the pharmaceutical industry. *Marketing Science*, 39(3):564–586, 2020.

M. L. Rebaiaia, D. Ait-kadi, and A. Jamshidi. Periodic replacement strategies: optimality conditions and numerical performance comparisons. *International*

Journal of Production Research, 55(23):7135–7152, 2017.

S. M. Ross. *Stochastic Processes*. Wiley, New York, 2nd edition, 1996.

K. Sabri-Laghaie and R. Noorossana. Reliability and maintenance models for a competing-risk system subjected to random usage. *IEEE Transactions on Reliability*, 65(3):1271–1283, 2016.

F. Sahling and G. J. Hahn. Dynamic lot sizing in biopharmaceutical manufacturing. *International Journal of Production Economics*, 207:96–106, 2019.

V. M. Saucedo and M. N. Karim. Experimental optimization of a real time fed-batch fermentation process using Markov decision process. *Biotechnology and Bioengineering*, 55(2):317–327, 1997.

M. Sharma. Maximizing biomanufacturing productivity in single-use applications, 2019. URL `https://www.medicaldesignbriefs.com/component/content/article/mdb/features/technology-leaders/35518`.

A. N. Shiryaev. *Optimal stopping rules*, volume 8. Springer Science & Business Media, 2007.

J. S. Stonebraker and D. L. Keefer. OR practice—modeling potential demand for supply-constrained drugs: A new hemophilia drug at Bayer biological products. *Operations Research*, 57(1):19–31, 2009.

N. Taneri and A. De Meyer. Contract theory: impact on biopharmaceutical alliance structure and performance. *Manufacturing & Service Operations Management*, 19 (3):453–471, 2017.

C. Terwiesch and C. H. Loch. Collaborative prototyping and the pricing of custom-designed products. *Management Science*, 50(2):145–158, 2004.

The European Biopharmaceutical Enterprises. Medical innovation that helps millions of patients around the world. 2015. URL `https://www.ebe-biopharma.eu/wp-content/uploads/2014/11/EBE-Little-Book-FINAL.pdf`.

B. Tomlin. Impact of supply learning when suppliers are unreliable. *Manufacturing & Service Operations Management*, 11(2):192–209, 2009.

Y.-S. Tsao, A. Cardoso, R. Condon, M. Voloch, P. Lio, J. Lagos, B. Kearns, and Z. Liu. Monitoring Chinese hamster ovary cell culture by the analysis of glucose

and lactate metabolism. *Journal of Biotechnology*, 118(3):316–327, 2005.

G.-J. Van Houtum and B. Kranenburg. *Spare parts inventory control under system availability constraints*, volume 227. Springer, 2015.

A. F. Villaverde, S. Bongard, K. Mauch, E. Balsa-Canto, and J. R. Banga. Metabolic engineering with multi-objective optimization of kinetic models. *Journal of Biotechnology*, 222:1–8, 2016.

N. Walker. Perfusion Appears to be Gaining Traction in Biopharma Manufacturing, 2017. URL `https://www.pharmasalmanac.com/articles/perfusion-appears-to-be-gaining-traction-in-biopharma-manufacturing`.

W.-b. Wang. A model to determine the optimal critical level and the monitoring intervals in condition-based maintenance. *International Journal of Production Research*, 38(6):1425–1436, 2000.

Y. Wang, W. Sun, S. Zheng, Y. Zhang, and Y. Bao. Genetic engineering of Bacillus sp. and fermentation process optimizing for diacetyl production. *Journal of Biotechnology*, 301:2–10, 2019.

World Health Organization. Neglected zoonotic diseases, 2019. URL `https://www.who.int/neglected_diseases/-diseases/zoonoses/en/`. Date accessed June 12, 2019.

R. Wu and M. C. Fu. Optimal exercise policies and simulation-based valuation for American-Asian options. *Operations Research*, 51(1):52–66, 2003.

W. Xiao and Y. Xu. The impact of royalty contract revision in a multistage strategic R&D alliance. *Management Science*, 58(12):2251–2271, 2012.

W. Xie, B. Wang, C. Li, J. Auclair, and P. Baker. Bayesian network based risk and sensitivity analysis for production process stability control. *Preprint, submitted September*, 10:2019, 2020.

Z. Xing, N. Bishop, K. Leister, and Z. J. Li. Modeling kinetics of a large-scale fed-batch CHO cell culture by Markov chain Monte Carlo method. *Biotechnology Progress*, 26(1):208–219, 2010.

Y. Yang and M. Sha. A Beginner's Guide to Bioprocess Modes – Batch, FedBatch, and Continuous Fermentation, 2019. URL `https://www.eppendorf.com/product-media/doc/en/763594/Fermentors-Bioreactors_`

Application-Note_408_BioBLU-f-Single-Vessel_A-Beginner%E2%80%99s-Guide-Bioprocess-Modes-Batch_Fed-Batch-Continuous-Fermentation.pdf.

J. Yuan, Y. Xue, K. Hu, H. Wu, and Q. Jia. On-line application oriented optimal scheduling for penicillin fed-batch fermentation. *Chemical Engineering and Processing: Process Intensification*, 48(2):651–658, 2009.

L. Zeng, X. Deng, and J. Yang. Constrained Gaussian process with application in tissue-engineering scaffold biodegradation. *IISE Transactions*, 50(5):431–447, 2018.

Summary

Optimal Decision Making under Uncertainty in Biomanufacturing

Biomanufacturing methods use living organisms (i.e., viruses and bacteria) to generate products. This leads to challenges that are different than those in any other industry. In this thesis we address these challenges and develop optimization models to improve biomanufacturing efficiency. In collaboration with MSD Animal Health (MSD AH), we focus on a novel technique: bleed–feed. Bleed–feed is promising in skipping intermediary setups. However, its optimal implementation involves unique trade-offs and challenges, and its potential benefits are not fully understood by the industry yet. We combine the biological dynamics of fermentation and the operational trade-offs of bleed–feed, and present stochastic optimization models. We investigate the optimal bleed–feed decisions in different contexts and generate insights for practitioners.

More specifically, in Chapter 2 we assume the batch condition is monitored regularly. We develop a finite-horizon, discrete-time Markov decision process (MDP) model to determine condition-based bleed–feed policies that maximize expected total yield per batch. We analyze the structural characteristics of the optimal policies and show that the optimal bleed–feed policies have a three-way control-limit structure under mild conditions. We present a sufficient condition

under which a risk-averse heuristic is optimal. Additionally, we characterize the behavior of the value function as a function of regulatory restrictions and observe that the marginal benefit of an additional bleed–feed decreases and converges to a certain value. We show that for a model extension the control limit structure is still valid. In addition, a case study from MSD AH is performed to demonstrate the impact of bleed–feed under different production settings. We observe that bleed–feed brings benefits for all scenarios. In the base case, total biomass production from one setup increases by 137% with two bleed–feed implementations.

As observed in Chapter 2, bleed–feed improves the batch yield. However, it also increases the fermentation processing time. Additionally, time-based policies are also attractive for practitioners as they can be easily incorporated in production planning. Thus, in Chapter 3 renewal reward theory is used to determine time-based bleed–feed policies maximizing the expected fermentation throughput. We optimize the bleed–feed time and the replenishment amount jointly and investigate the additional benefit of the joint optimization. We analyze structural properties of the optimization problem and present a sufficient condition under which the throughput function is convex for a specific range of bleed–feed time. Using this result, we discuss the settings where implementing bleed–feed is not beneficial. We also show (for a special case) that the expected yield obtained from the second cultivation is concave in the initial biomass amount for the second cultivation. Subsequently, the managerial insights are enhanced with a case study from MSD AH. Through several strategies and practically relevant scenarios, we assess the potential impact of implementing bleed–feed on current practice. Our numerical analysis indicates that the expected throughput can be improved by 17% with bleed–feed, and bleed–feed is not an attractive option for slow-growing cell cultures.

Then, in Chapter 4 we extend our renewal model by including practically relevant constraints. These constraints ensure that bleed–feed is implemented during a shift and consider biomanufacturer's risk-averse behavior while finding optimal bleed–feed policies. This model also captures waste accumulation, costs related to its purification and its effect on the exponential growth phase duration and determines the optimal bleed–feed time to maximize the fermentation profit per time unit. We generate managerial insights through numerical analysis. We relax the constraints to investigate the value of flexibility in bleed–feed decisions. Our results indicate that it is not necessarily better to implement bleed–feed earlier if bleed–feed time

is not in a shift, and chance constraints have more impact for low-risk batches. We observe that if we are too restrictive on bleed–feed time, or if the waste accumulation is fast, then bleed–feed is not an attractive option.

Finally, in Chapter 5 we present a portfolio of decision support tools to improve biomanufacturing efficiency. The tools consist of the bleed–feed, yield optimization and rhythm wheel tools, and use variety of operations research methods, such as renewal reward theory, Bayesian design of experiments, and simulation-optimization. We elaborate on development of the tools and their implementation at MSD AH. Thanks to these tools, MSD AH had a significant impact with up to 50% increase in the batch yield and an additional revenue of €50 million per year. In addition, the rhythm wheel tool allowed one extra batch production per week, and the bleed–feed tool resulted in 85% increase in the batch yield per setup using one bleed–feed.

About the author

Yeşim Koca was born in 1993 in Osmangazi (Bursa), Turkey. She received her bachelor's degree (2014) and master's degree (2017) in Industrial Engineering from Hacettepe Univesity, both as a high honor student. During her master's studies, she worked as a research and teaching assistant in the Department of Industrial Engineering at the same university.

In 2017, Yeşim started her PhD at the School of Industrial Engineering at Eindhoven University of Technology. She conducted research on stochastic modeling and optimization in biomanufacturing, under the supervision of Ivo Adan and Tugce Martagan. She collaborated with MSD Animal Health during her PhD. She also worked together with Lisa Maillart from University of Pittsburgh in Chapter 2. Yeşim's research was internationally recognized for its potential impact. She was a finalist in INFORMS Decision Analysis Practice Award, and EURO Excellence in Practice Award competitions in 2019.